PRELIMINARY CHARACTERIZATION OF A NOVEL MITOCHONDRIAL MYOPATHY MOUSE MODEL

by

Mehmet Yılmaz

B.S., Molecular Biology and Genetics, Boğaziçi University, 2019

Submitted to the Institute for Graduate Studies in
Science and Engineering in partial fulfillment of
the requirements for the degree of
Master of Science

Graduate Program in Molecular Biology and Genetics

Boğaziçi University

2022

ACKNOWLEDGEMENTS

I want to express my sincere gratitude to my M.Sc. supervisor Assist. Prof. Şükrü Anıl Doğan. He guided and encouraged me throughout my master's research. Even before, in my undergrad years, I was lucky enough to participate in his lecture and become enthusiastic about mitochondria research and inspired by him. I also want to thank my M.Sc. thesis jury members, Assist. Prof. Necla Birgül and Assist. Prof. Serkan Kır for evaluating my thesis.

I am very thankful for DoganLab members; especially Semin Erkul and Özlem Kartal, who helped me in every part of this research, and for their sincere friendships. I want to extend my thanks to our special project student Ayşenur Canfes who helped me with Western Blotting experiments, and our new members Bengi Bekmez, Sertan Atilla, and Erdost Irmak.

I want to thank Davod Khalafkhany and Ulduz Sobhiafshar for their guidance and recommendations in experiments, Yamanlab for their assistance with the qPCR machine, and Sumolab for their help in Western blotting experiments.

I want to thank my dearest mother Eşe Yılmaz, my father Kadir Yılmaz and my siblings Tayibe and Enver Yılmaz. They have always supported me and shared both my joys and sadness. I also want to thank my beloved grandma Tayibe Yılmaz, who passed away a few years ago. I miss her every second. She was the biggest supporter of my whole life.

I also want to thank and hug my great friends Tuğba Ecem Sakallı, Sevgi Çıracı, Tolga Gürcan, Yonca Altun, İsmet Tarık Gölge and Burak Andıç for making my life better and sharing their friendships with me. Taking time with them is priceless to me.

This project was supported by the Scientific and Technological Research Council

of Turkey (TÜBİTAK) research grant 119C022 to Şükrü Anıl Doğan. Mehmet Yılmaz has been supported by the TUBİTAK-BİDEB 2210-A scholarship.

ABSTRACT

PRELIMINARY CHARACTERIZATION OF A NOVEL MITOCHONDRIAL MYOPATHY MOUSE MODEL

Mitochondria provide a significant portion of the ATP to cells and govern cellular energy economics on ever-changing cellular energy requirements. Cells evolved to monitor mitochondrial stress and developed counteracting stress response mechanisms to counteract mitochondrial dysfunction. Mitochondrial diseases are rare but complex diseases; involvement of both nuclear and mitochondrial genomes, threshold effect, and tissue specific manifestations of the disease increase the conundrum. Neuromuscular involvement in mitochondrial diseases is usually associated with mitochondrial myopathies, which are progressive in nature and may cause premature death. For this study, we generated a novel mitochondrial myopathy mouse model by disrupting the function of the mitochondrial aspartyl-tRNA synthetase gene (*Dars2*) in the skeletal muscle. Mitochondrial aminoacyl-tRNA synthetases are vital for mitochondrial protein translation since they aminoacylate uncharged tRNAs, and their dysfunction hampers mitochondrial translation. In skeletal muscle-specific *Dars2* deleted mice, we observed severe and progressive mitochondrial myopathy that causes muscle atrophy and significant reduction in lifespan and body weight. Knockout mice exhibited exercise intolerance, decreased locomotor activity, and muscle strength compared to their littermates. We detected hypoglycemia and an overall decrease in electron transport chain complexes at the molecular level. On the other hand, various stress responses were evoked in the knockout mice. Terminal stage mice displayed increased mitochondrial biogenesis and mitochondrial integrated stress response in both cell-autonomous and non-autonomous manner. Moreover, an impairment in autophagy and an advanced antioxidant response were observed. Our findings may create windows of opportunity for additional interventions in mitochondrial diseases.

ÖZET

YENİ BİR MİTOKONDRİYEL MİYOPATİ FARE MODELİ'NİN ÖN KARAKTERİZASYONU

Mitokondri hücrenin ATP üretimin büyük bir kısmını sağlar ve sürekli değişen hücresel enerji gereksinimlerine göre hücresel enerji ekonomisini yönetir. Hücreler, mitokondriyal stresi takip etmek ve mitokondriyal işlev bozukluklarına karşı stres tepki mekanizmaları geliştirecek şekilde evrimleşmiştir. Mitokondriyal stress cevapları yeterli olmadığında mitokondriyal bozukluklar meydana gelebilir. Mitokondriyal hastalıklar nadir fakat karmaşık hastalıklardır hem nükleer hem de mitokondriyal genomların katılımı, eşik etkileri ve hastalığın doku özgüllüğü belirtileri bu karmaşıklığı arttırır. Mitokondriyal hastalıklarda nöromüsküler tutulum genellikle doğası gereği ilerleyici olan ve erken ölüme neden olabilen mitokondriyal miyopatilerle ilişkilidir. Bu çalışma için, mitokondriyal aspartil-tRNA sentetaz geninin (*Dars2*) işlevini bozarak yeni bir mitokondriyal miyopati fare modeli iskeleti oluşturduk. Mitokondriyal aminoasil-tRNA sentetazları, yüksüz tRNA'ları aminoasile ettiklerinden ve bunların işlevsizliği mitokondriyal translasyonu engellediğinden mitokondriyal protein translasyonu için hayati öneme sahiptir. İskelet kası spesifik *Dars2* silinmiş farelerde, kas atrofisine ve yaşam süresinde ve vücut ağırlığında önemli bir azalmaya neden olan şiddetli ve ilerleyici mitokondriyal miyopati gözlemledik. Nakavt fareler, kontrol grubuna kıyasla egzersiz intoleransı, lokomotor aktivite ve kas gücünde azalma sergiledi. Hipoglisemi ve moleküler düzeyde elektron taşıma zinciri komplekslerinde genel bir azalma gözlemledik. Öte yandan, nakavt farelerde güçlü bir stres tepkisi gözlendi. Yaşamlarının terminal aşamasında olan farelerde, sistemik bir şekilde artan mitokondriyal biyogenez ve hem hücresel otonom olarak hem de sistemik olarak mitokondriyal entegre stres tepkisi sergiledi. Ayrıca, otofajide bir bozulma ve antioksidan cevabı gözlendi. Bulgularımız mitokondriyal hastalıklarda müdahale için yeni fırsatlar oluşturabilir.

TABLE OF CONTENTS

ACKNOWLEDGEMENTS iii
ABSTRACT v
ÖZET vi
LIST OF FIGURES xi
LIST OF TABLES xiii
LIST OF SYMBOLS xv
LIST OF ACRONYMS/ABBREVIATIONS xvi
1. INTRODUCTION 1
1.1. Mitochondria 1
1.2. Mitochondrial Diseases and Mitochondrial Myopathy 3
1.2.1. Complexities in Mitochondrial Diseases 3
1.2.2. Primary and Secondary Mitochondrial Diseases 4
1.2.3. Mitochondrial Myopathies 5
1.3. Mitochondrial Aminoacyl tRNA Synthetases 7
1.3.1. Mitochondrial Aminoacyl tRNA Synthetases and Diseases . . . 9
1.4. Mitochondrial tRNAs 11
1.5. Mitochondrial Translation 13
1.6. Mouse Models for Mitochondrial Myopathy 15
1.6.1. Mitochondrial DNA Deletion Model 15
1.6.2. Mitochondrial DNA Depletion Model 16
1.6.3. Mitochondrial Transcriptional Deficiency Model 16
1.6.4. Mitochondrial Electron Transport Chain Deficiency Models . . . 17
1.6.5. Mitochondrial Translational Deficiency Models 18
1.7. Mitochondrial Stress Responses 18
1.7.1. Mitochondrial Biogenesis 19
1.7.2. Autophagy 19
1.7.3. Antioxidant Stress Response 20
1.7.4. Mitochondrial Integrated Stress Response 21
2. PURPOSE OF THE STUDY 24

3. MATERIALS 25
3.1. Disposables 25
3.2. Lab Equipment 26
3.3. Softwares 27
3.4. Chemicals 28
3.5. Solutions 30
3.6. Kits and Enzymes 32
3.7. Antibody List 32
3.8. QPCR Primers 34
4. METHODS 36
4.0.1. Animal Care 36
4.0.2. Tissue Specific Dars2 Deletion 36
4.1. Protein Related Experiment 36
4.1.1. Protein Isolation: 36
4.1.2. Protein Concentration Quantification 37
4.1.3. Western Blotting 37
4.2. Genotyping of Mice 38
4.2.1. DNA Isolation from Ear Biopsy 38
4.2.2. PCR Reactions 38
4.2.3. Agarose Gel Electrophoresis 40
4.3. Quantification at the Transcript Level 40
4.3.1. Total RNA Isolation from Mouse Muscle 40
4.3.2. cDNA Synthesis 41
4.3.3. QPCR 42
4.4. High Yield DNA Isolation from Mouse Muscle with Chloroform Isolation 43
4.5. Blood Glucose Measurement 43
4.6. Phenotypic Experiments 44
4.6.1. Treadmill 44
4.6.2. Rotarod 44
4.6.3. Grip Strength Test 44
4.6.4. Activity Cage 44

4.6.5. Life-span Measurement 45
4.6.6. Statistical Analysis 45
5. RESULTS 46
5.1. Mitochondrial Myopathy Mouse Model Generation 46
5.2. Phenotype of Mitochondrial Myopathy Mouse Model 48
5.3. Phenotypic Characterization of Mitochondrial Myopathy Mouse Model 49
5.3.1. Muscle Performance and Muscle Strength of Mitochondrial Myopathy Mouse Model 50
5.3.2. Locomotor Activity and Motor Coordination of Mitochondrial Myopathy Mouse Model 52
5.4. Molecular Characterization of mKOs 53
5.4.1. mKOs were Hypoglycaemic 53
5.4.2. OXPHOS were Downregulated in Mitochondral Myopathy Mouse Model 54
5.4.3. Mitochondrial Biogenesis Increases in Mitochondral Myopathy Mouse Model 55
5.4.4. Autophagy is impaired in Mitochondrial 58
5.4.5. Antioxidant Response in mKOs 59
5.5. Mitochondrial Integrated Stress Response in mKOs 60
6. DISCUSSION 65
6.1. Variability of Lifespan and Severity of Disease Phenotypes in Mitochondrial Myopathy Models 66
6.1.1. Deletor Mouse and Skeletal Muscle Specific *Dars2* Mouse 66
6.1.2. *Pus1* KO vs Skeletal Muscle Specific *Dars2* Mouse 67
6.1.3. COX10 KO vs Skeletal Muscle Specific *Dars2* Mouse 68
6.1.4. COX15 KO vs Skeletal Muscle Specific *Dars2* Mouse 70
6.1.5. *Ckmm-Cre* Mice and Myopathic Phenotpye 70
6.2. A Possible Fiber Type Switch in Skeletal Muscle Specific *Dars2* Mouse 72
6.3. Skeletal Muscle Specific *Dars2* Mouse are Hyopglycamemic 73
6.4. Reduction in ETC Complex Levels Skeletal Muscle Specific *Dars2* Mouse 73

6.4.1. Mitochondrial Biogenesis Response in Skeletal Muscle Specific *Dars2* Mouse 74
6.4.2. Autophagy Impairment in Skeletal Muscle Specific *Dars2* Mouse 76
6.4.3. Antioxidant Response in Skeletal Muscle Specific *Dars2* Mouse 77
6.4.4. ISR^{mt} in Skeletal Muscle Specific *Dars2* Mouse 79
7. CONCLUSIONS & FUTURE PERSPECTIVES 82
REFERENCES 84

LIST OF FIGURES

Figure 1.1. ETC complexes reside in the inner mitochondrial membrane. . . . 3

Figure 1.2. tRNA charging by mtaaRS occurs in a two-step, Figure is adapted from Antonellis and Green, 2008. 9

Figure 1.3. mt-aaRS related diseases may exert their effects on tissue specific manifestations. Figure is adapted from (Konovalova and Tyynissma, 2013). 11

Figure 5.1. Mutant generation strategy and *Dars2* transcript levels. Bars represent Mean ± SEM, asterisks display significance level between mKOs and WT group, n=5, Student's t test, ***: $p \leq 0.001$. . . . 47

Figure 5.2. Mating strategy of mice. Red colored figure represents mKOs. . . 49

Figure 5.3. Physical characteristics of mKOs. Bars represent Mean ± SEM, asterisks display significance level between mKOs and WTs, n = 5-18 (Student's t test, ***: $p \leq 0.001$, ****: $p \leq 0.0001$). 50

Figure 5.4. Muscle strength and muscle performance of mKOs differ from WT animals. Bars represent Mean ± SEM, asterisks display significance level between mKOs and WTs, n=4-25 (Student's t test, **: $p \leq 0.01$, ***: $p \leq 0.001$, ****: $p \leq 0.0001$). 52

Figure 5.5. mKOs are hypoglycaemic Bars represent Mean ± SEM, asterisks display significance level n = 8-12 (Student's t test, ***: $p \leq 0.001$, ****: $p \leq 0.0001$). 54

Figure 5.6. OXPHOS downregulation is evident in mKOs. Bars represent Mean ± SEM, asterisks display significance level n = 4 (Student's t test, ***: $p \leq 0.001$, ****: $p \leq 0.0001$). 55

Figure 5.7. Mitochondrial biogenesis in mKO skeletal muscles. Bars represent Mean ± SEM, asterisks display significance level n = 3-4 (Student's t test, *: $p \leq 0.05$, **: $p \leq 0.01$, ***: $p \leq 0.001$). 56

Figure 5.8. Mitochondrial biogenesis response increases mtDNA copy number. Bars represent Mean ± SEM, asterisks display significance level n = 5 (Student's t test, ns: not significant, ***: $p \leq 0.001$). 57

Figure 5.9. Mitochondrial chaperones in mKO skeletal muscle. Bars represent Mean ± SEM, asterisks display significance level n =3 (Student's t test, *: $p \leq 0.05$, **: $p \leq 0.01$). 58

Figure 5.10. Autophagy was impaired in mKOs. Bars represent Mean ± SEM, asterisks display significance level n = 4 (Student's t test, *: $p \leq 0.05$, **: $p \leq 0.01$). 59

Figure 5.11. Antioxidant response in mKOs. Bars represent Mean ± SEM, Asterisks display significance level n = 3-5 (Student's t test, *: $p \leq 0.05$, **: $p \leq 0.01$). 60

Figure 5.12. ISR^{mt} response in mKOs. Bars represent Mean ± SEM, asterisks display significance level n = 3 (Student's t test, ***: $p \leq 0.001$). 62

Figure 5.13. ATF4 targets and systemic ISR executers in mKO. Bars represent Mean ± SEM, asterisks display significance level n = 3-5 (Student's t test, *: $p \leq 0.05$, **: $p \leq 0.01$, ***: $p \leq 0.001$). 64

LIST OF TABLES

Table 3.1. Disposables. 25

Table 3.2. Lab equipment 26

Table 3.3. Softwares used in experiments. 27

Table 3.4. Chemicals 28

Table 3.5. Solutions 30

Table 3.6. Kits and enzymes. 32

Table 3.7. Antibody List 32

Table 3.8. Forward primers. 34

Table 3.9. Reverse primers 34

Table 4.1. PCR reaction mix for *Dars2* and Cre. 39

Table 4.2. PCR conditions - *Dars2*. 39

Table 4.3. PCR conditions - Cre. 39

Table 4.4. cDNA synthesis mix. 41

Table 4.5. cDNA synthesis (Reaction protocol). 41

Table 4.6. QPCR mix. 42

Table 4.7. QPCR conditions. 42

Table 4.8. Melting curve. 43

LIST OF SYMBOLS

α	Alpha
&	And
β	Beta
°C	Degree Celsius
g	Gram
g	Gravity
μ	Micro
μg	Microgram
μl	Microliter
μM	MicroMolar
mg	Milligram
ml	Milliliter
mM	MiliMolar
min	Minute
%	Percent
s	Second
V	Volt

LIST OF ACRONYMS/ABBREVIATIONS

aaRS	Aminoacyl-tRNA Synthetases
AcoA	Acetyl coenzyme A
ARE	Antioxidant Response Element
cDNA	Complementary DNA
COX	Cytochrome c Oxidase
Cre	Bacteriophage P1 derived site-specific recombinase
DARS2	Mitochondrial aspartyl-tRNA synthetase
DNA	Deoxyribonucleic Acid
ETC	Electron Transport Chain
FAD^+	Flavin adenine dinucleotide
IMM	Inner mitochondrial Membrane
IMS	Intermembrane Space
ISR^{mt}	Mitochondrial Integrated Stress Response
mKO	Muscle-knockout
MM	Mitochondrial Myopathy
mt-aaRS	Mitochondrial aminoacyl-tRNA Synthetases
mtDNA	Mitochondrial DNA
mt-tRNA	Mitochondrial tRNA
OMM	Outer Mitochondrial Membrane
NAD^+	Nicotinamide adenine dinucleotide
QPCR	Real Time PCR
PCR	Polymerase Chain Reaction
PBS	Phosphate Buffered Saline
RNA	Ribonucleic Acid
SEM	Standard Error of Mean
UPR^{mt}	Mitochondrial Unfolded Protein Response
WT	Wild Type

1. INTRODUCTION

1.1. Mitochondria

Thanks to great scientist Lynn Margulis, now it is widely accepted that mitochondria are derived from ancient alpha-proteobacterium and became organelles of their host cells during evolution (Sagan L., 1967). Mitochondrial incorporation into cells to form eukaryotic lineages opened up a range of possibilities to the course of evolution, allowing an expansion of the number of genes expressed up to 200000 times (Lane & Martin, 2010).

Mitochondria are double membranous organelles: Outer mitochondrial membrane (OMM) and inner membrane (IMM) are separated by intermembrane space; the lipid composition, permeability, and duties of transmembrane proteins of OMM and IMM differ from each other, probably a consequence of endosymbiosis (Protasoni & Zeviani, 2021). OMM is similar to eukaryotic membranes; on the other hand, IMM is more like bacterial membranes containing cardiolipin. Moreover, IMM has a sophisticated shape that consists of cristae via invaginations through the mitochondrial matrix and inner boundary membrane that lies parallel to the OMM (Protasoni & Zeviani, 2021). The inner boundary membrane and cristae are connected with the tight structures called the cristae junctions (Protasoni & Zeviani, 2021). In addition to these complex structures, mitochondria have double-stranded circular genomes that are minimized over time due to gene transfer to the cellular nucleus and are located in nucleoid spaces in the mitochondrial matrix (Nunnari & Suomalainen, 2012). Mitochondria also have translational machinery in the mitochondrial matrix, such as mitoribosomes and transfer RNAs (tRNAs) (Nunnari & Suomalainen, 2012).

Mitochondria play various roles in cells, from Adenosine triphosphate (ATP) production, Calcium (Ca^{2+}) homeostasis, apoptosis to Nicotinamide adenine dinucleotide (NADH) production, lipid synthesis, pyrimidine synthesis, and contribute to the one-carbon cycle and iron metabolism (Ducker & Rabinowitz, 2017; Nunnari & Suoma-

lainen, 2012). Among these functions, ATP production is the most popular as the mitochondria are frequently referred to as the "cell's powerhouses". ATP production supplies the cellular energy demand by cellular respiration comprised of glycolysis, tricarboxylic acid (TCA) cycle, and oxidative phosphorylation (Fernie et al., 2004). Mitochondrial involvement begins after glucose breakdown into pyruvate, which is transported into the mitochondrial matrix for the TCA cycle (Fernie et al., 2004). Pyruvate dehydrogenase mediates the conversion of pyruvate into Acetyl Co-enzyme A (ACoA) enters to the TCA cycle (Fernie et al., 2004). In addition to the glucose, amino acids, monosaccharides, and fatty acids can also be broken down into more minor metabolites and end up in acetyl-CoA, which is oxidized at the TCA cycle in the mitochondrial matrix, and its electrons are transferred to electron carriers; Nicotinamide Adenine Dinucleotide (NAD^+) and Flavin Adenine Dinucleotide (FAD^+) (Bezawork-Geleta et al., 2017). After the reduction of these two molecules in the TCA cycle, reoxidation of NADH and FADH2 is executed at IMM-located electron transport chain (ETC) complexes (Nolfi-Donegan et al., 2020).

ETC complexes comprise four macromolecular structures "Figure 1.1", Complex I (CI) is the largest of them all and contains 45 subunits (Sharma et al., 2009). CI accepts electrons from NADH, donates electrons to Co-enzyme Q (CoQ) and pump protons into intermembrane space. Complex II (CII) consists of 4 subunits: SDHA, SDHB, SDHC, and SDHD are the only ETC complex wholly encoded by the nuclear genome (Bezawork-Geleta et al., 2017). CII accepts electrons via Iron Sulphur (Fe-S) cluster from FADH2 and donates them to coenzyme Q. CII provides a second entry point into ETC, yet it does not pump protons. Electron transfer from CI or CII to CoQ reduces it to Ubiquinol (Nolfi-Donegan et al., 2020). Complex III (CIII) carries electrons from the Ubiquinol to cytochrome-C, by which Ubiquinol is oxidized back into the CoQ and cytochrome-C is reduced, and reduced cytochrome-C donates electrons to Complex IV (CIV). During cytochrome-C reduction, CIII pumps protons into the IMS (Li et al., 2021). CIV donates the electrons to oxygen and pumps protons into IMS. ATP Synthase (CV) utilizes the proton motive force generated by CI, CII, and CIV to produce ATP (Nolfi-Donegan et al., 2020).

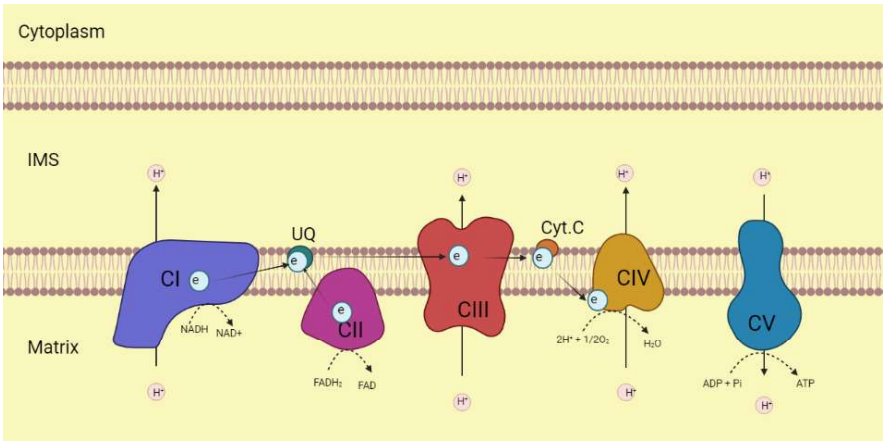

Figure 1.1. ETC complexes reside in the inner mitochondrial membrane.

1.2. Mitochondrial Diseases and Mitochondrial Myopathy

1.2.1. Complexities in Mitochondrial Diseases

Involvement of both nuclear and mitochondrial genomes and mitochondrial mode of inheritance increases the complexity of mitochondrial disorders. The mitochondrial way of inheritance is maternal, and paternal mitochondria are ubiquitinated for selective destruction (Pfeffer & Chinnery, 2013). In addition to these complexities, energy-demanding tissues like the brain, heart, endocrine system, and muscle are more vulnerable. Moreover, mitochondrial defects may lead to pathological problems at a metabolic and systemic level in humans (Pfeffer & Chinnery, 2013; Zeviani & di Donato, 2004).

Interestingly, mitochondrial dysfunctions caused by mutations in either nuclear or mitochondrial genome exert their effects on a phenotypical level when they pass a certain threshold (Rossignol et al., 2003). Mitochondrial homoplasmy and heteroplasmy concepts are being utilized for a better understanding of the threshold effect. Mitochondrial homoplasmy refers to a state in which all existing mitochondrial DNAs (mtDNAs) are mutant or variant; on the other hand, heteroplasmy refers to a state where normal and variant or mutant mtDNAs coexist (Zaragoza et al., 2010). 1 in 200 people carries the most ten pathological mtDNA point mutations with low hetero-

plasmy levels (Stewart & Chinnery, 2015). As the mitochondrial mode of inheritance is maternal, heteroplasmy of mtDNAs in the offspring may arise as a result of random transmission from the mother. Additionally, at the oocyte stage, a small group of dysfunctional mitochondria may exert their effect on the individual as these will be inherited in the whole body, which is known as the "bottleneck effect" (Pfeffer & Chinnery, 2013). Moreover, pathological deleterious mtDNA variants may cause a replicative advantage, in which smaller mtDNA sizes may accelerate the division rate and shift heteroplasmy towards a diseased phenotype (Stewart & Chinnery, 2015). Mitochondrial heteroplasmy can be observed among different species, organs, tissues, cells, and cellular compartments (Hahn & Zuryn, 2019). Due to the complexities of mitochondrial diseases, there is no cure for them; only some interventions and treatments exist to alleviate them (Garone & Viscomi, 2018).

1.2.2. Primary and Secondary Mitochondrial Diseases

Mitochondrial genome codes for 22 transfer RNAs (tRNAs), 13 ETC genes, and 2 ribosomal RNAs (rRNAs), and mitochondria contain approximately 1500 nuclear-encoded proteins (Calvo & Mootha, 2010). Primary Mitochondrial Diseases (PMDs) are caused by problems with those genes and are associated with OXPHOS dysfunction (Viscomi & Zeviani, 2020). Mitochondrial DNA-related defects may arise from large mtDNA deletions, protein-coding ETC subunit genes, and genes required for protein synthesis (rRNAs, tRNAs) (Viscomi & Zeviani, 2020). Most PMDs of nuclear DNA mutations are caused by defects in the structural proteins and assembly factors of the ETC complexes; mtDNA maintenance; mtDNA transcription and protein synthesis machinery; and quality control proteins (Viscomi & Zeviani, 2020).

Some known mtDNA-related mitochondrial diseases are Myoclonic Epilepsy with Ragged Red Fibers (MERFF), Leber's Hereditary Optic Neuropathy (LHON), Progressive External Ophthalmoplegia (PEO), Mitochondrial Encephalomyopathy with Lactic Acidosis (MELAS), Neuropathy Ataxia and Retinitis Pigmentosa (NARP), Barth's Syndrome, Kearns-Sayre Syndrome (KSS) and Leigh Syndrome: These diseases display heteroplasmy, meaning the severity of the problem depends on the heterogeneity level of conditions (Pfeffer & Chinnery, 2013; Zeviani & di Donato, 2004).

Nuclear DNA-related PMDs are pretty complex, and their mode of inheritance is mainly autosomal-recessive, X-linked or dominant (Niyazov et al., 2016). Multigenic point mutations in nuclear genes like *NDUFS1, SURF1*, etc., are associated with Leigh syndrome, and mutations in some nuclear genes like *POLG* and *TYMP* are engaged in Alpers-Huttenlocher and mitochondrial neurogastrointestinal encephalomyopathy (MNGIE) causing mtDNA deletion or depletion (Niyazov et al., 2016). Apart from these two groups of PMDs, there is another class of mitochondrial diseases called secondary mitochondrial disorders (SMDs) that may be caused by environmental or genetic factors, and worsen mitochondrial function but are not linked with ETC complex engagements (Sulaiman et al., 2020). Some SMDs are responsible for mutated genes can be exemplified as Spinal muscle atrophy by *SMN1*, Friedreich's Ataxia by *FXN*, Charcot-Maria-Tooth Type 2k by *GDAP1*, Hereditary spastic paraplegia seven by *SPG7*, and Wilson's disease by *ATP7B* gene (Niyazov et al., 2016).

1.2.3. Mitochondrial Myopathies

A notable group of PMDs is called mitochondrial myopathies (MMs) with OXPHOS dysfunctions and involvements of neuromuscular components (Hassani et al., 2010; Pfeffer & Chinnery, 2013). Mitochondrial myopathies often have a progressive nature that may lead to disabilities, even premature deaths (Pfeffer & Chinnery, 2013). Moreover, clinically multiorgan system involvement is observed in mitochondrial myopathies; for instance, renal tubular defects, diabetes mellitus, ataxia, optic atrophy, pigmentary retinopathy, psychosis, etc. may also accompany mitochondrial myopathy (Pfeffer & Chinnery, 2013).

Muscle and cardiac tissues are frequently affected by mitochondrial dysfunctions. Some explanations are proposed for this phenomenon; the first explanation states that muscle tissues are affected by mitochondrial defects more severely because of their higher energy demand (N. G. Larsson & Oldfors, 2001). The second one states that with organismal aging, mutational accumulation in postmitotic tissues passes a certain level and exerts its effects (N. G. Larsson & Oldfors, 2001). Lastly, the third one states a bias toward investigating muscle tissues in mitochondrial dysfunctions independently from the involvement of muscle tissues in mitochondrial defects (N. G. Larsson & Oldfors, 2001). Like other PMDs, MMs also display a threshold effect, in which disease progression requires passing a specific mutational load and disease progression depends on the heteroplasmy level (Pfeffer & Chinnery, 2013).

ETC dysfunctions in muscle may characterize mitochondrial myopathies, COX-negative but SDH-positive muscle fibers, aggregations of mitochondria in sub-sarcolemma [Ragged Red Fiber inclusions (RRFs)], aberrant-shaped mitochondria and cristae, and frequent mitophagosomes at the morphological level (Khan et al., 2017). An exciting study explained various ultrastructural changes of mitochondria in mitochondrial myopathy patients who displayed paracrystalline formations, cristae linearization, and geometric shapes by these linearized cristae, and onion-like structures of cristae composed of multilayered concentric membranes (Vincent et al., 2016). In addition to the mitochondrial matrix and intermembrane space, multiple mitochondrial compartmentalizations were noticed: Those compartments had a distinct molecular and ionic composition, also, nano-tunnelling between mitochondria and hyperbranched self-fused & doughnut-shaped mitochondria were observed (Vincent et al., 2016).

Apart from structural differences in mitochondria, in MM patients, decreased peak O_2 uptake, reduced mitochondrial volume density, and increased type II fiber ratio were also detected (Gehrig et al., 2016). Peak oxygen uptake in mitochondrial myopathy patients has been reduced to one-third of their sedentary controls also these patients also displayed exercise intolerance and reduced work capacity (Taivassalo & Haller, 2005). These severe phenotypes, threshold effects, and multisystem involvements in MMs require a deliberate analysis of the disease. Therefore, several mouse models have been developed to dissect mitochondrial myopathies in either whole body or tissue-specific manner with different types of defects.

1.3. Mitochondrial Aminoacyl tRNA Synthetases

Covalent attachment of tRNAs to their cognate amino acids is essential for protein synthesis (Wallen & Antonellis, 2013). This covalent attachment is catalyzed by aminoacyl-tRNA synthetases (aaRS) that aminoacylate transfer RNAs (tRNAs) via a two-step reaction in which tRNAs match with their cognate amino acids, and this tRNA aminoacylation process is also called "tRNA charging" (Konovalova & Tyynismaa, 2013).

In eukaryotic cells, there are two sets of aaRSs encoded by the nuclear genome; one is cytoplasmic, and the other is mitochondrial (Fine et al., 2019). Mitochondrial aminoacyl-tRNA Synthetases (mt-aaRS) are named according to "the first letter symbol of aminoacid-ARS-2", for example *AARS2* for Alanyl-tRNA Synthetase 2, or *YARS2* for Tyrosyl-tRNA Synthetase 2. The nuclear genome encodes 37 aaRS genes, 20 for cytoplasmic and 17 for mitochondrial. Glycyl-tRNA Synthetase and Lysyl-tRNA Synthetases, *GARS* and *KARS*, respectively, do not have a separate mitochondrial gene; instead, they are produced with the same gene as their cytoplasmic partner and are imported to mitochondria for protein synthesis like other mt-aaRSs (Tyynismaa, 2013). *GARS* gene has two translation initiation sites, one giving rise to the cytosolic, the other to the mitochondrial version. In the *KARS* gene, an alternative splicing pathway for mRNA decides whether the protein has a mitochondrial targeting signal or not (Bonnefond et al., 2005). Mt-aaRS for glutamine (glutamyl-tRNA synthetase)

have not been identified yet; it is thought that gln-mt-tRNAGln is formed by modification of glutamic acid after conjugation (Boczonadi et al., 2018; Echevarría et al., 2014). It is known that the GatCAB enzyme convert EARS2 catalyzed glu-mt-tRNAGlu into gln-mt-tRNAGln by transamidation reaction and utilizes free glutamine (D'Souza & Minczuk, 2018).

Aminoacylation of tRNA occurs in two steps: First, the amino acid is activated, and second, the activated amino acid is transferred to tRNA (Wallen & Antonellis, 2013). The first step of tRNA charging starts with amino acid and ATP binding to aaRS; then, aaRS attaches amino acid with AMP, forming aminoacyl adenylate and releasing two phosphates (Wallen & Antonellis, 2013). After aminoacyl-adenylate complex formation, the second stage of the reaction starts. In this step, aaRS binds to the anticodon binding domain of tRNA while removing amino acids from the AMP and covalently links amino acids to the tRNAs. Finally, both AMP and aminoacylated tRNA is released from the enzyme "Figure 1.2" (Wallen & Antonellis, 2013).

Significantly, identifying cognate tRNAs by aaRSs is determined by the 3-dimensional shape of tRNAs, especially the fold from stem-loop structures to ternary L-shape is critical for positioning and charging tRNAs (Garin et al., 2020). Specific nucleotides at the anticodon region and acceptor loop provide another layer of specificity (Garin et al., 2020). All aaRSs have an aminoacylation domain, and based on this domain, aaRSs are grouped into two distinct classes, each with 10 enzymes (Guo et al., 2010). First Class I aaRSs have nucleotide-binding Rossman fold, and Class II aaRSs have a seven-stranded β sheet structure with flanking α-helices (Guo et al., 2010). Interestingly half of aaRSs also have an editing function that detaches the wrong amino acid from the tRNA, and both aminoacylation and editing domains are common in all domains of life (Guo et al., 2010). In the course of evolution, eukaryotic aaRSs have gained non-canonical functions apart from their aminoacylation via new protein domains, and these new functions range from participating in angiogenesis, transcriptional control, and cell migration to tumorigenesis (Yao & Fox, 2013; Guo et al., 2010).

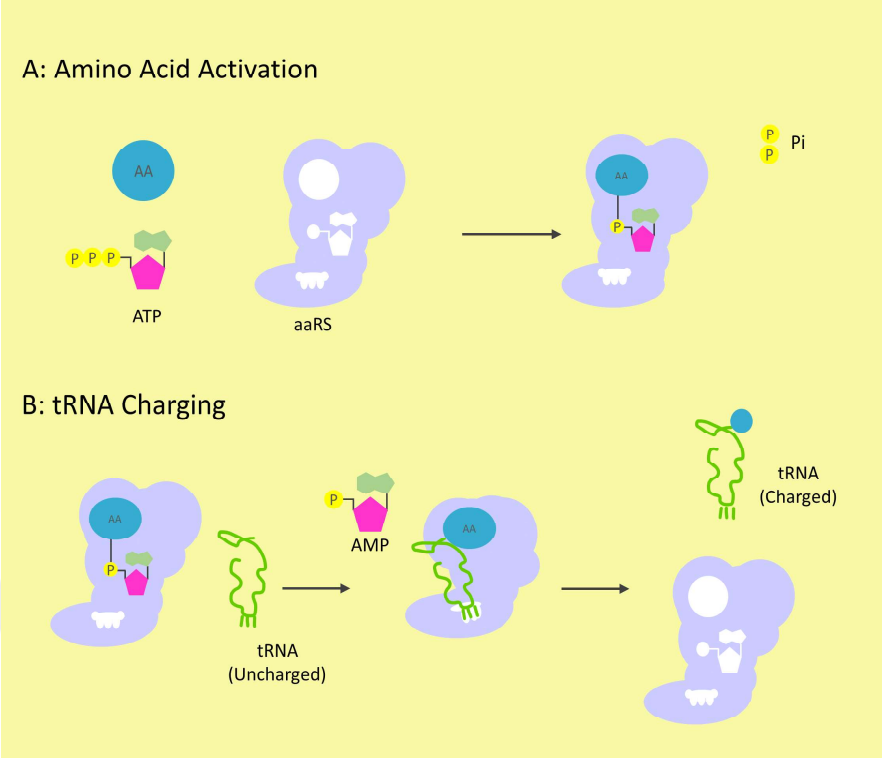

Figure 1.2. tRNA charging by mtaaRS occurs in a two-step, Figure is adapted from Antonellis and Green, 2008.

1.3.1. Mitochondrial Aminoacyl tRNA Synthetases and Diseases

Mutations in mt-aaRSs may affect phenotype by causing a broad range of diseases with tissue-specific involvements, which could appear at any age (Sissler et al., 2017). The diversity of these diseases changes from hearing loss, intellectual disability, and leukodystrophies to cardiomyopathies, yet mt-aaRS defects are biased towards the neural system involvements (Sissler et al., 2017).

The first identified mt-aaRS that led to human disease was the mitochondrial aspartyl-tRNA synthetase (*DARS2*); mutations of which caused leukoencephalopathy with the spinal cord and involvement of high lactate (LBSL) (Scheper et al., 2007). *DARS2* mutations are associated with spasticity, cerebellar ataxia, and mental faculty decline (Diodato et al., 2014). Elevated lactate levels and white matter changes are generally observed in patients (Diodato et al., 2014). Most DARS2 patients showed

mutations in intron 2 that may result in a problem of exon 3 splicing and exclusion of exon 3, leading to a frameshift and a shorter version of the original protein (van Berge et al., 2012). Of note is that the observed mutation is leaky, which means a small amount of the WT version of DARS2 protein is synthesized (van Berge et al., 2012). Most LBSL patients with either *DARS2* or *DARS1* mutations are compound heterozygous; only a few cases were reported as homozygous (Muthiah et al., 2021). LBSL mutations caused by *DARS2* also do not always produce the same phenotype. For example, in a case, a Japanese patient with compound heterozygous *DARS2* mutation [c.358_359delinsTC (p.Gly120Ser) and c.228-15C4G (splicing error)] presented the first clinical symptoms in childhood. Still, the patient exhibited leukoencephalopathy involvement with brainstem and spinal cord (Shimojima et al., 2017). As for other mitochondrial diseases, *DARS2* mutations can also exert their clinical symptoms at any age. For example, in the case of an adult female, clinical signs appeared at the age of 43 (N'gbo N'gbo Ikazabo et al., 2020). MRI results showed white matter abnormalities, and the disease is caused by compound heterozygous mutation at one allele combined with polymorphism in the other allele (N'gbo N'gbo Ikazabo et al., 2020). Other mt-aaRSs mutations also display various diseases as well. In "Figure 1.3", mt-aaRSs and their clinical manifestations are summarized.

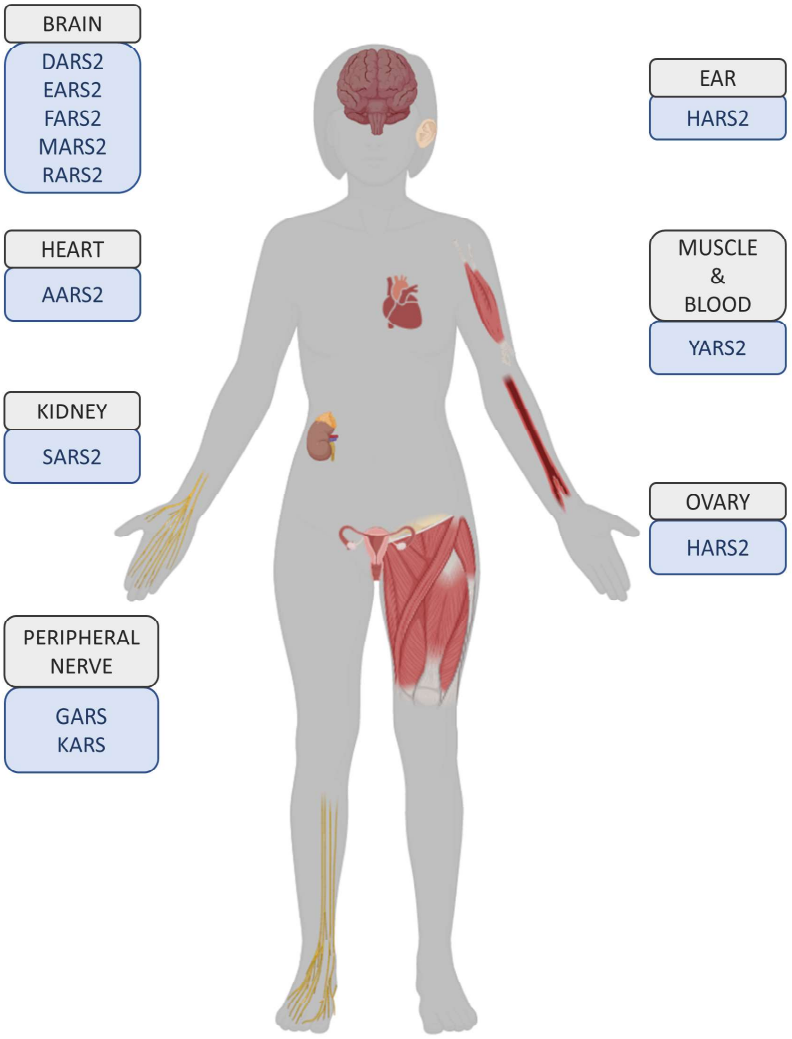

Figure 1.3. mt-aaRS related diseases may exert their effects on tissue specific manifestations. Figure is adapted from (Konovalova and Tyynissma, 2013).

1.4. Mitochondrial tRNAs

Mitochondrial tRNAs (mt-tRNAs) In some eukaryotic species like *Trypanosoma brucei*, all mt-tRNAs are encoded in the nuclear genome and transferred into mitochondria; in some other species, a similar case with specific amino acid import is observed, i.e. in *S. cerevisiae*, only tRNAGln is transferred from the cytoplasm (Niemann et al., 2017; Rubio et al., 2008). Although human mitochondria code for their tRNAs, it has been shown that mammalian mitochondria have the inherent ability to import their

tRNAs from nuclear-encoded ones (Rubio et al., 2008). Despite this surprising innate ability in mammalians, there are clear distinctions between mitochondrial and nuclear tRNAs. Firstly, the D-loop was not observed in mammalian mt-tRNASer(AGY), which is the only tRNA without a D-loop in all 3 domains of life (Suzuki et al., 2011). Another distinct mt-tRNA is mt-tRNASer(UCN) which has only 1 base between the D stem and Acceptor stem with a short D loop and one additional loop (Suzuki et al., 2011). Numerous mt-tRNAs also do not have canonical D-T loop interactions in tRNAs (Suzuki et al., 2011).

Mitochondrial transcription occurs in a polycistronic mode in which tRNAs punctuate proteins and rRNAs on the primary transcript (D'Souza & Minczuk, 2018). Releasing proteins, tRNAs, and rRNAs from this primary transcript is mediated by endonucleolytic cleavage of tRNAs by RNase P, & RNase Z. This model is called the "tRNA punctuation model" (D'Souza & Minczuk, 2018). Some rRNAs or proteins are not punctuated by tRNAs; thus, FASTK proteins have roles in mtRNA transcript stabilizing and precursor processing, particularly those with non-canonical cleavage sites (D'Souza & Minczuk, 2018). After transcription, tRNAs undergo various modifications such as at a wooble base in anticodon to recognize non-Watson Crick base pairing at position 34 or another common modification at position 37 of mt-tRNA to increase the fidelity of codon-anticodon interaction. Last but not least, Pseudouridylation is another mt-tRNA modification that provides structural rigidity and stability (D'Souza & Minczuk, 2018). Mature mt-tRNAs might be aminoacylated by mt-aaRSs in which the amino-adenylation occurs; then, an activated amino acid is transferred to tRNA so that aminoacylated tRNAs can enter mitochondrial translation reactions (Salinas-Giegé et al., 2015).

Mutations that directly affect tRNA codon recognition abilities or aminoacylation reaction impair tRNA function severely; mutations in less critical positions may also threaten tRNA biogenesis or function (Suzuki et al., 2011). Nonetheless, very few tRNA point mutations on critical points have been associated with pathological cases; most mutations were in the less critical regions implying that these essential point mutations must be unsuited for embryo development (Suzuki et al., 2011). A point mutation in

mt-tRNALys at position 8344 is associated with a severe encephalomyopathy, MERRF. Moreover, from cardiomyopathy to ophthalmoplegia, other mitochondrial dysfunctions were associated with 15 distinct point mutations at mt-tRNAIle (Suzuki et al., 2011).

1.5. Mitochondrial Translation

Mitochondrial translation comprises of four main stages, translation initiation, elongation, termination of translation, and ribosome recycling (Pearce et al., 2013). Mitochondrial translation machinery requires nuclear DNA-encoded mitochondrial initiation factor 2 (mtIF2) and mitochondrial initiation factor 3 (IF3) (D'Souza & Minczuk, 2018). IF3 resides at the P site of the small subunit of mitochondrial ribosome (SSU) to inhibit early SSU and large subunit of mitochondrial ribosome (LSU) joining (D'Souza & Minczuk, 2018). Like other protein synthesis systems, mitochondrial protein synthesis requires a mitochondrial version of tRNAmet for translation initiation; nevertheless, mitochondria have a nuance; instead of normal methionine, they need formylated methionine (mt-tRNAf-met). mt-tRNAf-met has increased affinity for IF2, associates mt-tRNAf-met and mRNA, and navigates mitochondrial monosome assembly (D'Souza & Minczuk, 2018). Interestingly, as IF2 and IF1 (Initiation factor 1) are universal in all domains of life, mitochondria lack IF1, which binds to the A site of a small subunit to inhibit tRNA binding (Kummer & Ban, 2021). It was shown that in mammalians, IF2 could compensate for this function of IF1 by protruding its 37 amino acid long moiety at A subunit (Acceptor Site) in SSU (Kummer & Ban, 2021). In translation elongation, ribosomes proceed through mRNA. This elongation can be grouped into three stages, decoding in which aminoacylated tRNA couples with mRNA, formation of a peptide bond, peptide chain and tRNA presented amino acid, and translocation of mRNA-tRNA complex to E site (Kummer & Ban, 2021). EF-Tu assembles a complex incorporating aminoacylated tRNAs and GTP; it also mediates the guidance of tRNA to the A site for codon anti-codon interaction establishment (D'Souza & Minczuk, 2018). Upon GTP hydrolysis, peptide bond forms, and EFTu is released. Mitochondrial EFG1 disengages deacylated tRNAs from the P site, relocates peptidyl-tRNAs from the A-P site to the P-E site, and shifts the mRNA to one codon (D'Souza &

Minczuk, 2018). Translation termination is performed when stop codons are read. Mitochondria have UAG and UAA as a stop codon, and UGA codes for tryptophan (Christian & Spremulli, 2012). In the final stage, polypeptide release is followed by mitochondrial recycling factor (mtRRF) and EF-G2mt-mediated disassembly of ribosomal subunits, deacylated tRNA in the E site, and mRNA in the P site, which form a post-termination complex (PoTC). Binding of EF-G2mt.GTP to RRF.PoTC complex releases the PoTC complex elements (F. Wang et al., 2021).

Mitochondrial translation defects may have arisen from either mitochondrial or nuclear genomes since these two genomes contribute to the translation. Mt-tRNAs constitute 10% of the mitochondrial genome, yet they cause most mitochondrial mutations in human diseases (Pearce et al., 2013). A3243G mutation in mt-tRNALeu(UUR) accounts for 80% of patients with MELAS syndrome, which is frequently observed in children and young adults with signs of recurrent vomiting, headache similar to migraine, and hemiparesis (Pearce et al., 2013). Another significant mt-tRNA mutation is A8344G in mt-tRNALys, which is associated with MERFF, a multisystem disorder described as myoclonus and is succeeded by ataxia, dementia, epilepsy, and weakness (Pearce et al., 2013). Mt-tRNA mutations may be caused by various reasons like mt-tRNA processing, reduced aminoacylation, and impaired taurine modification. Still, these different mutations have similar conclusions, in which mt-tRNA stability is reduced (Pearce et al., 2013).

Like defects in mt-tRNAs genes, mitochondrial translational dysfunctions may frequently originate from the mtDNA pathologies and leads to OXPHOS deficiencies. Still, mutations in the nuclear genome may result in mitochondrial translation defects (Sasarman et al., 2002). Mutations in nuclear DNA-encoded ribosomal proteins are associated with various metabolic multisystem diseases ranging from cardiomyopathy to hearing loss (F. Wang et al., 2021). In addition to mitochondrial ribosomal proteins and mt-tRNAs, mutations in RNA modification enzymes, mitochondrial translation factors, and mt-aaRS may cause mitochondrial translational defects (F. Wang et al., 2021). Of note that although different mt-aaRS defects lead to mitochondrial translation deficiency and OPXHOS dysfunctions, each mt-aaRS defect may exert different tissue-specificity (Webb et al., 2020).

1.6. Mouse Models for Mitochondrial Myopathy

To study mitochondrial myopathy, numerous mouse models have been utilized. The general aim of these mouse models is to change the mtDNA expression profiles by knocking out or overexpressing nuclear-encoded genes (Kuszak et al., 2018). These different MM mice models can be classified as:

1.6.1. Mitochondrial DNA Deletion Model

PstI endonuclease enzyme was expressed in the skeletal muscles of mice to delete mtDNA (Srivastava & Moraes, 2005). Mouse mtDNA have two PstI endonuclease restriction sites at nucleotides 8424 and 12242; also, PstI-mediated restriction may result in a similar deletion condition to human m.8483_13459del4977 that accumulate throughout aging and disease progression (Bacman et al., 2014). In mitoPstI mice, mitochondrial myopathy onset was around 6-7 months. Mitochondrial DNA depletion, ETC defects, RRF formation, and numerous mitochondrial DNA deletions were observed in the skeletal muscles of mitoPstI mice. These deletions were mostly nearby to PstI regions in mtDNA (Srivastava & Moraes, 2005).

1.6.2. Mitochondrial DNA Depletion Model

Deletor is a transgenic mouse model with a mutated *Twinkle* gene under a ubiquitous promoter to generate a DNA depletion model (Tyynismaa et al., 2005). TWINKLE is a ring-shaped mtDNA helicase needed for mitochondrial H-strand synthesis by unwinding mt-DNA and progressing with the replicative fork (Peter & Falkenberg, 2020). Importantly TWINKLE is the only mitochondrial helicase, which is required for mtDNA maintenance (Peter & Falkenberg, 2020). Deletor mice made mistakes in mtDNA replication, and the accumulation of mtDNA deletion by mutated TWINKLE proteins showed a late onset mouse phenotype, in which the symptoms started to be observed around one year (Tyynismaa et al., 2005). Deletor mice displayed a phenotype similar to progressive PEO with ETC dysfunction, chronic late-age mitochondrial diseases, and COX (cytochrome c oxidase) deficiency (Tyynismaa et al., 2005).

1.6.3. Mitochondrial Transcriptional Deficiency Model

TFAM (Transcription Factor A, mitochondrial) is a mitochondrial protein vital for the organization of mtDNA and its transcriptional activation in both heavy and light strands of mtDNA by binding their promoter regions (Ngo et al., 2014). Additionally, it binds mtDNA and compacts the genome or serves as an RNA primer for the initiation of mtDNA replication (Kang et al., 2018). The onset of myopathy started to be observed around 3-4 months in skeletal muscle-specific deletion of *Tfam*, and the knockouts' lifespans were decreased to 4-5 months (Wredenberg et al., 2002). RRF formation, deterioration of ETC function, and decreased muscle force were also observed (Wredenberg et al., 2002). Paracrystalline inclusions were not observed but the cristae were disrupted in the skeletal muscle-specific *Tfam* knockouts (Wredenberg et al., 2002). Another TFAM mouse model is the whole body heterozygous version, in which an impediment of ROS generation and ATP production by OXPHOS was noted (N.-G. Larsson & Rustin, 2001).

1.6.4. Mitochondrial Electron Transport Chain Deficiency Models

A chaperone protein SURF1 is essential for COX assembly and is located in the IMM; although its exact role is unknown, *SURF1* mutations are one of the leading causes of Leigh syndrome in the population (Kose et al., 2020). Surf1 mice were generated to recapitulate Leigh Syndrome, caused by *SURF1* mutations in humans. However, Surf1-ablated mice, in which exon 7 was targeted, had only mild effects and surprisingly lived longer than wild-type and heterozygous mutant mice (Dell'Agnello et al., 2007). *Surf1* ablation has a neuroprotective effect, probably caused by a decreased Ca^{2+} uptake of mitochondria (Dell'Agnello et al., 2007).

NDUFS4 protein is involved in mitochondrial complex I (CI) assembly and stabilization, thus affecting CI function (van de Wal et al., 2022). Whole body *Ndufs4* KO mice did not reveal any problems up until 5 weeks, then exhibited ataxic signs, which included lower clasping of their back limbs and lost gait balance, and died around 7 weeks (Kruse et al., 2008). Their O_2 consumption rate, muscle ATP, and phosphorcreatine levels were within the physiological intervals of WT mice. However, they had subsarcolemmal mitochondrial accumulation and relatively low NADH dehydrogenase activity (Kruse et al., 2008).

COX10 protein is an assembly factor for CIV and catalyzes the conversion of protoheme (heme B) to heme O via farnesylation reaction (Antonicka, Leary, et al., 2003). Skeletal muscle-specific COX10 KO mice were generated to assess COX deficiencies in humans for a single ETC component level (CIV). From 3 months of age, mice started developing progressive mitochondrial myopathy, in which females are more severely affected than males, and both had a shorter lifespan than WT mice (Diaz et al., 2005). Fatigability of COX10 is lower than in skeletal muscle-specific TFAM KO mice; no signs of oxidative damage or apoptosis were observed as well (Diaz et al., 2005). Like COX10, COX15 protein is also involved in heme A synthesis and performs the last step of the reaction; it also contributes to the COX assembly (Bareth et al., 2013). Skeletal muscle-specific COX15 KO mice were generated to mimic the ETC problem. COX15 defects lead to deadly encephalocardiomyopathy in children. In the mouse

model, mitochondrial myopathy with severe COX deficiency was observed within 6 months of median survival rate and mice performed worse in treadmill tests than WT mice (Civiletto et al., 2015; Viscomi et al., 2011).

1.6.5. Mitochondrial Translational Deficiency Models

Mitochondrial Translational Deficiency Models PUS1 protein modifies mt-tRNAs with pseudouridylation reaction, in which pseudouridine molecule is attached to RNA molecules to improve the stability of their tertiary structure for efficient and accurate mitochondrial translation (Czudnochowski et al., 2013). *PUS1* mutation causes mitochondrial myopathy with lactic acidosis and sideroblastic anemia (MLASA) in humans. *Pus1* KO mice revealed decreased exercise capacity and COX activity around 14 weeks of age (Mangum et al., 2016). As DARS2 is an mt-aaRs, its skeletal muscle and heart-specific deletion (*Ckmm-Dars2*$^{-/-}$) led to a translational defect, which results in substantial COX deficiency (Dogan et al., 2014). DARS2-deficient mice exhibited severe hypertrophic cardiomyopathy and muscle atrophy with a drastically short lifespan of 6-7 weeks (Dogan et al., 2014). Although the disorganized myocardial structure and mitochondrial accumulation were observed in the hearts of DARS2 deficient mice, the authors could not find mitochondrial aggregations or fiber disruptions in the skeletal muscle; only occasional fused mitochondria were observed (Dogan et al., 2014).

1.7. Mitochondrial Stress Responses

Mitochondria govern cellular energy economy via communicating with the nuclear genome and participating in various cellular processes from apoptosis to calcium homeostasis (Nunnari & Suomalainen, 2012). Mito-nuclear communication upon mitochondrial stress and cellular rewiring to alleviate mitochondrial stressors are crucial for cellular homeostasis.

1.7.1. Mitochondrial Biogenesis

The economics of cellular energy regulation is a highly delicate and interactive process; when cellular energy demand increases or mitochondrial ATP production decreases, mitochondrial copy number is upregulated as a stress response (Valera-Alberni et al., 2018). Since ATP is the energy currency in living organisms, energetic status changes can be tracked by the change of ATP amount in cells by the sensor protein AMPK (AMP-activated protein kinase). When ATP:ADP ratio decreases, the myokinase reaction generates 1 ATP and 1 AMP from 2 ADP molecules. This reaction leads to the accumulation of AMP in the cell, and AMP binding allosterically activates AMPK (Ren et al., 2010).

AMPK activation can directly activate PGC-1α (Pparg coactivator 1 alpha) by phosphorylation or by upregulating NAD^+ levels, resulting in phosphorylation of Sirtuin 1 (SIRT1). Upon activation, SIRT1 can de-acetylate PGC-1α and stimulate mitochondrial biogenesis. PGC-1α can initiate various pathways and transcription factors to increase mitochondrial biogenesis, including NRF1/PAL- α, NRF2/GABP, and estrogen-related receptors (Palikaras & Tavernarakis, 2014; Pasyukova et al., 2019). NRF1 and NRF2 can regulate nuclear-encoded OXPHOS proteins and bind to the promoters of the proteins that regulate mtDNA transcription and replication, like *TFAM* (Pasyukova et al., 2019). TFAM can wrap, bend, and package the mtDNA and play a role in mtDNA replication and transcription. Also, a moderate TFAM increase is followed by increased mtDNA transcripts (Rebelo et al., 2011).

1.7.2. Autophagy

Autophagy is an adaptive response to various cellular stressors, such as starvation, cellular growth factor deficiency, hypoxia, or damaged mitochondria (Dikic & Elazar, 2018). Mitochondrial biogenesis and mitochondrial-specific autophagy have a delicate relationship; damaged mitochondria need to be cleared, and new mitochondria should be generated (Palikaras & Tavernarakis, 2014). ULK1 (Unc-51 like autophagy activating kinase) is an autophagy-impairing protein downstream of mitochondrial biogenesis

protein AMPK. AMPK or ULK1 loss ends in the abnormal aggregation of autophagy mediator protein Sequestosome 1 (P62) and mitophagy impairment (Egan et al., 2007; Palikaras et al., 2015). Ubiquitinated proteins are carried by P62 and moved to autophagosomes by P62 interacting with autophagosome bound Microtubule-associated proteins 1A/1B light chain 3B (LC3-II) (W. J. Liu et al., 2016). An increase in autophagy is expected to decrease P62 levels. Defects in the formation of LC3-II and autophagosome were observed in P62 loss (W. J. Liu et al., 2016).

ATG proteins regulate the maturation of autophagosomes. Mammalian ATG proteins have three isoforms (LC3A, LC3B, LC3C), and these proteins are subjected to posttranslational modifications by the attachment of phosphatidylethanolamine (PE) residue. PE conversion of LC3-I to LC3-II enables them to bind selectively to autophagic membranes. PE conjugation increases in cellular stress conditions. It is thought that LC3-II has roles in the induction of autophagy and determining phagophore size (Hwang et al., 2022; Parzych & Klionsky, 2014).

1.7.3. Antioxidant Stress Response

Oxidative stress is caused by the unbalanced relationship between Reactive Oxygen Species (ROS) and ROS detoxifying enzymes. OXPHOS processes produce ROS as a by-product an mitochondria are the leading producers of most cellular ROS (Murphy P.M., 2009). During OXPHOS processes, most O_2 is converted to H_2O, yet a minute amount of O_2 is converted to superoxide. Mitochondrial detoxifying enzyme SOD2 converts superoxide to less toxic hydrogen peroxide (Kasai et al., 2020). ROS accumulation might cause mitochondrial dysfunction, membrane potential change, and reduced mitochondrial biogenesis (Bhatti et al., 2017).

The antioxidant response is mediated by NFE2L2/NRF2 protein. In basal conditions, it binds to KEAP1 protein, and KEAP1 recruits E3 Ubiquitin ligase to degrade constantly NFE2L2 by the Ubiquitin-Proteosome system. Oxidative stress leads to dissociation of the NFE2L2, which accumulates in the nucleus and binds to antioxidant response elements (ARE) of promoters to initiate antioxidant stress response (Hellyer

et al., 2021). *SOD1, SOD2, CATALASE,* and *NFE2L1* constitute some targets of NFE2L2. (Frias et al., 2020; Merry et al., 2016).

1.7.4. Mitochondrial Integrated Stress Response

While established proteotoxic stress response in *C. elegans* is UPR^{mt}, its mammalian stress response counterpart is named Mitochondrial Integrated Stress Response ISR^{mt} and is comprised of various metabolic pathways, including UPR^{mt} response (Suomalainen & Battersby, 2018). UPR^{mt} is coordinated by transcription factor ATFS1 that continuously targets mitochondria; when mitochondrial protein import decreases, it localizes in the nucleus and activates amino acid response elements (AAREs) of the target chaperones, proteases, ROS detoxifying enzymes in *C. elegans* (Melber & Haynes, 2018; Suomalainen & Battersby, 2018). Although mammalian ATF proteins and worm ATFS1 activate the mitochondrial stress response by binding to the AARE regions, their downstream pathways of postmitotic tissues differ from the targets of cultured cells and *C. elegans* (Suomalainen & Battersby, 2018). From worm to the patient, heat shock proteins (HSPs) and protease CLPP is conserved in UPR^{mt}; interestingly, these inductions are associated with the mitochondrial biogenesis program, too (Suomalainen & Battersby, 2018).

ISR^{mt} is the collection of various molecular pathways and proteins induced by mitochondrial stress and the convergence point of these multifaceted pathways is the activation of ISR by eIF2α phosphorylation, which four kinases can mediate that was activated upon amino acid deprivation (GCN2), Heme deficiency (HRI), endoplasmic reticulum stress (PERK), Viral Infection (PKR) (Pakos - Zebrucka et al., 2016). OXPHOS dysfunctions phosphorylate eIF2α via two axes. The first axis involves declining cellular asparagine and aspartate levels through OXPHOS dysfunction and activation of GCN2 because of amino acid deprivation (S. Liu et al., 2021). On the second axis, OXPHOS deficiency causes OMA1-DELE1-HRI activation (S. Liu et al., 2021).

ISR activation causes two significant events: global protein synthesis attenuation, and the translation of a group of genes with upstream open reading frames, includ-

ing transcription factors *ATF4, ATF5,* and *CHOP* (Eckl et al., 2021). Transcription factor ATF4 and its dimerization partner CHOP bind to their target genes' open reading frames (ORF) to boost mitochondrial one-carbon metabolism, serine biosynthesis, transsulfuration, proline biosynthesis, and mitokines for systemic changes in a stage-wise manner (S. Liu et al., 2021).

Cell-autonomous responses are prominent in the early stages of ISR^{mt}, primarily in the mitochondrial folate cycle, which is an essential part of one-carbon metabolism and crucial for formyl methionine production (Suomalainen & Battersby, 2018). Methylenetetrahydrofolate dehydrogenase 2 (*MTHFD2*) is a regulator of the folate cycle and contains AARE in its promoter. MTHFD2 enyzme is not observed in healthy postnatal tissues; its expression is increased in mitochondrial dysfunction (Suomalainen & Battersby, 2018). The cell-autonomous response also supplies the cell with nucleotides, glutathione for an antioxidant response, and phospholipids; this variety of these diverse metabolic responses might be initiated by the upstream mechanistic target of rapamycin complex I (mTORC1) pathway through induction of MTHFD2 (Suomalainen & Battersby, 2018). Importantly, serine is a crucial donor of one carbon cycle, and an ATF4-dependent increasing in serine biosynthesis boosts one-carbon metabolites, and both serine biosynthesis and one carbon cycle produce NADH, whose accumulation is undesirable (S. Liu et al., 2021).

Mitochondrial deficiencies may also cause depletion in proline and asparagine, both of their production are glutamate-dependent (Bilen et al., 2022). Like MTHFD2, the PYCR1 enzyme, which catalyzes the final step of proline synthesis from glutamate, also has lower expression in most healthy tissues and increased in diseases. Interestingly, PYCR1 is a target of Myc, which can activate the PERK-eIF2α axis of ISR and may also contribute to regulating the cell's redox status (Licari et al., 2021; Nilsson et al., 2014).

ISR^{mt} may also act in a paracrine or endocrine manner, and elicit a systemic stress response in mitochondrial dysfunction can cause the secretion of two characterized mitokines, Fibroblast growth factor 21 (FGF21) and growth differentiation factor 15

(GDF15), to blood vessels (Klaus & Ost, 2020). FGF21 and GDF15 are secreted from skeletal muscle in mitochondrial dysfunctions and contribute to early-stage ISR^{mt}; additionally, they are elevated during organismal aging (Klaus & Ost, 2020).

FGF21 is persistently secreted from the heart and skeletal muscles of mitochondrial myopathy patients and mice. (Forsström et al., 2019). FGF21 can be activated on fasting and prompts lipolysis and ketogenesis; also, its activation depends on ATF4. Although liver and adipose tissues constitute the primary targets of FGF21, other tissues are also targeted depending on the context (Bar-Ziv et al., 2020). It is known that FGF21 enhances energy expenditure via white adipose tissue browning and increases insulin sensitivity and glucose tolerance, enabling mice to have resistance against a high-fat diet, making them leaner (Bar-Ziv et al., 2020).

Like FGF21, GDF15 is secreted by skeletal muscle during mitochondrial stress, shown experimentally in Ucp1 transgenic mice that have a reduction in the OXPHOS function by respiratory uncoupling (Ost et al., 2020). Interestingly, GDF15 ablation in Ucp1 mice did not influence cell autonomous ISR^{mt}, and muscle atrophy; on the other hand, it abrogated the browning of white adipose tissue, systemic metabolic flexibility upon the stress, and insulin sensitivity, and caused fat accumulation (Ost et al., 2020).

2. PURPOSE OF THE STUDY

Mitochondrial diseases often present a complex phenotype with multiorgan presentations, especially in high energy-demanding tissues, and these complexities make the assessment and treatment difficult. That is why a "cure" for mitochondrial diseases has not been developed yet. Investigation of mitochondrial dysfunctions under more definite conditions is required to comprehend them better for future medical interventions. In this study, our primary purpose was to generate a mitochondrial myopathy mouse model in a tissue-specific manner by causing mitochondrial translation defects upon *Dars2* deletion. Our secondary goal was to analyze whether these novel mutant mice display mitochondrial myopathy hallmarks at both phenotypical and molecular levels. Our final purpose for this thesis work was to investigate whether the new myopathy model induced any stress responses against mitochondrial dysfunction.

3. MATERIALS

3.1. Disposables

Disposables are given in table Table 3.1.

Table 3.1. Disposables.

Equipment	Company
15 ml Falcon Tubes	Sarstedt
50 ml Falcon Tubes	Sarstedt
96-Well Plates	Topscien
Accu-Check Glucometer Strips	Roche
Cryotubes	Sarstedt
Micropipette Tips	Axygen
Micropipette Tips	BioPointe
Nitrocellulos Membrane	Amersham
Parafilm	VWR
PCR Tubes	Axygen
Serological Pipets	Sarsted
Serological Pipette Tips	CAPP
Tubes (1.5ml 2ml)	CAPP
Weighing Container	Isolab
Whatmann Extra Thick Filter Papers	Thermo Fisher

3.2. Lab Equipment

Lab equipments are given in table Table 3.2.

Table 3.2. Lab Equipment.

Equipment	Company
+4° & -20° Fridge	Arçelik
+4° Room	Birikim Elektrik
-80° Deep Freezer	Thermo
Accu-Check Glucometer	Roche
Activity Cage	Ugo Basile
Agarose-Electrophoresis System	Anayltik Jena
Autoclave	Astell
Benchtop Centrifuge	Hitachi
Biometra TSC ThermoShaker	Analytik Jena
G-Box Chemi	Syngene
Gel-Doc	Biorad
Glass Bottles	Isolab
Grip Stength Meter	Ugo Basile
Heat Block	Techne
Ice Flaker	Brema
Magnetic Stirrer	Chiltern
Micropipetts	Axygen
Microplate Reader	VersaMax
Micro-wave	Arçelik
Minifuge	LMS
PCR Machine	Biorad
pHmeter	Hanna Instruments
Pipettor Autorep	Rainin
Pipettor MotoPet	Aygen

Table 3.2. Lab Equipment. (cont.)

Power Supply	Biorad
Rotating Rod	Ugo Basile
QPCR Machine	Bioneer Exicycler
Serological Pipettes	CAPP
Shaker	Onilab
Spectrophotometer	Nanodrop
Treadmill	Ugo Basile
Vortex	IKA
Water Distillator	UTES

3.3. Softwares

Softwares are given in table Table 3.3.

Table 3.3. Softwares used in experiments.

ImageJ
GraphPad
Microsoft Excel
Microsoft PowerPoint
Microsoft Word
Biorender
GeneSys

3.4. Chemicals

Chemicals are listed in table Table 3.4.

Table 3.4. Chemicals.

Chemical	Company
2-Propanol 2.5 lt	Merck
Acetic Acid (Glacial) 100% Anhydrous	Isolab
Acetyl coenzyme A Lithium Salt	Sigma
Acrylamide-Bisacrylamide 40%	Neofroxx
Agarose	GeneOn
Chemical	Company
Ammonium Acetate	Merck
Ammonium Persulfate	Bioffroxx
Asetik Asit	Saf Kimya Ş.
Boric Acid	Merck
Bromophenol Blue	Sigma
BSA	Neofroxx
Chloroform	Merck
Citric acid	BDH
Coomassie Brilliant Blue R250	Neofroxx
COmplete™, Mini, Protease Inhibitor Cocktail	Sigma (Roche)
di-Sodium Hydrogen Phosphate	Merck
dNTP Solution Set	NEB
EDTA	Bioffroxx
Ethanol Absolute For Analysis 2.5Lt	Merck
Ethanol Absolute≥ 99.9%	Isolab
Ethidium Bromide	Neofroxx
Glycine	Neofroxx
HEPES Buffer	Bioffroxx

Table 3.4. Chemicals. (cont.)

Hydrogen Peroxide	Merck
Isoamyl Alcohol	Sigma
K2HPO4	Merck
Methanol $\geq$ 99.8%	Isolab
MgCl2 Solution	Sigma
Milk Powder	Havancızade
NuPAGE LDS Sample Buffer (4X)	Invitrogen
NuPAGE™ Sample Reducing Agent (10X)	Invitrogen
PageRuler Plus Protein Ladder, 10 to 250	Thermo Fisher
PageRuler™ Protein Ladder, 10 to 180 kDa	Thermo Fisher
Chemical	Company
Ponceau S - 500 ml	Ecotech
Potassium Acetate	Neofroxx
SDS	Bioffroxx
Sodium Acetate	Merck
Sodium Chloride	Merck
Sodium Fluoride	Labochem international
Sodium Hydroxide	Merck
Sodium Orthovanadate	Sigma
Sodium Phosphate dibasic dihydrate	Sigma
TBE 10X, 500 ml	Ecotech
TEMED	Neofroxx
Tris Buffer	Bioffroxx
Triton X-100	Bioffroxx
TWEEN20	Neofroxx

3.5. Solutions

Solutions are listed in table Table 3.5.

Table 3.5. Solutions.

Solutions	Content)
DNA Extraction Buffer for Genotyping	100mM NaCl 10 mM Tris.Cl (pH: 8) 25 mM EDTA (pH: 8) 0.5% SDS 0.1 mg/ml proteinase K
Organ Lysis Buffer	50 mM HEPES 1% TRITON-X 0.1 M NaF 10 mM Na-Orthovanadate 10 mM EDTA 0.1% 20X SDS 100 mM NaCl
10X PBS	100mM NaHPO42H_2O 1.8mM KH2PO4 1.37M NaCl 26mM KCl
1X PBS-T	100 ml 10X PBS 900ml ddH_2O 0.1% Tween-20
10X Running Buffer	250 mM Tris 1.92M Glycine 34.7mM SDS
10X Transfer Buffer	250 mM Tris 1.92M Glycine

Table 3.5. Solutions. (cont.)

Solutions	Content)
1X Transfer Buffer	100μL 10X Transfer Buffer 200μL Absolute Methanol 700μL ddH_2O
10% Resolving Gel	3.94 mL ddH_2O 2 mL Tris (pH:8.8 & 1.5M) 1.98 mL 40% Acrylamide 80 μL 10% SDS 8 μL TEMED 80 μL 10% APS
5% Stacking Gel	2.45 mL ddH_2O 1 mL Tris (pH:6.8 & 1M) 487.5 μL 40% Acrylamide 40 μL 10% SDS 4 μL TEMED 20 μL 10% APS
TBE Buffer	0.02 M EDTA 1 M Tris Base 1 M Boric Acid

3.6. Kits and Enzymes

Kits and enzymes are listed in table Table 3.6.

Table 3.6. Kits and enzymes.

Name	Company
WesternBright ECL - HRP Substrate	Advansta
WesternBright Sirius Chemiluminescent Detection Kit	Advansta
Directzol RNA MiniPrepPlus	Zymo Reserach
Proteinase K	Biofroxx
Dc Protein Assay Kit	Biorad
GoTaq G2 DNA Polymerase	Promega
iScript cDNA Synthesis Kit	Biorad
DNase1	Roche
RealQ Plus 2x Master Mix Green	Ampliqon

3.7. Antibody List

Antibodies are listed in table Table 3.7.

Table 3.7. Antibody List.

Name	Company	Catalogue Number
Grp75/MOT	Abcam	ab53098
Hsp60	Abcam	ab46798
TFAM	Abcam	ab131607
HSC70 (B-6)	Santa Cruz	D0318
Tom20 (F-10)	Santa Cruz	A2919
PGC-1α (D-5)	Santa Cruz	sc-518025
Total OXPHOS Blue Native WB Cocktail	Abcam	ab110412

Table 3.7. Antibody List. (cont.)

Name	Company	Catalogue Number
VDAC1/Porin	Proteintech	55259-1-AP
DARS2	Proteintech	13807-1-AP
PYCR1	Proteintech	13108-1-AP
SQSTM1	Abnova	H00008878-M01
LC3B	Cell Signaling	2775S
eIF2-α	Cell Signaling	9722
Phospho-eIF2-α	Cell Signaling	3398
S6 Ribosomal Protein (5G10)	Cell Signaling	2217
Phospho-S6 Ribosomal Protein (Ser235/236)	Cell Signaling	4858
Phospho-AMPKa (Thr172)	Cell Signaling	2531S
AMPKa	Cell Signaling	2532S
SOD2 (D3X8F) XP®	Cell Signaling	13141S
Ubiquitin (P4D1)	Cell Signaling	3936S
NRF2 (D1Z9C) XP®	Cell Signaling	12721S
ATF-4 (D4B8)	Cell Signaling	11815S
Mouse Secondary	Cell Signaling	7076S
Rabbit Secondary	Cell Signaling	7074S

3.8. QPCR Primers

Primers used in QPCR reactions are listed in table Table 3.8 and Table 3.9.

Table 3.8. Forward primers.

Gene Name	Sequence
Sod1	CAAGCGGTGAACCAGTTGTG
Catalase	TGGCACACTTTGACAGAGAGC
Sod2	GCCTGCACTGAAGTTCAATG
Gpx1	CCACCGTGTATGCCTTCTCC
Nfe2l2	TCCATTCCCGAATTACAGTGTCT
Atf4	GCAAGGAGGATGCCTTTTC
Atf5	CCTTGCCCTTGCCCACCTTTGAC
Chop	CTGGAAGCCTGGTATGAGGAT
CoxI	TGCTAGCCGCAGGCATTACT
Hprt	TCCTCCTCAGACCGCTTTT
RnaseP	GCCTACACTGGAGTCCGTGCTACT
Fgf21	AGATCAGGGAGGATGGAACA
Gdf15	CAACCAGAGCCGAGAGGAC
Mthfd2	CATGGGGCATATGGGAGATAAT

Table 3.9. Reverse Primers.

Gene Names	Sequence
Sod1	TGAGGTCCTGCACTGGTAC
Sod2	ATCTGTAAGCGACCTTGCTC
Catalase	CCTTTGCCTTGGAGTATCTGG
Gpx1	AGAGAGACGCGACATTCTCAAT
Nfe2l2	GCCCACTTCTTTTTCCAGCG
Atf4	GTTTCCAGGTCATCCATTCG

Table 3.9. Reverse Primers. (cont.)

Atf5	CCAGAGGAGGAGGCTGCTGT
Chop	CAGGGTCAAGAGTAGTGAAGGT
CoxI	CGGGATCAAAGAAAGTTGTGTTT
Hprt	CCTGGTTCATCATCGCTAAT
RnaseP	CTGACCACACACGAGCTGGTAGA
Fgf21	TCAAAGTGAGGCGATCCATA
Gdf15	TGCACGCGGTAGGCTTC
Mthfd2	CCGGGCCGTTCGTGAGC

4. METHODS

4.0.1. Animal Care

All animals were raised in Boğaziçi University, and experiments were conducted according to governmental ethical frames and ethical permit number 2020-02 granted by "Boğaziçi Üniversitesi Kurumsal Hayvan Deneyleri Yerel Etik Kurulu (BÜHADYEK)". Animals were raised under 12 hours light to 12 hours dark cycle, and between 20°C-24°C. They were fed with an ad-libitum diet and sacrificed with cervical dislocation.

4.0.2. Tissue Specific Dars2 Deletion

Dars2LoxP/LoxP mice were previously generated by Dogan et al, 2014. Those $Dars2^{LoxP/LoxP}$ mice were mated with $Dars2^{+/LoxP,+/Cre}$. The cre-driver was a human alpha actin-1 *(ACTA1)* promoter, that was strongly expressed in the striated muscle cells and some myocardial cells (Miniou et al., 1999).

4.1. Protein Related Experiment

4.1.1. Protein Isolation:

500 μL fresh organ lysis buffer was added to each Roche Tubes that contain magnetic beads. Tissues were taken from liquid nitrogen, minced with a scalpel, and added to the tubes. After being placed in Magna-Lyser, tissues were homogenized at 6500rpm for 2x 30 seconds. The lysates were centrifuged at the pre-cooled centrifuge for 45 minutes and +4°C. The supernatants were transferred into Eppendorf tubes. Protein lysates were stored in -80°C.

4.1.2. Protein Concentration Quantification

Protein concentration was quantified according to Biorad's DC Protein Assay. 1:10 and 1:20 lysate:ddH_2O dilution series were prepared. 5μl 1:10 and 1:20 diluted samples and BSA standards were loaded into wells of 96 well-plate as duplicates. A $'$ solution was freshly prepared in the Eppendorf tube by adding 20 μL S solution for every 1ml of A solution. 25μL A $'$ solution, then 200μL B solution was added to samples respectively. 96 well plate was covered with aluminum folio and shaken by a plate reader, and. 15 minutes later, a plate reader measured OD values at 750 nm. Then using OD values and BSA concentrations, protein concentration was calculated.

4.1.3. Western Blotting

The Western blot reaction mix was prepared with 25μg protein lysate, 4X Nu-Page Reaction Buffer, 10X Nupage reducing agent, and the remaining reaction volume was completed with ddH_2O. Samples were heated at 70°C for 10 minutes, then pulse centrifuged. In the first lane of polyacrylamide gel, a protein ladder was loaded, then samples were loaded in the other lanes, respectively. The voltage was set to 80V until the proteins passed the stacking gel, then the voltage was set to 120V. For wet transfer, Whatmann Filter papers, nitrocellulose membrane, and acrylamide gel was incubated with 1X fresh transfer buffer; after incubation wet transfer sandwich was set. Wet Transfer was performed at 100V and for 120 minutes. Transfer quality and total protein amount were controlled with Ponceau S. staining. After Ponceau S. staining which was removed by a PBST wash. 1 hour of blocking with 5 % Milk powder in PBST was followed by membrane washing with 5% PBST for 1x10 minutes and 2x5 minutes. Then, membranes were incubated overnight in primary antibody solution at +4°C. The next day PBST wash was done 2x10 minutes, 1x 5 minutes. Secondary antibody was incubated at room temperature for 1 hour, followed by a PBST wash for 3x10 minutes. Imaging was performed with the Syngene machine. Usually, 1:1 ECL: Peroxide solution was used for protein signals; however, 1:1 Sirius-red: Peroxide solution was added to enhance the faint signal.

4.2. Genotyping of Mice

4.2.1. DNA Isolation from Ear Biopsy

Mouse-ear biopsies were placed in the Eppendorf tubes, then 500μL DNA Extraction Buffer and 5 μL Proteinase-K (20mg/ml) were added into the tubes. Samples were shaken on the Thermo Shaker at 55°C and 1000rpm overnight. The following day samples were pulse centrifuged, and 500μL isopropanol was loaded to each piece; then, samples were centrifuged at maximum speed (15000rpm) for 20 minutes at +4°C with a benchtop centrifuge. After centrifuging, the supernatant was discarded, 500ul cold EtOH was loaded into tubes, and samples were centrifuged at maximum speed for 15 minutes. The supernatant was discarded again. Tubes were placed into a heat block at 60°C for 10 minutes to remove EtOH remnants. 50μL ddH_2O was added to each tube, and tubes were placed onto Thermo Shaker at 37°C for 1 hour. Isolated DNAs were stored at +4°C.

4.2.2. PCR Reactions

After DNA Isolation, PCR reactions were run for *Dars2* and Cre. The reaction mix of *Dars2* and Cre were different from each other. Their specific PCR reaction mixtures were prepared according to the parameters in Table 4.1. After preparation of PCR mix, samples were shortly vortexed and spun-down. PCR reactions were performed with PCR machine according to conditions that were listed in Table 4.2 and Table 4.3.

Table 4.1. PCR reaction mix for *Dars2* and Cre.

1X Reaction	*Dars2*	Cre
DNA	1μL	1 μL
H_2O	11.1 μL	11.15 μL
GoTaq 5X Reaction Buffer	4 μL	4 μL
dNTP Mix(1.25mM)	1 μL	1 μL
Forward Primers (10μM)	0.8 μL	0.8 μL
Reverse Primers (10μM)	0.8 μL	0.8 μL
Flexi-GoTaq Enzyme (5U/10μL)	0.1 μL	0.05 μL
Mg^{+2}	1.2 μL	1.2 μL
Total Reaction Volume	20 μL	20 μL

Table 4.2. PCR conditions - *Dars2*.

Temperature (°C)	Time	Cycle
95	5 min	1
95	30 s	30
60	30 s	
72	45 s	
12	∞	

Table 4.3. PCR conditions - Cre.

Temperature (°C)	Time	Cycle
95	5 min	1
95	30 s	35
62	30 s	
72	30 s	
12	∞	1

4.2.3. Agarose Gel Electrophoresis

Agarose gel electrophoresis followed PCR reactions. %1 agarose was dissolved with 1X TBE in microwave and solidified in trays.3 μL DNA ladder and 10 μL samples were loaded into wells. Samples were run at 140V for 20 minutes. After running, gel was incubated in Ethidium Bromide solution and shaken slowly for 40 minutes. Imaging was done with Geldoc device. %1 agarose was solved with 1X TBE in a microwave and solidified in trays. 3 μL DNA ladder was loaded into the first well, and 10 μL samples were loaded in other wells, respectively, run at 140V for 20 minutes. After running, Ethidium Bromide incubation and imaging with GelDoc device were done.

4.3. Quantification at the Transcript Level

4.3.1. Total RNA Isolation from Mouse Muscle

Total RNA extraction was performed with respect to Direct-zol RNA Miniprep Plus Kit's protocol, and the procedure was performed on ice. 600 μL TRI reagent was added into Roche tubes with beads. Animal tissues were cut into pieces and added into Roche tubes. Magna-Lyser was used for tissue lysis at 6500rpm and 2x30 seconds. Lysates were centrifuged at +4°C for 5 minutes, and the supernatant was transferred into new Eppendorf tubes. Equal volume 100% EtOH was added into the supernatant. 600 μl of this mixture was loaded in Zymo-Spin IIICG Column. The column was centrifuged at 4°C for 30 seconds, and the flow through was discarded. If the mixture was more than 600 μl, the remaining mixture should have followed the same steps. 400 μL RNA wash buffer was loaded into the column, and the column was centrifuged at +4°C for 30 seconds. DNaseI powder was solved in 275 μL nuclease-free water. A mixture of 5 μL DNaseI solution and 75 μL DNA digestion buffer was prepared for each tissue sample. The DNA digestion mixture was added to the column and incubated for 15 minutes at room temperature. 400 μL of RNA prewash buffer was added to the column and centrifuged at +4°C for 30 seconds. This prewash step was repeated one more time. 700 μL RNA wash buffer was added and centrifuged at +4°C for 2 minutes,

and flow through was discarded. 50 μL nuclease-free water was added to the column matrix and centrifuged for 3 minutes. Concentrations were calculated by nano-drop, and samples were stored at -80°C.

4.3.2. cDNA Synthesis

cDNA was prepared according to Biorad's iScript cDNA Synthesis Kit. 1000ng RNA was used from each sample. The reaction was prepared and run with respect to the manufacturer's instructions, shown in Table 4.4 and Table 4.5.

Table 4.4. cDNA synthesis mix.

Component	Reaction Volume
5X iScript Reaction Mix	4 μL
iScript Reverse Transcriptase	1 μL
Nuclease Free Water	(15-X) μL
RNA Template	X μL
Total Reaction Volume	20 μL

Table 4.5. cDNA synthesis (Reaction protocol).

Step	Temperature(°C)	Time
Priming	25	5 min
Reverse Transcription (RT)	46	20 s
RT Inactivation	95	1 min
Optional Stage	4	∞

4.3.3. QPCR

Forward and Reverse primers were solved in Nuclease-free water with respect to the manufacturer's instructions. 10 ng DNA and 2.5 pmol Forward and Reverse Primers were used. The reaction mix was prepared according to the parameters in Table 4.6. In 96 well plates, this reaction mix was loaded for 5 WT samples, 5 knockout samples, and 1 Negative Template control for each gene. QPCR conditions and Melting Curve are listed Table 4.7 and Table 4.8 respectively.

Table 4.6. QPCR mix.

Ingredients	Amount (μL)
Forward Primers	0.25
Reverse Primers	0.25
Nuclease Free H_2O	2.5
DNA	2
Master Mix	5
Total	10

Table 4.7. QPCR conditions.

Temperature (°C)	Time	Cycle
95	15 min	1
95	15 s	40
60	30 s	
72	30 s	

Table 4.8. Melting curve.

Starting Temperature	60°C
End Temperature	95°C
Hold Time	00:01 s
Temperature Increment After Hold	0.2°C

4.4. High Yield DNA Isolation from Mouse Muscle with Chloroform Isolation

About 1/3rd of the gastrocnemius muscle of wild-type (WT) mice and 1/2 of or whole gastrocnemius of knockout (mKO) animals have been minced and placed in Eppendorf tubes. 0.4 ml lysis solution and 4 μl proteinase-K (10mg/mL) was added. Samples were incubated overnight at Thermo-shaker for 750rpm and 55 °C. The next day 150μl of 8M potassium acetate and 0.5mL chloroform were added to each tube. Samples were vortexed and incubated -80°C for 15 minutes, then centrifuged at max speed on the benchtop centrifuge. Two separate liquid phases were observed with an interface. The upper aqueous layer was decanted to new Eppendorf tubes without touching interfaces. 1mL absolute ethanol was added to the aqueous phase, and tubes were inverted several times. White precipitates may be visible at his stage. After inverting tubes, samples were centrifuged at the max speed on the benchtop centrifuge. Pellet was rinsed with 70% Ethanol, then centrifuged for 5 minutes at maximum speed. Ethanol was removed, pellets were air dried, and 100 μL nuclease-free H_2O was added to the samples. DNA concentrations were measured by nanodrop.

4.5. Blood Glucose Measurement

The lateral vein of mice was punctured with a needle of a syringe. The glucose strip was directly applied to a drop of blood, and glucose levels were recorded. This procedure was repeated from 3rd weeks of age to the terminal stage every week.

4.6. Phenotypic Experiments

4.6.1. Treadmill

Treadmill was used at 10° slope. The electric stimuli pulses 200msec/pulse, intensity 3Hz, and 1.22mA were set. Before starting an experiment, new mice were adapted to the exercise and the device for 2 days with a speed of 6.5m/min for 10 minutes. In 3^{rd} day, mice were placed on the treadmill; the initial speed was 6.5m/min and every 3 minutes device got faster by 0.5m/min. Mice are considered exhausted when day get an electric shock 10 times a minute.

4.6.2. Rotarod

Mice were adapted to the system for 2 days. They were placed on the rod for adaptation and stayed for 5 minutes without movement. Then the machine was started to rotate for 5 minutes at a constant speed of 10. On the 3^{rd} day, mice were placed on a rotarod with an accelerating pace for 2 to 50 in 5 minutes. Their falling time was recorded. This procedure was repeated 3 times at 20-minute intervals.

4.6.3. Grip Strength Test

Mice were placed on a grid. They were pulled from their tail; the grip strength meter measured their maximal resistance force (grip force) against the pulling force. This step was repeated 5 times at 1-minute intervals. The best 3 values were used in calculating their muscle strength in the gram-force units.

4.6.4. Activity Cage

A mouse was placed in an activity cage. The activity cage has two sets of infrared laser systems. The 1^{st} set is placed at the lower stage, and measures movement counts on the horizontal axis. The other lase set is placed onto the first laser set and counts when mice stand up on their back limbs. In the activity cage, each time, a single mouse

was let move freely for 30 minutes, and their movement counts were recorded.

4.6.5. Life-span Measurement

5 control and 5 knockout mice were monitored each week, their body weights were recorded, and their health conditions were examined. We noted their death age, and some terminally ill mice were sacrificed when they worsened above ethical limits, which state 15

4.6.6. Statistical Analysis

An unpaired t-test was used to analyze the significance between mKOs and WTs. Values lower than 0.05 were accepted as significant. Error bars indicate the Standard error of the mean (S.E.M). *$p \leq 0.05$, **$p \leq 0.01$, ***$p \leq 0.001$, ****$p \leq 0.0001$

5. RESULTS

5.1. Mitochondrial Myopathy Mouse Model Generation

To generate a novel mitochondrial translation-deficient myopathy mouse model, previous floxed *Dars2* (*Dars2*$^{\mathrm{LoxP/LoxP}}$) (Dogan et al., 2014) mice, whose second intron and the third exon was floxed, was mated with *Acta1-Cre* mice "Figure 5.1a". Since DARS2 is a mitochondrial protein, its deletion, specifically in skeletal muscle, was expected to give rise to mitochondrial myopathy phenotype by exhibiting exercise intolerance, reduced locomotor activity, and muscle atrophy. *ACTA1* (Human alpha actin 1, HSA) promoter was aimed to confer a skeletal muscle-specific expression of Cre recombinase to delete the *Dars2* gene. Research has shown that the *ACTA1* promoter is uniformly active in adult striated muscle fibers such as triceps, gastrocnemius, etc., and expression in some cardiomyocytes that have no connection with known cardiac structures was observed as well; on the other hand, no *ACTA1* activation was observed in other tissues like brain, kidney, liver, thymus, etc. (Miniou et al., 1999). In the embryonic stage, the *ACTA1* promoter was active since 9 d.p.c (days post coitum) at myotomal muscles, and some cardiomyocytes have no connection with known cardiac structures (Miniou et al., 1999). interestingly, at 9 d.p.c ectopic expressions in the trigeminal nerves were noted, but at 12 d.p.c, there was no signal in them (Miniou et al., 1999).

Offspring numbers obtained from the optimized matings between *Dars2*$^{\mathrm{LoxP/LoxP}}$ mice with *Dars2*$^{+/\mathrm{LoxP},\ +/\mathrm{Cre}}$, followed expected Mendelian proportions: Out of 200 pups, 58 pups were *Dars2* $^{+/\mathrm{LoxP},\ +/\mathrm{Cre}}$, 53 pups *Dars2* $^{\mathrm{LoxP/LoxP},\ +/\mathrm{Cre}}$ (from now on called mKO), 40 pups *Dars2*$^{\mathrm{LoxP/LoxP}}$ and 49 pups *Dars2*$^{+/\mathrm{LoxP}}$. We did not characterize the heterozygous mice (*Dars2* $^{+/\mathrm{LoxP},\ +/\mathrm{Cre}}$) in this study, as whole-body heterozygous *Dars2* mutant was shown to be haplo-sufficient (Dogan et al., 2014), and no visible signs of illness were observed in *Dars2* $^{+/\mathrm{LoxP},\ +/\mathrm{Cre}}$ mice up until the death of mKOs. Genotypes of mice were monitored by PCR and agarose gel electrophoresis "Figure 5.1b". To confirm *Dars2* deletion in mice, transcript levels were analyzed.

Dars2 mRNA was markedly decreased in the skeletal muscles of mKOs, but not in wild-type (WT) mice "Figure 5.1c".

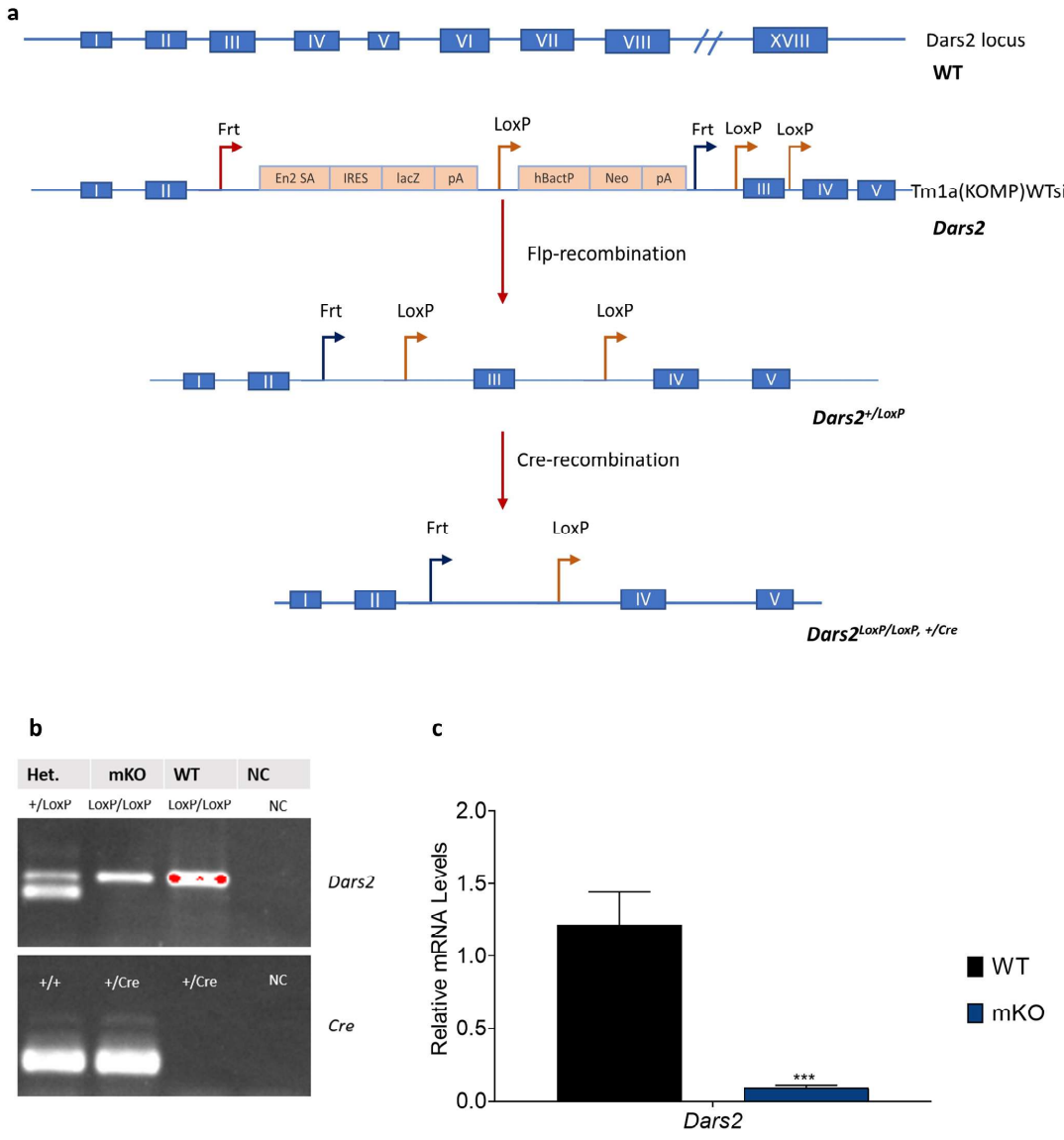

Figure 5.1. Mutant generation strategy and *Dars2* transcript levels. Bars represent Mean ± SEM, asterisks display significance level between mKOs and WT group, n=5, Student's t test, ***: $p \leq 0.001$.

Our mating strategy involved 3 steps, and our founder mice had been sent to us by Aleksandra Trifunovic as a kind gift. Genotypes of these founder mice were *Dars2*$^{\text{LoxP/LoxP}}$ and *Dars2*$^{+/\text{Cre}}$, and their mating gave us either *Dars2*$^{+/\text{LoxP, }+/\text{Cre}}$ or *Dars2*$^{+/\text{LoxP, }+/+}$, which were utilized in the second step of the mating strategy and 1/8$^{\text{th}}$ of offspring was expected to homozygous knockout in this stage. The best strategy in the third mating stage could be mating homozygous *Dars2*$^{\text{LoxP/LoxP, }+/\text{Cre}}$ mutants with *Dars2*$^{\text{LoxP/LoxP}}$ mice to obtain 1/2 homozygous mutants accordingly to Mendelian proportions; however, homozygous mutants had a severe phenotype and had a short lifespan. Therefore, we chose the next "best" strategy by mating *Dars2*$^{\text{LoxP/LoxP}}$ mice with *Dars2*$^{+/\text{LoxP, }+/\text{Cre}}$ in which offspring was expected to have a 1/4$^{\text{th}}$ ratio of homozygous mutant "Figure 5.2".

5.2. Phenotype of Mitochondrial Myopathy Mouse Model

Considerable health differences were observed in mKOs with respect to their WT counterparts. The fur of mKOs was not dense as their WT siblings, their body size was markedly smaller than WTs "Figure 5.3d", and they had reddish colorations in muscles. There were significant differences in the bodyweight of mKOs, which was almost half of their WT siblings, and this difference was apparent in both males "Figure 5.3a" and females "Figure 5.3b". Although mKO's body weight was lower at three weeks of age, this difference got pronounced when the mice got older. While WTs gained weight as the weeks progressed, weight gain stopped for mKOs around 4$^{\text{th}}$-5$^{\text{th}}$ weeks of age, and they slowly lost weight until their terminal stage. WT mice can live up to two to three years; however, the median lifespan of mKOs drastically decreased to 54 days (7-8 weeks) "Figure 5.3c". Throughout the studies in this thesis, mKOs were accepted to be in their terminal stage as of their seventh week of age, especially in molecular experiments performed in 7-week-old mice. The maximal lifespan of the mKOs was decreased to 75 days. As seen in myopathies, severe skeletal muscle atrophy was evident in mKOs; consistent with this observation, elevated transcript levels of atrophy markers *Atrogin* (muscle atrophy F-box gene) and *Murf1* (muscle RING-finger protein-1) were detected "Figure 5.3f".

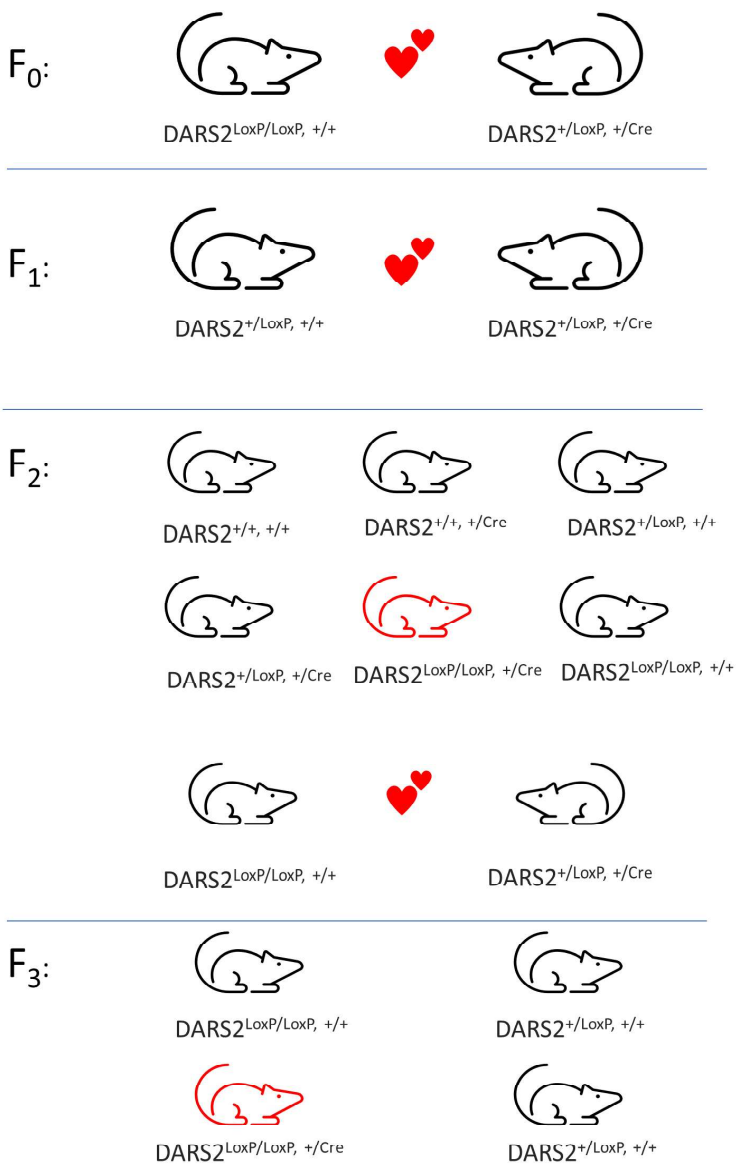

Figure 5.2. Mating strategy of mice. Red colored figure represents mKOs.

5.3. Phenotypic Characterization of Mitochondrial Myopathy Mouse Model

Various assays were utilized to further investigate DARS2 deficiency in skeletal muscle on a phenotypical level: muscle strength, performance, coordination, and locomotor activities were assessed by several behavioral tests.

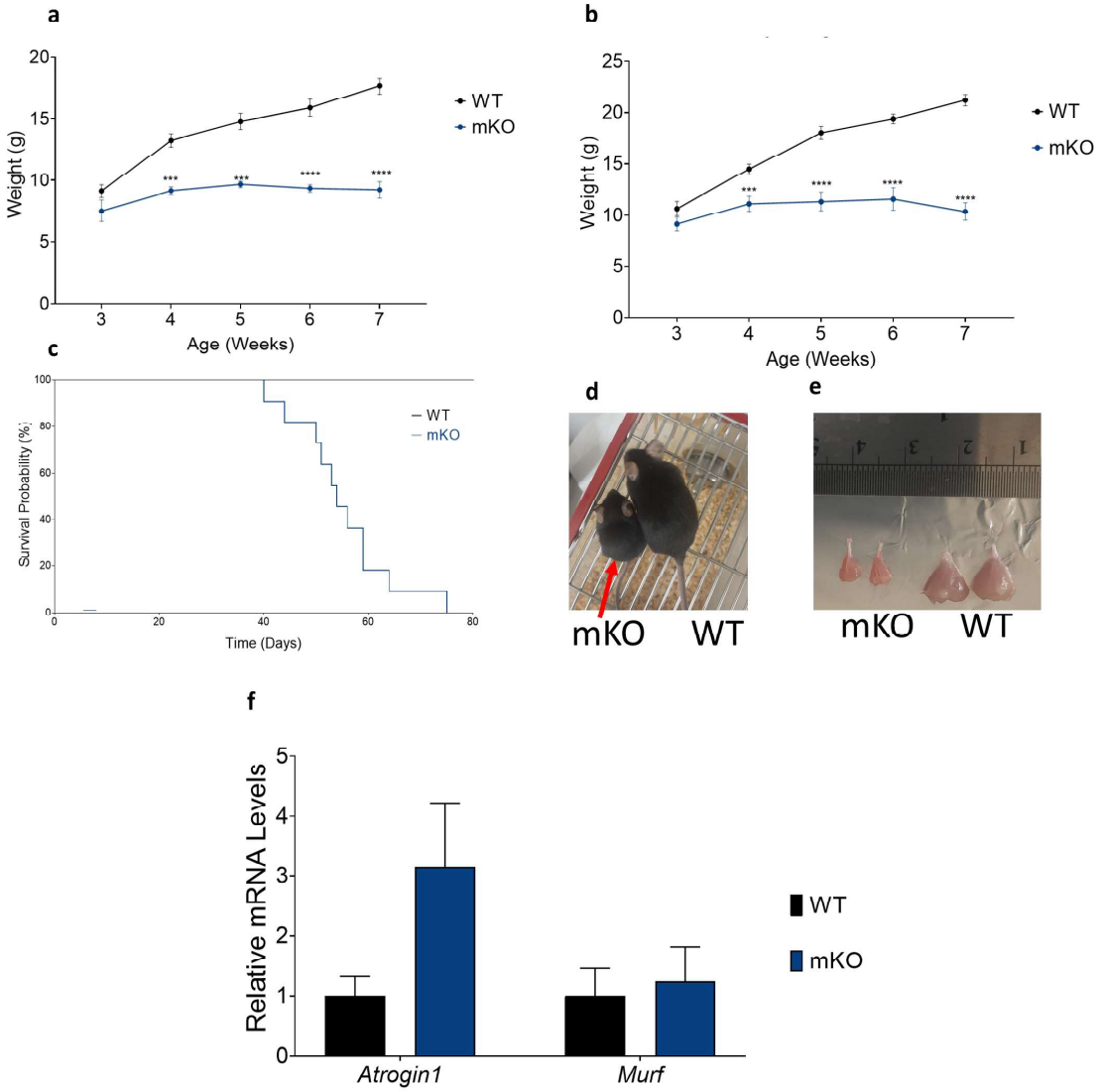

Figure 5.3. Physical characteristics of mKOs. Bars represent Mean ± SEM, asterisks display significance level between mKOs and WTs, n = 5-18 (Student's t test, ***: p $\leq$ 0.001, ****: p $\leq$ 0.0001).

5.3.1. Muscle Performance and Muscle Strength of Mitochondrial Myopathy Mouse Model

Muscle performances of mKO mice were expected to be different compared to WTs. The treadmill is a forced exercise and exhaustion test to assess exercise intolerance and maximal muscle performance capacity. The average running distance of WT

animals was above 1000 meters; on the other hand, the distance run by mKOs was remarkably lower than their controls “Figure 5.4a”. The running distance progressively declined each successive week compared to the previous ones. The running distance of 3-week-old mKOs was on average 134 meters, gradually decreasing to 60 meters in the 4^{th} week, then to 22, 6, and 5 meters in the following weeks. Around their terminal stage, mKOs could barely run on the treadmill. We concluded that the gradual decrease in muscle performance might be due to the progressive nature of myopathy in these mice.

Muscle strength was measured with Ugo Basile®'s grip strength meter. Mice were placed on a rectangular grid, and the device measured their maximum resistance against pulling. At the third week of age, mKOs had slightly lower grip strength than WT animals; yet the difference was minute “Figure 5.4b”. As they got older and more accustomed to the test, WT mice performed better at grip strength. Although there was a slight increase through the 4^{th} week of mKOs, this increase reached a plateau. Thus, the difference between mKOs and their littermates progressively increased and became prominent “Figure 5.4b”.

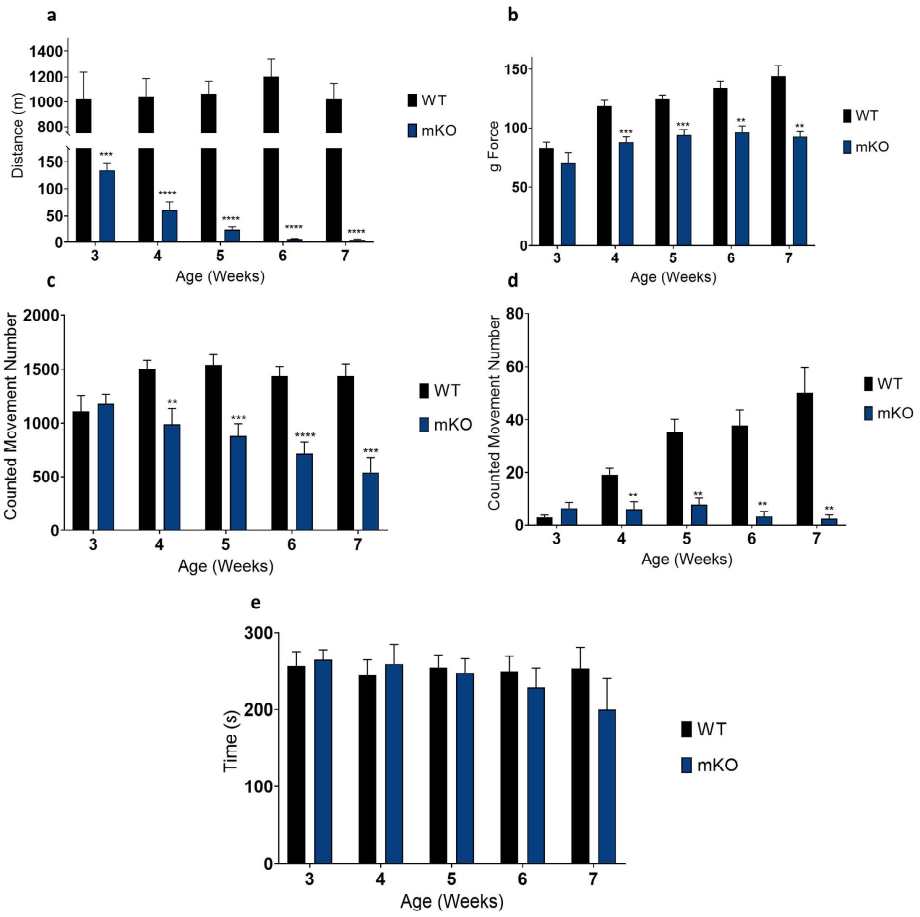

Figure 5.4. Muscle strength and muscle performance of mKOs differ from WT animals. Bars represent Mean ± SEM, asterisks display significance level between mKOs and WTs, n=4-25 (Student's t test, **: $p \leq 0.01$, ***: $p \leq 0.001$, ****: $p \leq 0.0001$).

5.3.2. Locomotor Activity and Motor Coordination of Mitochondrial Myopathy Mouse Model

After assessing muscle strength and performance, we wanted to monitor voluntary movement with an activity cage. These cages have previously been employed for behavioral, neurological, and toxicology tests (Schwarting et al., 2022)

Ugo Basile®'s activity cage has two sets of infrared lasers and sensors. The lower stage counts the horizontal movement of the mice, whereas the upper stage counts the times mice stand up on the vertical axis on their hind limbs. The experiment lasts for 30 minutes. In the third week, at both horizontal and vertical axes, mKOs displayed slightly lower performance than the WT mice, yet the difference was minute "Figure 5.4c and d". In the following weeks, this difference became more drastic. Although WT counterparts did not reveal a tendency towards a decrease, a progressive reduction in the movement on the horizontal axis was apparent in mKOs "Figure 5.4c". On the vertical axis, the number of standing up by hindlimb increased in WT mice in each successive week, probably caused by their body size increase and easily caught by sensors at the upper stage; contrarily, consistent reduction in mKOs was evident "Figure 5.4d". Activity cage results show that, on both axes, mKOs had lower locomotor activity than controls.

As a final behavioral test, rotarod was utilized to assess motor coordination. Animals were placed on a rotarod device for up to 300 seconds. WT animals managed to stay on the rotating rod for around 245 - 260 seconds throughout the observation period "Figure 5.4d". On the rotating rod, mKOs performed similarly to their WT counterparts in the third to fifth weeks. However, in the sixth and seven weeks, mKOs showed a slight decrease in rotarod performance and could stay on the rotating rod for 227 and 200 seconds, respectively "Figure 5.4d". Although the time the mKOs on rotarod decreased, this reduction was not statistically significant. It seems the motor coordination of mKOs was not affected severely.

5.4. Molecular Characterization of mKOs

5.4.1. mKOs were Hypoglycaemic

As phenotypical experiments suggested progressive mitochondrial myopathy, we wanted to strengthen these observations with molecular cues. Hypoglycemia occurs relatively frequently in individuals with mitochondrial disorders (Ashfaq et al., 2021). We monitored the post-prandial blood sugar of both mKO and WT mice between the

third week and the terminal stage (7^{th} week). In the third week, mKOs already had a lower blood glucose level (121mg/dL) compared to WTs (141 mg/dL), and again this difference got more drastic in the following weeks "Figure 5.5". Hypoglycemia also advanced progressively, especially at the terminal stage; it dropped to 70mg/dL, almost half of the WT mice "Figure 5.5".

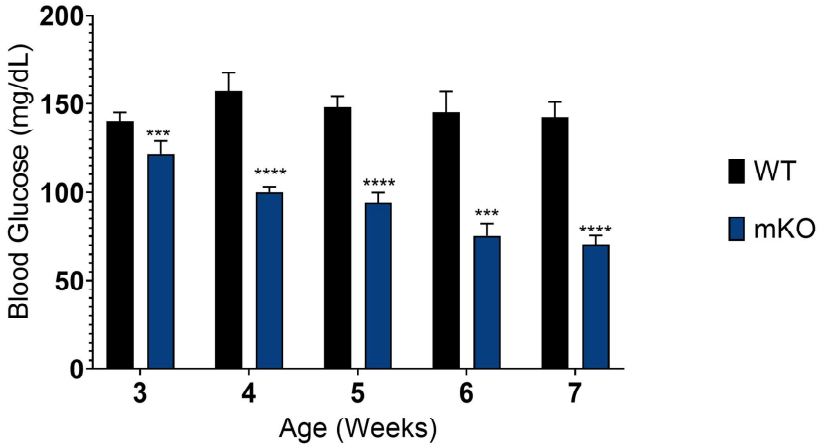

Figure 5.5. mKOs are hypoglycaemic Bars represent Mean ± SEM, asterisks display significance level n = 8-12 (Student's t test, ***: $p \leq 0.001$, ****: $p \leq 0.0001$).

5.4.2. OXPHOS were Downregulated in Mitochondral Myopathy Mouse Model

As explained, primary mitochondrial diseases and mitochondrial translation defects led to OXPHOS downregulation, and mKOs have mitochondrial translation defects in their skeletal muscles; their OXPHOS complexes may be affected adversely. Therefore, we analyzed OXPHOS complexes of terminal stage mKOs and their WT littermates. Substantial reduction in the levels of COX IV and UQCRC2 was detected and the decrease in NDUFA9 was moderate "Figure 5.6". Contrarily, protein levels were elevated in SDHA and ATP5A "Figure 5.6". Apart from mitochondrial complex V, there was a tendency toward downregulation of complexes in which mtDNA encoded proteins take parts. It is worth mentioning that mitochondrial complex II is entirely encoded by the nuclear genome and CV has two subunits (F0 and F1), and the F1

subunit is entirely encoded by the nuclear genome (Signes & Fernandez-Vizerra, 2018). An increase in their protein levels may indicate a possible mitochondrial biogenesis response in mKOs.

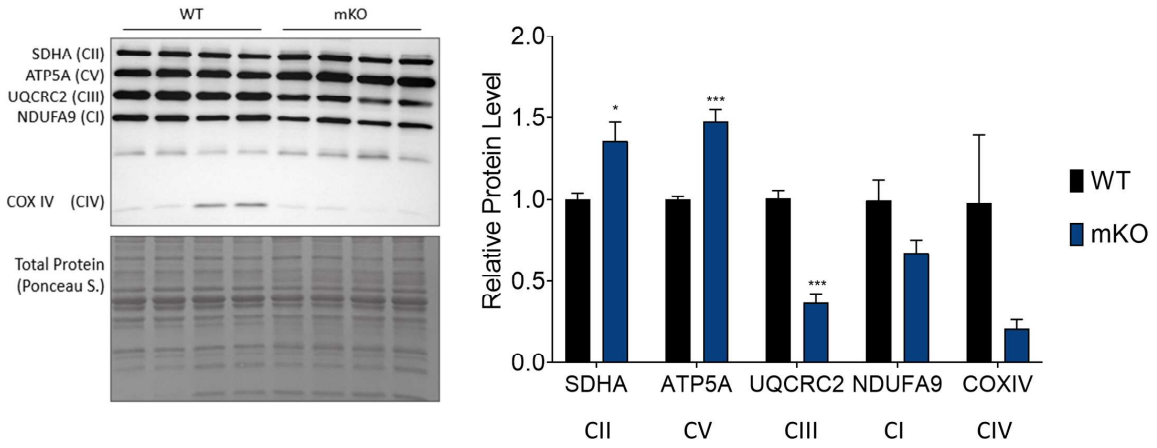

Figure 5.6. OXPHOS downregulation is evident in mKOs. Bars represent Mean ± SEM, asterisks display significance level n = 4 (Student's t test, ***: $p \leq 0.001$, ****: $p \leq 0.0001$).

5.4.3. Mitochondrial Biogenesis Increases in Mitochondral Myopathy Mouse Model

As mentioned above, mKOs displayed reddish muscle colorations, which may result from PGC-1α mediated mitochondrial accumulation and fiber type switch towards type 1; a mouse model with transgenic *Pgc-1α* showed fiber type switching and displayed reddish muscle (Lin et al., 2002). Moreover, a general decrease in OXPHOS complexes and an increase in CII and CV imply a possible biogenesis response. Mitochondrial biogenesis was measured at the protein level either directly by observing the levels of the master regulator of mitochondrial biogenesis, PGC-1α, and the activity of its regulator protein AMPK, or indirectly by assessing mitochondrial biogenesis-related proteins like TFAM, VDAC1, and TOM20.

Surprisingly, we did not observe an increase in PGC-1α levels of the mKOs; however, AMPK phosphorylation increased almost 1.5 times compared to WTs "Figure 5.7a and b". It is known that energy sensor and PGC-1α regulator AMPK can directly phosphorylate PGC-1α to increase its transcriptional activity (Cantó & Auwerx, 2009; Jäer et al., 2007). Consistent with AMPK phosphorylation increase, the levels of mitochondrial biogenesis-related proteins TFAM, VDAC1, and TOM20 were upregulated "Figure 5.7a". Since VDAC1 and TOM20 are in the mitochondrial membranes, an increase in mitochondrial surface or number may elevate their protein levels too; therfore, their increase may indicate a biogensis response.

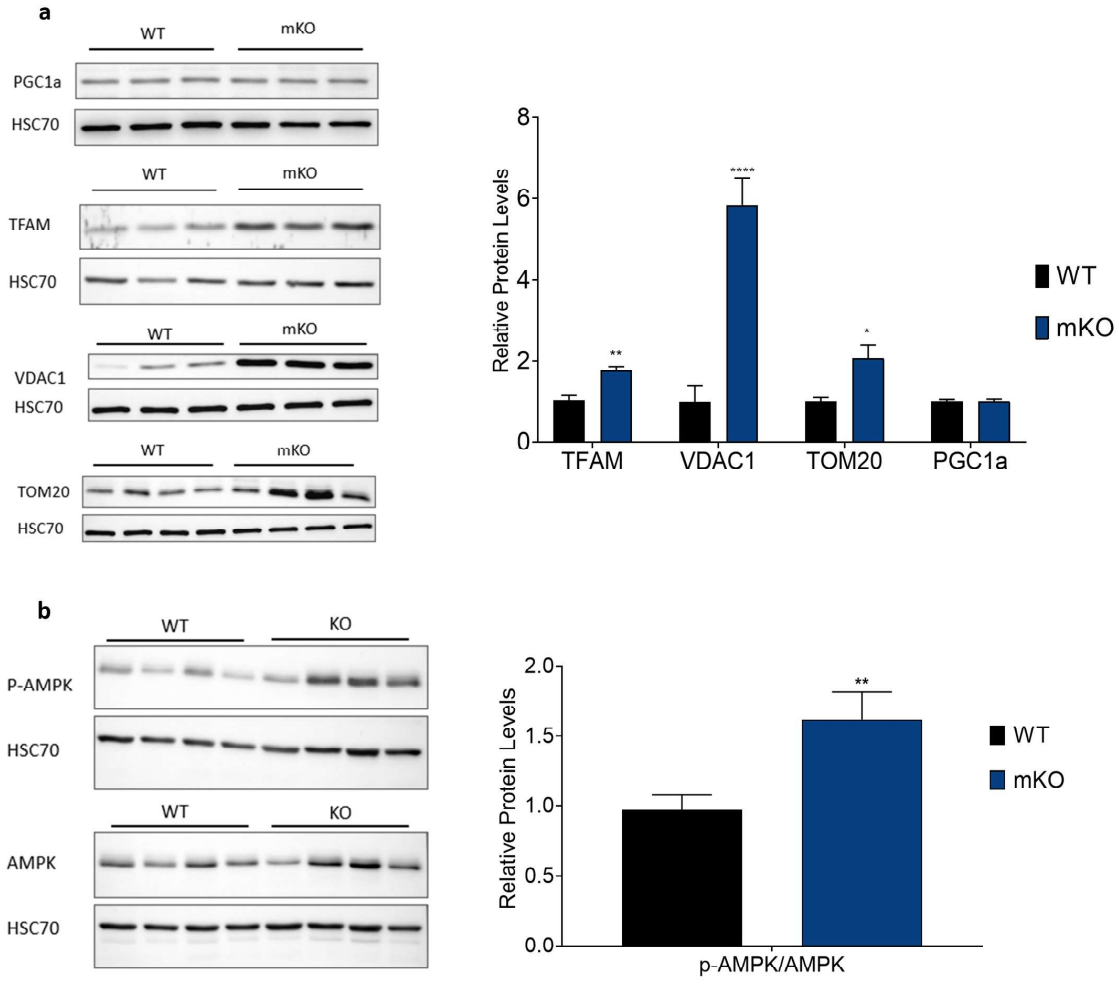

Figure 5.7. Mitochondrial biogenesis in mKO skeletal muscles. Bars represent Mean ± SEM, asterisks display significance level n = 3-4 (Student's t test, *: $p \leq 0.05$, **: $p \leq 0.01$, ***: $p \leq 0.001$).

As mentioned before, TFAM binds mtDNA and directly contributes to mitochondrial activities involving mitochondrial transcription and translation. We next wondered whether TFAM protein increase was also mirrored in mtDNA levels. Indeed, relative mtDNA levels measured by RT-qPCR were elevated up to 8-fold in mKOs compared to WT animals. These results demonstrate that mitochondrial translational deficiency leads to mitochondrial biogenesis in mKO mice "Figure 5.8".

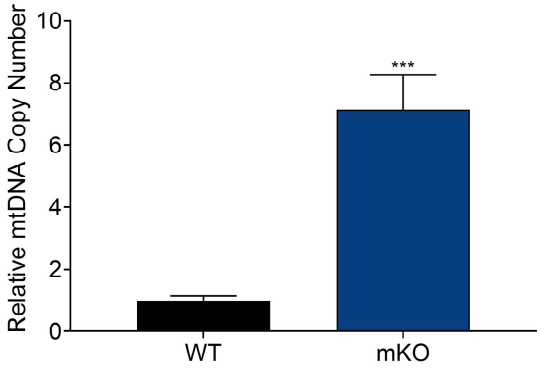

Figure 5.8. Mitochondrial biogenesis response increases mtDNA copy number. Bars represent Mean ± SEM, asterisks display significance level n = 5 (Student's t test, ns: not significant, ***: $p \leq 0.001$).

A subtle increase in mitochondrial chaperones in patients was noted, and those inductions were attributed to their functional connections with the mitochondrial biogenesis program (Suomalainen & Battersby, 2018). mtHSP70 and HSP60 are two mitochondrial chaperones, and they are critical for the correct folding of imported mitochondrial preproteins. The physical interaction of HSP60 and newly imported preproteins in the mitochondrial matrix was also proven(Voos & Röttgers, 2002). Thus, we wanted to measure the protein levels mtHSP70/GRP75 and HSP60 and observed an elevation in both chaperons in the terminal stage of mKOs "Figure 5.9". We concluded that these increase in mitochondrial chaperones may conribute the both mitochondrial biogenesis and ISR^{mt} mechanisms.

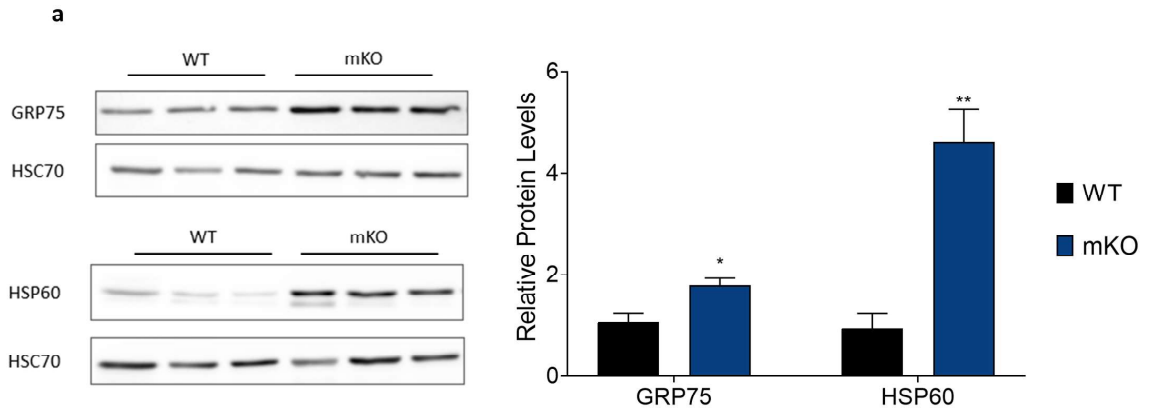

Figure 5.9. Mitochondrial chaperones in mKO skeletal muscle. Bars represent Mean ± SEM, asterisks display significance level n =3 (Student's t test, *: $p \leq 0.05$, **: $p \leq 0.01$).

5.4.4. Autophagy is impaired in Mitochondrial

In healthy organisms, mitochondrial homeostasis depends on balancing mitochondrial biogenesis and autophagy. We then wondered if autophagy was affected as a quality control mechanism. P62 and LC3B are two main markers used to measure autophagy. Since P62 carries ubiquitinated proteins into the autophagosomes, its rate is inversely proportional to the autophagy rate. P62 accumulation and LC3B-II increase were noted in the skeletal muscle of terminal stage mKOs by western blot "Figure 5.10a". This increase points out an impairment in autophagy. Since P62 binds ubiquitinated proteins via ubiquitin associating domain (UBA), it can also boost aggregation via multimerization domain PB1 and carries protein aggregates to autophagic membranes via LC3 associating LIR and PB1 domains (Su & Wang, 2012). In agreement with the P62 increase, ubiquitinated proteins were elevated in mKOs "Figure 5.10b". Thus, due to impaired autophagy, P62-mediated ubiquitinated protein aggregates increased but could not be degraded in autophagosomes.

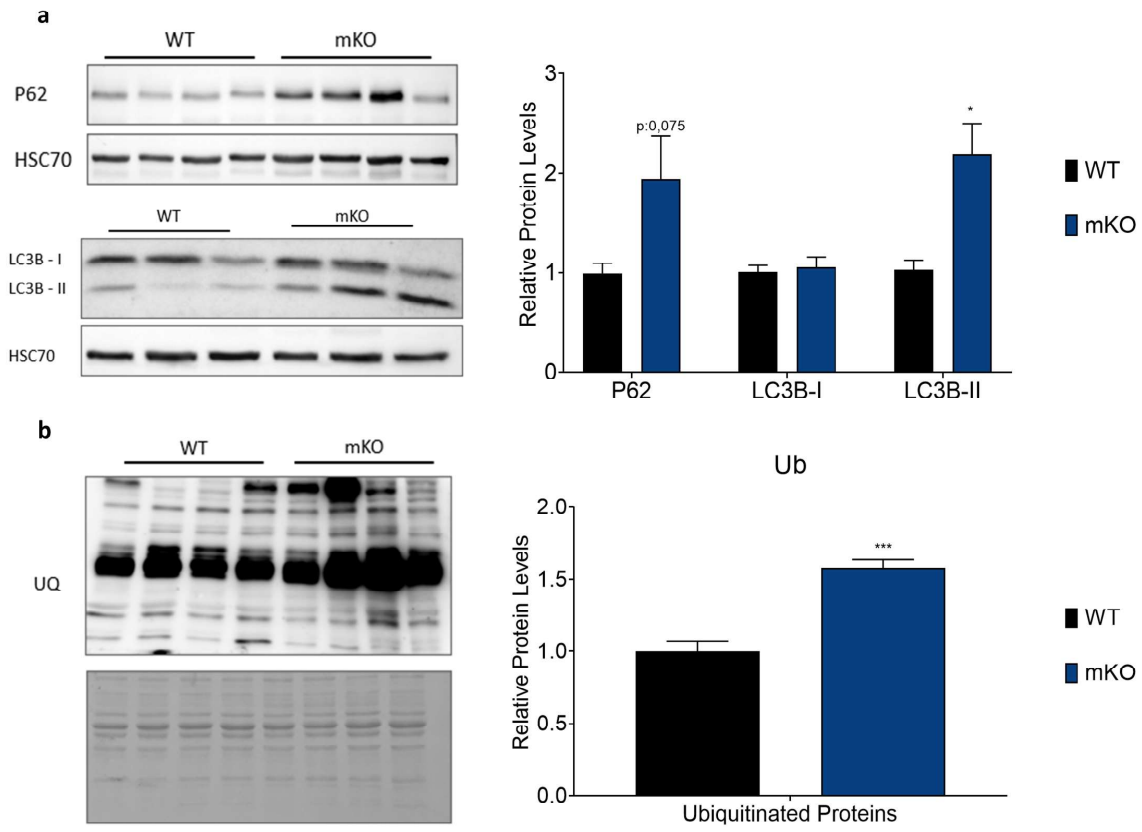

Figure 5.10. Autophagy was impaired in mKOs. Bars represent Mean ± SEM, asterisks display significance level n = 4 (Student's t test, *: $p \leq 0.05$, **: $p \leq 0.01$).

5.4.5. Antioxidant Response in mKOs

The *P62* gene has an AARE element in its promoter, activated by NFE2L2 accumulation in the nucleus; in turn, the P62 protein assists activation of NFE2L2 (Jain et al., 2010). Nitric oxide production by overactive heme oxygenase-1 triggers mitochondrial biogenesis through NFE2L2 binding to ARE elements of *NRF1/PAL-α* (Piantadosi et al., 2008). In the terminal stage mKOs, mitochondrial antioxidant enzyme SOD2 and antioxidant response mediator protein NFE2L2 levels were increased in their skeletal muscle "Figure 5.11a". However, transcript levels of *Sod2, Gpx1,* and *Nfe2l2* were decreased, and no significant change was observed in *Sod1,* and *Catalase* transcripts "Figure 5.11b". These differences between transcript and protein level imply the requirement of a thorough investigation of whether ROS-involved antioxidant

response is mediated or the protein increase attempts to contribute to the balance between mitochondrial biogenesis and autophagy.

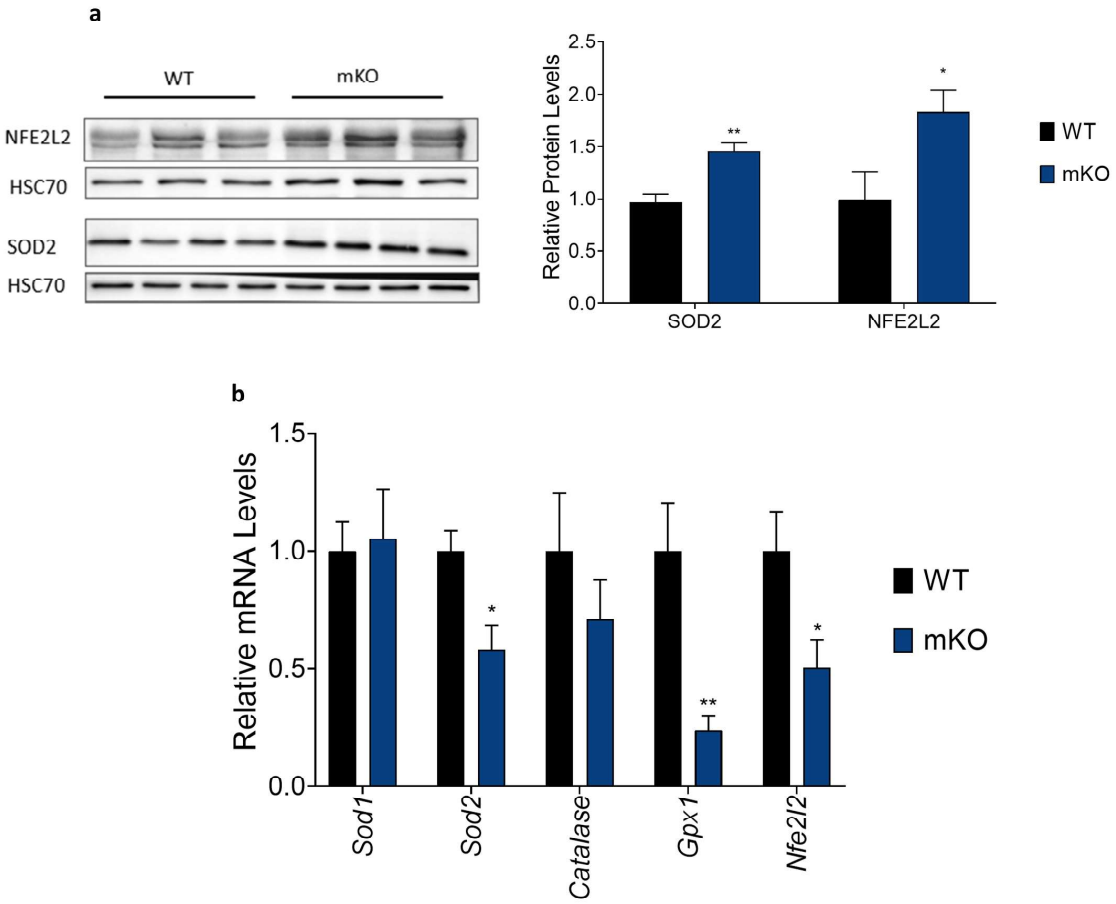

Figure 5.11. Antioxidant response in mKOs. Bars represent Mean ± SEM, Asterisks display significance level n = 3-5 (Student's t test, *: $p \leq 0.05$, **: $p \leq 0.01$).

5.5. Mitochondrial Integrated Stress Response in mKOs

Proteotoxic stress leads UPR^{mt} induction in *C. elegans*; however, in mammalians, UPR^{mt} is a part of a stress response that comprises the rewiring of various metabolic pathways upon mitochondrial insult, which is called mitochondrial integrated stress response ISR^{mt} (Suomalainen & Battersby, 2016). Various branches of this ISR^{mt} response pathways were investigated in our mitochondrial translation deficient mKOs.

Since eIF2α phosphorylation initiates ATF4-dependent activation of downstream targets, phosphorylation of eIF2α was assessed by Western blotting. Although total eIF2α levels were similar in both groups, significant elevation in p-eIF2-α was markedly high in mKOs demonstrating an active stress response "Figure 5.12a". Our following targets were *Atf4* and *ATF5* since they are located downstream of eIF2α phosphorylation. Surprisingly, there was no *Atf4* or *Atf5* increase in the transcript levels, a slight but non-significant decrease was observed "Figure 5.13c". Although amino acid starvation increases *Atf4* mRNA levels, other studies also showed that *Atf4* mRNA decrease in cells and pointed out ATF4 regulation at the transcriptional level (Dey et al. 2010). A modest but not-significant upregulation was noted in ATF4 protein levels "Figure 5.12b". This subtle increase may be caused by a lower available *Atf4* transcript level (Dey et al., 2010). We could observe a solid increase in protein level if mRNA levels were increased or not changed. Another reason could be obtained signal was very faint. A stronger immunoblot signal could give a more reliable signal. We also observed an increase in the transcript levels of *Chop*, the binding partner of ATF4 in ISR^{mt}.

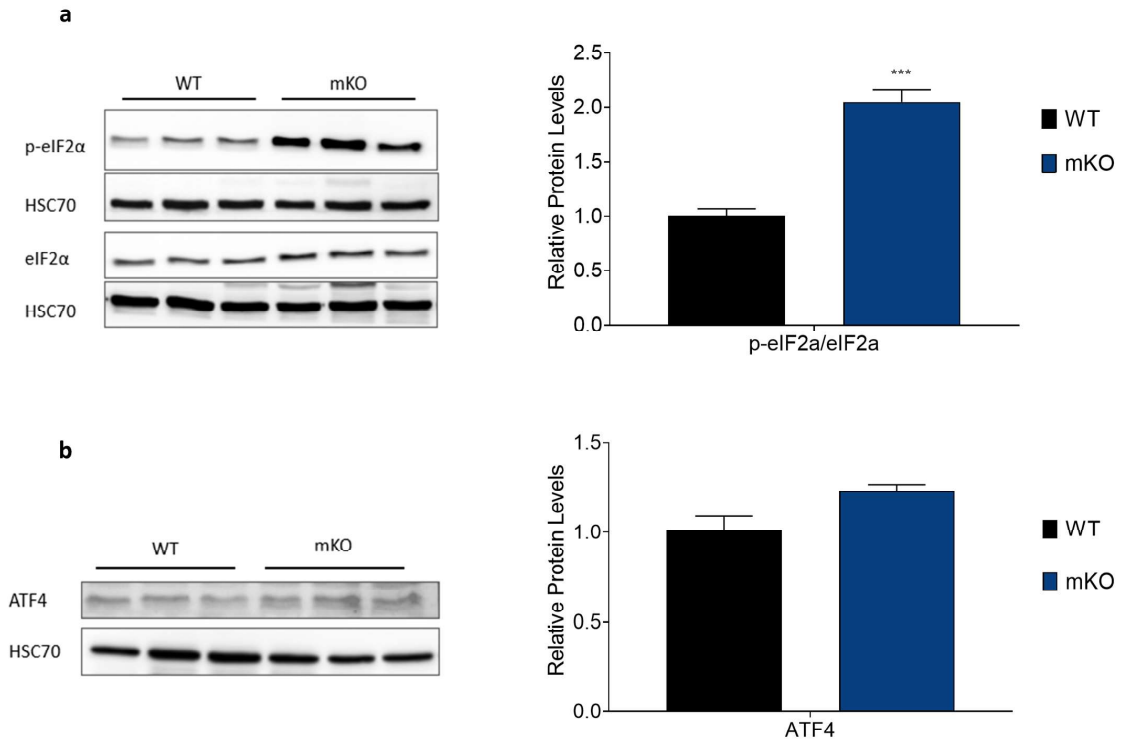

Figure 5.12. ISR^{mt} response in mKOs. Bars represent Mean ± SEM, asterisks display significance level n = 3 (Student's t test, ***: $p \leq 0.001$).

As mammalian post-mitotic tissues respond to mitochondrial stress via upregulation of various metabolic pathways in ATF4 dependent manner, downstream targets of ATF4 were also monitored. MTHFD2 is the rate-limiting enzyme of the folate cycle and one-carbon metabolism whose transcription was strongly upregulated in mKOs "Figure 5.13c". An increase in one-carbon metabolism may result in the rewiring of many cellular pathways as it yields biosynthetic pathway elements like purines and thymidine and influences amino acid metabolism by producing formylated methionine, serine, glycine, etc. (Ducker & Rabinowitz, 2017). Thus, these downstream pathways may also be rewired in mKOs via eIF2α – ATF4 axis. Proline biosynthesis is another metabolic pathway that is downstream of ATF4. This pathway was upregulated in both the protein (PYCR1) and transcript levels (*Aldh18a1*) "Figure 5.13a and c".

The mammalian target of rapamycin complex 1 (mTORC1) is upstream of stress

response pathways in mitochondrial defects with manifestations in muscle (Khan et al., 2017). Independently from eIF2α phosphorylation, mTORC1 activates ATF4 and leads to mitochondrial folate cycle activation (Ben-Sahra et al., 2016). Thus, we also wondered whether mTORC1 activation was visible in mKO and showed that ATF4-dependent activation of ribosomal protein S6 was also evident in mKOs as an indicator of mTORC1 activation "Figure 5.13b".

Early ISR^{mt} mediators FGF21 and GDF15 enforce systemic ISR^{mt} execution and are secreted upon skeletal muscle mitochondrial dysfunction. They participate in energy homeostasis in which FGF21 boosts energy expenditure and GDF15 decreases energy intake (Klaus & Ost, 2020). FGF21 and GDF15 increase may exert a threshold effect in which higher levels of increase may cause a worsening of phenotype; on the other hand, a mild increase in their levels can be an adaptive response (Klaus & Ost, 2020). In the skeletal muscles of our mKOs, *Fgf21* elevated up to 500 folds, and *Gdf15* to 25-folds "Figure 5.13d". These results indicate that mitochondrial translational stress on the skeletal muscles of mKOs activates ISR^{mt} in both a systemic and cell-autonomous manner.

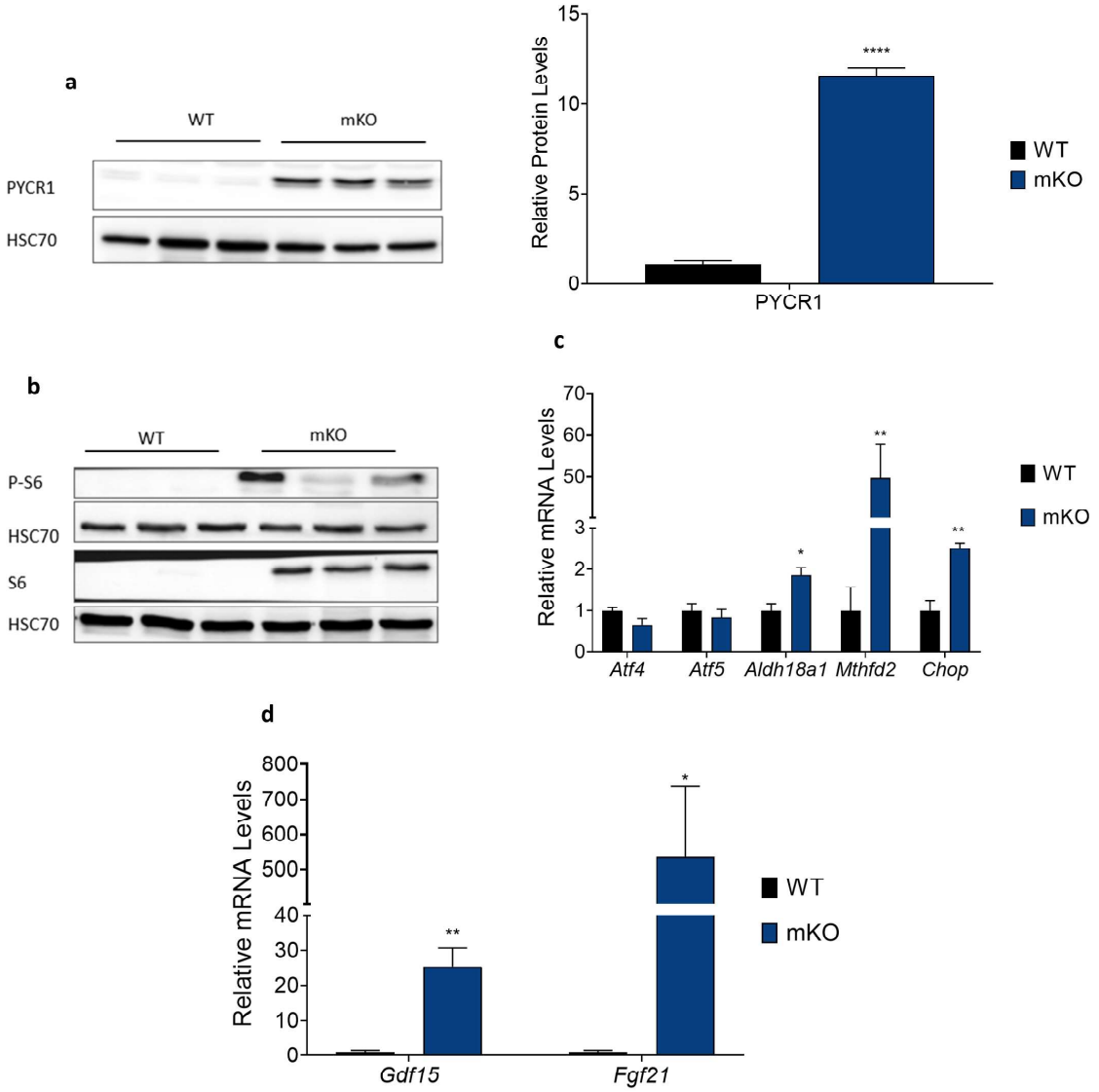

Figure 5.13. ATF4 targets and systemic ISR executers in mKO. Bars represent Mean ± SEM, asterisks display significance level n = 3-5 (Student's t test, *: $p \leq 0.05$, **: $p \leq 0.01$, ***: $p \leq 0.001$).

6. DISCUSSION

As mitochondria are responsible for the majority of cells' energy production, their fidelity is tightly monitored for cellular wellbeing. Ensuring mitochondrial homeostasis is even more significant in high energy-demanding tissues like skeletal muscles as mitochondrial dysfunction could result in disease (Eckl et al., 2021). At the molecular level, mitochondria are highly complex organelles considering their genome, rich proteome, mode of inheritance, communication with the rest of the cell, solid surveillance, and a stress response system should be established in cells to maintain mitochondrial homeostasis.

Mitochondrial inheritance adds unforeseen challenges to dissecting the mechanisms of mitochondrial diseases. Mitochondria do not abide by the Mendelian law of inheritance when mitochondrial diseases are considered. In a cell, the number of mitochondria is numerous as well as the number of mtDNA that are present in a mitochondrion (Zhang et al., 2015). In addition to mtDNA inheritance, the mitochondrial threshold effect also adds another layer of complexity. Defective mitochondria may clonally expand to cause increased mitochondrial heterogeneity towards disease phenotype; an exciting paper showed mitochondrial deletion defects may gain an advantage to deleted mtDNAs to propagate better than heathy mtDNAs because of constitutive UPR^{mt} activation by OXPHOS defect (Lin et al., 2016). The ratio between healthy and unhealthy mitochondria also matters in this respect. Last but not least, every tissue differs in their energy demands, and even the same type of mitochondrial dysfunction results in disease conditions in one tissue but not in the other (Vincent & Picard, 2018). Therefore, the dissection of tissue-specific manifestations of mitochondrial dysfunctions provides us with valuable knowledge.

We specifically generated and dissected the consequences of defective mitochondrial translation in skeletal muscles by generating a novel mitochondrial myopathy mouse model. For this, *Acta1-Cre* mice have mated with mice Floxed for the *Dars2* gene. Tissue specificity was conferred by Cre recombinase expressed under the human

α-alpha skeletal actin (*ACTA1*) promoter. Distal regulatory element at *ACTA1* gene enables strong muscle-specific expression, although, in the embryonic stage, it also has expression at striated muscle cells at the somite and some in the heart (Miniou et al., 1999). As DARS2 protein is a mitochondrial tRNA synthetase, its depletion leads to mitochondrial translation defects and results in an OXPHOS deficiency in a tissue-specific manner.

6.1. Variability of Lifespan and Severity of Disease Phenotypes in Mitochondrial Myopathy Models

6.1.1. Deletor Mouse and Skeletal Muscle Specific *Dars2* Mouse

The median lifespan of mKOs was about 54 days, corresponding to 7 to 8 weeks, which is an utterly short lifespan compared to the WT mice, which may live up to 2 to 3 years. This level of lifespan shortening, especially in tissue-specific deletion of the target gene, is striking. Although our mKOs had severe early-onset mitochondrial myopathy, there are significant variations among different mitochondrial myopathy mouse models. For instance, transgenic Deletor mice with mutated TWINKLE helicase present with late-onset mitochondrial myopathy and a normal life span, in which the first visible signs of mitochondrial myopathy appear in 1 year (Tyynismaa et al., 2005). Since TWINKLE is the mtDNA helicase responsible for the synthesis of the H strand of mtDNA, defective TWINKLE causes mtDNA mutations that accumulate over time leading to myopathy. mtDNA depletions caused by *Twinkle* mutations led to compromised ETC function as expected, but interestingly these changes were not severe enough to lead to early aging (Tyynismaa et al., 2005).

Apart from lifespan, other indicators in our mKOs also differ from the Deletor mice. Deletor mice have shown to have similar body weight and locomotor activity, measured with an activity cage, compared to their WT counterparts (Tyynismaa et al., 2005). Conversely, body weight loss was apparent in our mKOs even in the 4^{th} week of their lives, and locomotor activity in the activity cage was severely affected compared to the Deletor mouse. Moreover, decreased voluntary movement on both

axes accompanies the progression of the disease in the mKOs. In the vertical axis, the movement number of our WT mice increased continuously. This could be caused by increase in their body sizes as vertical sensors are placed higher than the horizontal ones to be able to detect only the hindlimb movement. When the mice grew in size, sensors for the vertical axis was able to quickly catch the signal. The opposite was true for mKOs; since their growth was stunted, the sensors could not detect the signal for the vertical axis. Thus, mKOs might have performed slightly better in the vertical axis than the observed data, even if this would not be nearly as close to the WT performance.

6.1.2. *Pus1* KO vs Skeletal Muscle Specific *Dars2* Mouse

Pus1 knockout (PUS1 KO) mouse is another whole-body knockout model, which presents with mitochondrial myopathy (Magnum et al., 2016). PUS1 pseudouridylate tRNAs and the pseudouridylation process is essential for the structure and function of RNAs. Loss of function at the *Pus1* gene is accompanied by a low mitochondrial translation rate (Fernandez-Vizarra et al., 2007; Mangum et al., 2016). When the PUS1 KO mice were 14 weeks of age, they did not exhibit body weight change, and their muscles were not atrophic, which was assessed by dividing the gastrocnemius mass by the body weight (Magnum et al., 2016). However, a 46% reduction was noted on the treadmill at 14-week-old PUS1 KOs, indicating a reduction in muscle performance; interestingly, the grip strength test, which measures muscle strength, did not reveal any substantial difference compared to their littermates (Magnum et al., 2016). Regarding neuromuscular coordination at the rotarod test, a significant change was not observed between PUS1 KO and WTs.

Phenotypical assessments in our mKO mouse model exhibited highly severe manifestations compared to PUS1 KO. First, the lifespan of mKOs was markedly less, and they had highly atrophic muscles. In their 3rd week, our mKOs had already shown decreased muscle performance. For instance, the best performance among all observed mKOs on the treadmill was 182 meters in their 3rd week, but the average running distance of WTs is more than 1000 meters at the same age. Muscle strength in mKOs

is also significantly different than in the controls. Like PUS1 KO, our mKOs have shown similar rotarod performance with their controls. These rotarod test results may indicate that neuromuscular coordination might not necessarily be worsened in mitochondrial myopathies.

Consistent with Deletor and PUS1 KOs, mitochondrial myopathy phenotype was apparent in mKOs, in which reduced muscle performance, decreased locomotor activity, atrophied muscle, and decreased body weight were apparent. However, Deletor and PUS1 KOs are whole-body knockout mouse models so comparing mKOs with skeletal muscle-specific models would also be beneficial.

6.1.3. COX10 KO vs Skeletal Muscle Specific *Dars2* Mouse

COX10 is a nuclear genome-encoded assembly factor that plays a role in mitochondrial complex IV (COX) biogenesis and mitochondrial heme biosynthesis pathway (Antonicka, Leary, et al., 2003). COX10 mutations are associated with leukodystrophy, tubulopathy, Leigh Syndrome, and fatal infantile hypertrophic cardiomyopathy (Antonicka, Leary, et al., 2003).

Skeletal muscle-specific COX10 KO mice displayed severe and progressive myopathy, yet the phenotypical symptoms of mitochondrial myopathy were not apparent in the first 2 and a half months (Diaz et al., 2005). Among noted phenotypical symptoms, decreased muscle size and spontaneous activity can be exemplified; the body weight of males was similar to their control group for the first 3 months but progressively declined over time; this difference is markedly lower at female knockouts compared to their littermates even at the early stages (Diaz et al., 2005). The knockout mice could hardly reach to 20 grams when they were three months old, although their female counterparts were between 25-30 grams. Muscle performance was measured with a treadmill, in which male and female COX10 KOs displayed lower performance, especially females (Diaz et al., 2005). The authors also noted that knockouts could hardly run even at the slowest speed at their terminal stage. 50% of female knockouts died around the 4^{th} month, but 50% of males died around the 7^{th} month. Maximal muscle force was

measured with electrodes, which is a different method than grip strength meter test, and COX10 KO mice showed progressively lower maximal muscle force (Diaz et al., 2005).

COX10 model showed progressive and severe myopathy with sex-specific differences at the phenotypical level. In our case, progressive treadmill reduction was very evident too, and again in the final stage, mKOs could not run on the treadmill platform. Moreover, in our mKOs, WT muscle force increased over time, but there was no considerable decrease in the grip strength test. Nevertheless, it is evident that in both groups, the muscle strength of myopathic animals is markedly lesser than their WT littermates. Despite the similarity and severity of phenotypes between skeletal COX10 KOs and mKOs, there are some differences to consider. First, COX10 deletion leads primarily to COX10 protein depletion, which is directly related to COX deficiency (Diaz et al., 2005). Conversely, DARS2 deletion leads to a translation defect in mitochondria, and overall, down-regulation in mtDNA-encoded proteins with aspartic acid residues, resulting in a generalized compromised OXPHOS (Dogan et al., 2014). These molecular differences might account for the severity of some traits, including the beginning disease symptoms and early lethality in mKOs compared to COX10 KO. Both DARS2 and COX10 deletion in muscle cause lifespan, body weight, and muscle performance reductions. In mKOs, these signs were more pronounced; however, sex-specific phenotyping was not performed in mKOs as we have not noticed any visible differences gender wise, apart from body weight. This was also in accordance with the heart and skeletal muscle-specific DARS2 mutant, in which authors have not observed any sex-specific differences (Dogan et al. 2014). Another essential difference can be attributed to tissue specificity conferred by different promoters. COX10 model was generated with *Mlc1f-Cre*; however, the mKOs were generated with *Acta1-Cre*. As explained *ACTA1* promoter is mainly active in striated muscle and expression few cardiomyoctyes in adults and in embryonic stage it was active in myotomes and some cardiomyocytes with no known cardiac structure (Miniou et al., 1999). *MLC1F* promoter is active myoblast-myotube transtiotion in the embryonic stage (Cohen et al., 1998). Although both promoters are skeletal muscle-specific, it is not apparent whether these promoter differences contribute to the severity of mutants by themselves.

6.1.4. COX15 KO vs Skeletal Muscle Specific *Dars2* Mouse

Skeletal muscle-specific COX15 knockout (COX15 KO) is another tissue-specific mitochondrial myopathy mouse model of ETC deficiency. COX15 is an essential protein for the complex IV, mainly participating in heme A synthesis, a prosthetic group in the COX complex. It is known that COX15 deficiency is associated with mitochondrial myopathies like Leigh Syndrome and hypertrophic cardiomyopathy (Antonicka, Mattman, et al., 2003; Bugiani et al., 2005; Halperin et al., 2020). Similarly, COX15 KO mice displayed severely reduced muscle performance by treadmill results; they could run at most for a couple of minutes, which is markedly lower than their WT littermates (Viscomi et al., 2011). Half of COX15 KO mice died around six months, significantly showing severe decline in lifespan (Civiletto et al., 2015). Both our mKOs and COX15 KO have markedly compromised muscle performance and reduced lifespan, yet COX15 mice have a better survival rate.

Both COX10 and COX15 contribute to COX assembly, and their mutations are associated with Leigh Syndrome, a severe myopathy. The median lifespan of COX10 KO was 4 months for females and 7 months for males (Diaz et al., 2005). Similarly, the median survival of COX15 KOs was 5 months and the body weight loss started around the 8^{th} week in COX15 KO (Dogan et al., 2018). On the other hand, COX10 KO males had similar body weight to their controls until three months of age, but the females had lower body mass already around the 1^{st} month (Diaz et al., 2005). Similar COX defects with different promoters seem to generate roughly similar phenotypes in terms of myopathy phenotype, lifespan, and severity. Thus, comparing severe decline in health and lifespan, mKOs were directly affected by their translational defect, and types of defects (i.e. translation defective vs COX defective) result in different survival rates even in the same tissue knockouts.

6.1.5. *Ckmm-Cre* Mice and Myopathic Phenotpye

Ckmm-Cre is a transgenic overexpressor mouse model generally used for modeling heart-related defects because the creatine kinase muscle promoter (*Ckmm*) is

expressed in heart and skeletal muscle (Lyons et al., 1991). In the last decades, several *Ckmm-Cre* mediated tissue-specific knockouts were generated. One of these models was *Ckmm-Dars2*$^{-/-}$ mice, which has the same DARS2 construct, and the protein was deleted both in the heart and skeletal muscle (Dogan et al, 2014). *Ckmm-Dars2*$^{-/-}$ mice displayed severe cardiomyopathy, ETC deregulation, and impaired mitochondrial protein synthesis in both tissues. Nevertheless, activation of stress responses was only observed in the heart, not skeletal muscle (Dogan et al., 2014). Similar phenomena were also observed in other knockout mouse models utilizing *Ckmm-Cre*. For example, *Ckmm-Tfam*$^{-/-}$ mice did not show any abnormal morphological signs in the skeletal muscle as well as a mitochondrial myopathy phenotype (J. Wang et al., 1999). The muscles had similar ETC function as their WT counterparts; only mtDNA copy number decrease was detected in muscle (J. Wang et al., 1999). That might be reasonable as TFAM directly contributes to mtDNA replication, its depletion results in mtDNA depletion. Another example is the *Ckmm-MTERF3*$^{-/-}$ mouse model, MTERF3 is a mitochondrial transcriptional repressor and its germline deletion is embryonic lethal (Park et al., 2007). Terminal stage *Ckmm-MTERF3*$^{-/-}$ mutants showed similar skeletal muscle morphologies to their controls (Park et al., 2007). On the other hand, they had mitochondrial cardiomyopathy, and their maximal life span was 18 weeks (Park et al., 2007). MCL-1 is similar to BCL-2 a pro-survival protein germline deletion led embryonic lethality (Chin & Fu, 2021). *Ckmm-Mcl-1*$^{-/-}$ mice showed a similar pattern as the other models, with a solid cardiomyopathic phenotype but no visible signs of myopathy (X. Wang et al., 2013).

To summarize, *Ckmm-Cre* mediated excision, hence deletion in cardiac and skeletal muscle, worsened the cardiac tissues extensively but not the skeletal muscles to that extent (Dogan et al., 2014). Then, *Acta1-Cre* mediated excision on mKOs showed severe and progressive myopathy phenotype on *Dars2* deletion. Both *Ckmm-Dars2*$^{-/-}$ and mKOs displayed atrophy, shortening in lifespan, and significantly less body weight compared to their WT counterparts. However, an extensive phenotypical study on *Ckmm-Dars2* mice had not been done like exercise intolerance to locomotor activity observation, etc, and further comparison remains lacking on those assays. Interestingly, an exciting similarity was observed in *Tfam* knockouts. As mentioned *Ckmm-Dars2*$^{-/-}$

mice did not exhibit a myopathic phenotype, but skeletal muscle-specific deletion of *Tfam* also exhibited a progressive mitochondrial myopathy phenotype and molecular signatures of disease (Wredenberg et al., 2002). Compelling question remains if other *Ckmm-Cre* mediated would display myopathy phenotype when their skeletal muscle-specific deleted.

6.2. A Possible Fiber Type Switch in Skeletal Muscle Specific *Dars2* Mouse

We have observed muscle atrophy and reddish muscle in mKOs. ETC abnormalities might accompany muscle loss by the sarcopenia, and it is known that white-colored, fast twitching type II fibers are more susceptible to muscle loss than type I fibers, which are slow twitching and red-colored (Bua et al., 2002). Type I muscle fibers depend more on oxidative metabolism, but type II fibers depend more on glycolysis metabolism (Yan eta al., 2011). We showed that mitochondrial translation defect leads reduced ETC complexes which resulted in mitochondrial biogenesis increase in mKOs. It is also known that fiber type switch is mediated by mitochondrial biogenesis master regulator PGC-1α that shifts type II fibers toward type I to increase OXPHOS metabolites, type I proteins like myoglobin, troponin, and type II fibers become more reddish (Lin et al., 2002). Moreover, research on rats showed that age-dependent sarcopenia is accompanied by ETC defects and the percentage the type II fibers decreased while type I fibers increased in soleus and adductor longus muscles (Bua et al., 2002). These findings are coherent with our findings in which mitochondrial biogenesis increased via the transcriptional activity of PGC-1 α and severe muscle atrophy was evident. On the other hand, a research showed that adult mitochondrial myopathy patients displayed a decreased percentage of type I fibers and increased type II fibers, yet they have not observed a significant change a cross-sectional area specific to type I and type II fibers between patients and controls (Gehrig et al., 2016). They also mentioned type I predominance in children with mitochondrial myopathy (Gehrig et al., 2016). Additionally, PUS1 KO mice also displayed type II dominant fibers and they underlined the similarity between PUS1 KO and MLASA patients in terms of

utilization of glycolytic metabolism (Mangum et al, 2016). These findings suggest further immunohistochemical experiments need to be performed to fully support this hypothesis.

6.3. Skeletal Muscle Specific *Dars2* Mouse are Hyopglycamemic

Another significant condition was hypoglycemia in mKOs, which is commonly observed in mitochondrial dysfunction (Ashfaq et al., 2021). Similar observations were made on other mouse models with mitochondrial problems: Heart-specific deletion of VLCAD which catalyzes the first reaction in mitochondrial fatty acid oxidation resulted in hypoglycemia in mice (Xiong et al., 2014). Also, VLCAD deficiency is associated with dilated cardiomyopathy, hypoketotic hypoglycemia, and skeletal myopathy in patients (Xiong et al., 2014). On the other hand, encephalomyopathy mice with globally-ablated *Ndufs4* exhibited blood glucose within the healthy range, as the Deletor mice (Kruse et al., 2008; Tyynismaa et al., 2010). A child with defective glutamyl-tRNA synthetase 2, Mitochondrial (EARS2), like mKOs, presented with hypoglycaemia as well (Danhauser et al., 2016). Another example is translation-related mutations in mitochondrial protein MRPS2: Biallelic mutations in the gene caused OXPHOS deficiencies and hypoglycaemia (Gardeitchik et al., 2018). As can be deduced from the examples, blood glucose levels sometimes change in some mitochondrial problems but not in all. The low blood sugar levels we observed might be caused by the ETC defect inducing disrupted fatty acid oxidation in skeletal muscles and higher glucose uptake rate. Thus, further research should be conducted to see whether glucose uptake increased such as monitoring with GLUT4, and fatty acid oxidation decreased or not measuring the levels of non-esterified fatty acids (NEFA) in blood.

6.4. Reduction in ETC Complex Levels Skeletal Muscle Specific *Dars2* Mouse

Mitochondrial translation defect on *Dars2* deletion in skeletal muscles accompanied a down-regulation in CI, CIII, and CIV in mKOs. It is known that OPXHOS defects might induce a mitochondrial biogenesis response to compensate for defects

(Moraes, 2009). Biogenesis response can explain CII elevation in our mKOs since it is also known that the nuclear genome completely encodes CII (Signes &Vizarra, 2018). Furthermore, CV elevation in mKOs also be explained by mitochondrial biogenesis response because CV consists of two subunits (F0 and F1), and the nuclear genome entirely encodes the F1 subunit (Signes &Vizarra, 2018). Therefore, CII and CV (F1 subunit) protein levels may also be elevated to compensate for ETC deficiency.

6.4.1. Mitochondrial Biogenesis Response in Skeletal Muscle Specific *Dars2* Mouse

Since PGC-1α is a master regulator of mitochondrial biogenesis, firstly, PGC-1α levels were examined, and multiple bands were observed at the western blot, probably different isoforms of it. The most potent bands were visible at 70kd. The other signal, just above 100kd, was not quantified since a band was not available in some of the WT samples. Surprisingly, we could not observe an increase in the protein levels of PGC-1α. This could be due to the antibody used. Regardless, mKO muscles have upregulated AMPK phosphorylation, which is a regulator of PGC-1α activation and a significant energy sensor activated upon ATP reduction. AMPK can directly activate the transcriptional activity of PGC-1α by phosphorylation. Especially considering the decline in OXPHOS subunit levels on mitochondrial translational stress, it is reasonable to increase the transcriptional activity of PGC-1α by an energy sensing axis (Cantó & Auwerx, 2009).

PGC-1α may activate the transcriptional program for mitochondrial biogenesis via NRF1/NRF2, which would lead to the upregulation of genes in mitochondrial biogenesis like *TFAM* (Dillon et al., 2012). As a part of the biogenesis program, both NRF1 and NRF2 regulate nuclear DNA-encoded ETC proteins: NRF1 can directly bind to *Tfam* promoter, and NRF2 can regulate critical mitochondrial proteins like TOM20 (Pasyukova et al., 2019). The increase we observed in TFAM and mtDNA copy number in mKO skeletal muscles strongly supports a robust response, probably by PGC-1α & NRF1 axis. The upsurge in mitochondrial membrane proteins VDAC1 and TOM20 also strengthens the idea of increased mitochondrial mass in mKOs, supporting

PGC-1α & NRF2 axis. Nevertheless, one interesting question remains: Is the biogenesis response adaptive? That means if the mitochondrial biogenesis response can counteract mitochondrial ailment and alleviate the disease or could not resolve the stress and cause an aggravation of the condition. Pathologies like ragged-red fiber formation is closely linked with mitochondrial biogenesis, which was observed in several clinical cases and some mouse models as well.

Similar biogenesis responses have also been observed in other mitochondrial myopathy mouse models. Mitochondrial aggregation at the subsarcolemmal region of the soleus and increased *Pgc-1α* RNA in muscle was observed in *Vlcad*$^{-/-}$ mice (Exil et al., 2003). Skeletal muscle-specific *Tfam* deletion also caused mitochondrial accumulation and RRF formation. Abnormal mitochondria with distorted cristae were observed, yet paracrystalline aggregates were not detected. As expected, *Tfam* deletion reduced mtDNA content and *Tfam* transcript levels, and resulted in OXPHOS activity decline. Microarray analysis of PUS1 KO mice exhibited an enrichment of mitochondrial biogenesis elements in red gastrocnemius muscle to some extent, not in white skeletal muscle. Interestingly, PUS1 KO animals had smaller and fewer mitochondria in their muscles. Also, there were no paracrystalline mitochondrial inclusion bodies also observed in PUS1 KO mice (Mangum et al., 2016). Likewise, whole-body *Surf1*$^{-/-}$ deletion displayed an activated mitochondrial biogenesis program with elevated PGC-1α, TFAM, mtDNA copy number, CII levels, and Porin/VDAC1 proteins in both heart and skeletal muscle (Pulliam et al., 2014). The authors also discovered substantial COX activity decline in both tissues, but other complex activities were in a normal range (Pulliam et al., 2014). All in all, mitochondrial biogenesis was observed in many other mitochondrial myopathy mouse models, consistent with our observations in mKOs. Contrarily to these mitochondrial myopathy models, *Ckmm-Dars2*$^{-/-}$ mice displayed mitochondrial biogenesis response only in the heart, yet neither mitochondrial biogenesis nor RRF formation was observed in their skeletal muscle even if they had apparent muscle atrophy (Dogan et al., 2014). Since they did not observe RRF formation in skeletal muscle, we did not investigate whether there is an RFF formation or not in our mKOs too.

Although mitochondrial biogenesis increased as a stress response, some of the mentioned mitochondrial myopathy models exhibited mitochondrial accumulations, RRF formations, or ultrastructural distortions. The formation of RRFs can be due to the chronic mitochondrial dysfunction observed in the aforementioned knockout models and due to this chronic nature, stress responses could not resolve the problems and give rise to an aggravated phenotype even with an active quality control mechanism. Not all mitochondrial myopathies exhibit RRF formations in both human cases and murine models. Sometimes between 1% - 30% of the stained muscles can exhibit RRF formation (Punsoni et al., 2014; Vogel, 2001). Additionally, the interaction of the mitochondrial biogenesis program with quality control mechanisms is essential to govern a healthy mitochondrial biogenesis program and stress response resolution. To sum up, histochemical and microscopy analyses are needed to determine whether our mKOs exhibit RRFs or ultrastructural disruptions.

6.4.2. Autophagy Impairment in Skeletal Muscle Specific *Dars2* Mouse

Mitochondria-specific autophagy opposes mitochondrial biogenesis: When mitochondrial biogenesis increases, autophagy decreases, and vice versa. In dysfunctional states, either mitochondrial accumulation and defective autophagy or overactive autophagy and decreased mitochondrial mass can be observed (Palikaras & Tavernarakis, 2014). P62 is an established autophagy marker that binds ubiquitinated or polyubiquitinated proteins, forms aggregates and carry autophagic cargo to autophagosomes. LC3 is another autophagic marker that plays a role in the formation of autophagosomes; LC3B-I is an inactive and cytoplasmic form of LC3; LC3B-II is an active autophagosome membrane-bound form. P62 serves polyubiquitinated proteins to autophagosomes by interacting with LC3B-II, and ubiquitinated protein aggregates are degraded in active autophagosomes (Liu et al., 2016; Niklaus et al., 2017). As our terminal stage mKOs displayed increased mitochondrial biogenesis, we wondered whether autophagy was affected. We have observed upregulated protein levels of LC3B-II and P62, and elevated ubiquitinated proteins; contrarily, LC3B-I levels were not changed. These results show that although autophagosome number is increased, autophagic cargos could

not be efficiently degraded. Especially the higher levels of P62 and polyubiquitinated proteins implies impaired autophagy, most probably in the formation of autolysosomes. Compromised autophagy may also be associated with RRF formation and mitochondria accumulation as the autophagy system could not turnover dysfunctional mitochondrial aggregates. A study, in which catabolic processes, including autophagy, were inhibited by PGC-1α mediated biogenesis response to evade mitochondrial atrophy, gives credence to this claim (Cannavino et al., 2014). Moreover, AMPK phosphorylation may lead to the activation of ULK1/2, which promotes autophagy. Additionally, AMPK boosts the activity of PGC-1α as a mitochondrial biogenesis response. In this respect, AMPK has a bipartite role and is essential for homeostasis (Palikaras & Tavernarakis, 2014). In our case, even if the increased phosphorylation of AMPK might induce autophagy, the last steps of autophagy pathway might be defective, i.e. autolysosome formation. Further experiments measuring the autophagic flux could be useful in dissecting this pathway further.

Similar autophagy impairments were observed in other mitochondrial myopathy models. COX15 KO mice exhibited increased LAMP and P62 levels (Civiletto et al., 2015). Deletor mice showed overall increased mitophagy in muscle tissue but selectively impaired mitophagy at RRFs (Mito et al., 2022). Lysosomes were dispersed around a disorganized mitochondrial network of RRFs, and their size was small; on the other hand, mitophagy levels were regular in morphologically normal parts of skeletal muscle and centrally nucleated fibers. P62 and LC3B-II levels also increased, showing impaired autophagy in muscle (Khan et al., 2017; Mito et al., 2022).

6.4.3. Antioxidant Response in Skeletal Muscle Specific *Dars2* Mouse

NFE2 Like BZIP Transcription Factor 2 (NFE2L2) mediated antioxidant response is essential for both mitochondrial biogenesis and autophagy responses. Accumulated NFE2L2 in the nucleus binds the ARE element of the *NRF1* gene, which activated *TFAM* and mtDNA replication (Merry et al., 2016; Wu et al., 1999). It is also known that NFE2L2 plays a role in autophagy by activating some macro-autophagy genes like *P62, ULK1,* and *ATG7* (Pajares et al., 2016).

Our results revealed discrepancies between protein and transcript levels of the key components of the antioxidant response. SOD2 and NFE2L2 protein levels were upregulated, whereas the transcript levels of *Sod2, Nfe2l2,* and *Gpx1* were downregulated. This discrepancy between protein and RNA levels may be caused by the factors contributing to different protein stability and RNA turnover rates. NFE2L2 phosphorylation by the MAPK pathway is known to increase NFE2L2 stability allowing longer activation (Nguyen et al., 2003). Another study on C. cerevisiae showed that mRNA levels of antioxidant genes returned to baseline level 1 hour of diamide treatment mediated oxidative stress induction; however, protein levels were still changing (Vogel et al., 2011). This data also point to a dynamic change between mRNA and protein levels in the stress response mediation. Moreover, the levels of nuclear-localized NFE2L2, than the total protein level in the cell, is more important for the activation of the antioxidant response. Nevertheless, these activated proteins suggest an upregulated antioxidant response, but whether this activation is ROS-dependent or a complementary part of biogenesis and autophagy-related response, is needed to be further investigated. Further studies, such as ROS, protein carbonylation, lipid peroxidation, and DNA damage measurements, should be employed to understand whether mKOs suffer from oxidative damage.

Mitochondrial dysfunction models exhibiting antioxidant response ranges from none to some extent. For example, protein levels of antioxidant enzymes (SOD1 and SOD2) were not changed in the skeletal muscles of COX10 KO animals. Additionally, oxyblot analysis of mitochondria and muscle lysates were not different in knockout mice compared to their controls (Diaz et al., 2005). In the heart and skeletal muscle of *Ckmm-Dars2*$^{-/-}$ mice, neither protein carbonylation nor SOD2 increase was observed (Dogan et al., 2014). Similarly, GPX1 and SOD2 levels were unchanged in the heart and liver of the Mutator mice (Trifunovic et al., 2005). Whole-body knockout *Surf1*$^{-/-}$ mice did not show increased ROS, interestingly antioxidant response elements (NRF2 and HO-1) were only upregulated in the hearts but not skeletal muscle homogenates (Pulliam et al., 2014). An increase in the antioxidant response element *Nfe2l2* and its target genes *Gpx1* and *Sod2*; additionally, the transcripts of *Catalase* and *Sod1* were observed in *Acta1-Cox15*$^{-/-}$ mice (Dogan et al., 2018). ROS upregulation was also

evident as a result of increased H_2O_2 levels and decreased Aconitase2 activity (Dogan et al., 2018). All these results demonstrate that mitochondrial myopathies do not always lead to increased ROS or antioxidant response. Sometimes both can be observed as in the case of *Acta1-Cox15*$^{-/-}$ mice or just antioxidant response as in the *Surf1*$^{-/-}$ mice. Our mKOs showed an increase in NFE2L2 and SOD2 in protein level, yet transcript levels were not coherent with protein level. Therefore, we could not conclude whether antioxidant response increased or not in our mKOs just by looking at these data. Also increased, NFE2L2 or SOD2 does not necessarily indicate an accompanying ROS increase. NFE2L2 could modulate mitochondrial biogenesis or autophagy responses via activating its target on these pathways. In either case, further experiments are needed regarding the ROS response of mKOs to comprehend the underlying molecular reason.

6.4.4. ISR^{mt} in Skeletal Muscle Specific *Dars2* Mouse

Mitochondrial unfolded protein response (UPR^{mt}) is the central mediator of proteotoxic stress response in *C. elegans*, which is mediated by ATFS-1 that accumulates in the nucleus and upregulates chaperones and proteases (Forsström et al., 2019). This pathway proved to be more complicated in mammals and the term "mitochondrial integrated stress response (ISR^{mt})" was coined, which comprises various metabolic pathways and UPR^{mt} as well. The central element in ISR^{mt} is eIF2α phosphorylation by various kinases like HRI, GCN2, PKR, PERK (Zebrucka et al., 2016).

Upon eIF2α phosphorylation at serine51, global translation initiation is prevented and by counteracting in ternary complex formation that is a significant event for 5'Cap dependent translation (Eckl et al., 2021). This phosphorylation leads to a translation program for special uORFs to counteract mitochondrial insult and decreases global protein synthesis. Transcription factors *Atf4, Atf5,* and *Chop* are expressed in this cap-independent program (Eckl et al., 2021; Ryoo & Vasudevan, 2017). When we analyzed ISR^{mt} response in our terminal stage mKOs, we have observed increased eIF2α phosphorylation; however, transcript levels of *Atf4* and *Atf5* were not significantly but relatively decreased. An established mitochondrial myopathy model Dele-

tor mouse also exhibited non-significant *Atf4* transcript levels in their skeletal muscles (Forsström et al., 2019). The authors argued that ATF4 might be regulated at the post-transcriptional level; this might also be the case for our mKOs. Atf5 transcript increase was evident in Deletor mice at an early stage. If we could also quantify the *Atf5* transcripts earlier than the terminal stage of mKOs, we might obtain a similar observation.

Interestingly, a significant elevation in ATF4 protein level was not recorded, only a subtle increase was observed. We believe that a stronger signal with different ATF4 antibodies may give us better results.

Even if there was not a clear upregulation in the ATF4 levels as expected, we observed an increase in ATF4 downstream pathways. Folate metabolism is induced by ATF4 activation, and skeletal muscle tissues of our mKOs showed 50 folds increase at the rate-limiting step enzyme *Mthfd2* transcript. Apart from the eIF2α phosphorylation axis as a part of translation defect response, MTHFD2 induction can be mediated by the mTORC1-ATF4 axis. mTORC1 axis leads to purine synthesis in one carbon cycle as a part of ISR^{mt} (Ben-Sahra et al., 2016; Khan et al., 2017). In addition to the purine synthesis pathway, mTORC1 also modulates protein biosynthesis by phosphorylating its target proteins S6K1 and EIF4EB1 proteins (Chang et al., 2022). EIF4EB1 sequester a protein that is a part of cap binding complex for protein translation, mTORC1 mediated phosphorylation of EIF4EB1 protein to release its sequestered protein and cause protein synthesis increase (Chang et al., 2022). mTORC1 also contributes to ribosome biosynthesis by phosphorylating S6K1 protein which in turn phosphorylates S6 protein and S6 protein is a significant element of ribosomal biogenesis (Chang at al., 2022). Therefore, elevated S6 phosphorylation rates in mKOs show mTORC1-S6 axis activation. That is in line with the mTORC1-activated ATF4-dependent one carbon metabolism activation and serine biosynthesis (Ben-Sahra et al., 2016) Proline biosynthesis is a downstream pathway of the phosphorylated eIF2α-activated ATF4 axis (Kühl et al., 2017). In accordance with these results, we observed a robust increase in PYCR1 protein and *Aldh18a1* transcript levels. Intriguingly, mTORC1 activation inhibits autophagy and leads to a polyu-

biquitinated aggregate. That could be the indication that may explain the impaired autophagy in mKOs (Khan et al., 2017). In the 3rd stage of ISR^{mt}, chaperone activity might be observed (Forsström el al., 2019). Chaperone activity is essential for appropriate mitochondrial biogenesis as well since HSP60 and GRP75/HSP70 proteins fold imported mitochondrial preproteins. Considering most mitochondrial proteins are nuclear-encoded and translocated into the mitochondrial matrix in their unfolded forms, chaperons play a vital role in mitochondrial proteostasis. mtHSP70/(GRP75) carries out both chaperone activity and mitochondrial protein import via PAM machinery, which is crucial for assembling ETC complexes. The preproteins were observed to be folded by HSP60 after being released by GRP75, which suggests cooperation between these two chaperones (Voos & Röttgers, 2002).

Increased mitochondrial chaperone activities were detected in other mitochondrial myopathy models as well. Examples include the heart and skeletal muscle of *Surf1*$^{-/-}$ mice (Pulliam et al., 2014) and the skeletal muscles of the Deletor mice (Forsström et al., 2019).

FGF21 and GDF15 are mammalian mitokines that early elements of ISR^{mt}, and they activate systemic ISR^{mt} response. FGF21 is also responsible for the induction of ATFs at the second stage of ISR^{mt} (Forsstöm et al., 2019; Dogan et al., 2018). Both *Fgf21*and *Gdf15* transcript levels were increased, supporting the view of ATF4 and a general ISR^{mt} induction in the skeletal muscles of our mKOs.

In addition to our mKOs and Deletor mice, five different cardiomyopathy mouse models (*Ckmm-Twnk*, *Ckmm-Tfam*, *Ckmm-Polrmt*, *Ckmm-Lrpprc*, and *Ckmm-Mterf4*) also showed increased ISR^{mt} at their hearts (Kühl et al., 2017). However, a significant ailment in their muscles was not reported. Whether skeletal muscle-specific deletion in these genes would also recapitulate the findings at mKOs would be interesting to delve into.

7. CONCLUSIONS & FUTURE PERSPECTIVES

To sum up, skeletal muscle-specific deletion of *Dars2* led to a mitochondrial translational defect; which resulted in a severe and progressive mitochondrial myopathy phenotype. The mKO mice weighed half of their WT littermates and had severely reduced lifespan of 7 to 8 weeks. mKOs had decreased voluntary movement as tested by the activity cage, and their muscle performance is also remarkably low as observed by the treadmill and grip strength meter. Marked muscle atrophy, slight reddish muscle coloration, and lesser body hair were observed. Molecular cues also supported the myopathy phenotype: *Dars2* transcript levels in the muscle were almost diminished, atrophy markers were increased, and hypoglycaemic blood was detected in mKOs. Likewise, a reduction in OXPHOS complexes was observed. As a compensatory mechanism, we observed an overall increase in mitochondrial biogenesis, mitochondrial chaperones, antioxidant response, ISR^{mt}, and impairment in autophagy.

This study primarily performed phenotyping of a novel mitochondrial myopathy model and overall stress response induction. Nevertheless, to gain more insight into the myopathy phenotype of this mouse mode, some areas should be further investigated thoroughly. Firstly, histochemistry and microscopy studies need to be performed to reveal the possibility of mitochondrial ultrastructural disruptions and RRF formation. Moreover, mitochondrial oxygen consumption and membrane potential should be measured to understand the degree of mitochondrial dysfunction. Blue-Native PAGE and aminoacylation assays can be performed to understand whether this new mutant also recapitulates the translational defects observed in *Ckmm-Dars2*$^{-/-}$ hearts and skeletal muscles. The stress responses can also be further characterized. Although we observed an increase in the antioxidant response elements, we should check what happens to the ROS levels. Similarly for fatty acid oxidation, glucose uptake and fatty acid levels may be measured.

Finally, the characterization of this novel myopathy mouse model could also benefit from possible interventions to ameliorate the disease phenotype. These interventions

could lead into the detailed elucidation of the underlying molecular mechanisms that can eventually be exploited to design new rational therapeutic approaches for mitochondrial myopathies.

REFERENCES

Antonellis, A. and E.D. Green, 2008, "The Role of Aminoacyl-tRNA synthetases in Genetic Diseases", *Annual Review of Genomics and Human Genetics*, Vol. 9, pp. 87–107.

Antonicka, H., S.C. Leary, G.H. Guercin, J.N. Agar, R. Horvath, N.G. Kennaway, C.O. Harding, M. Jaksch and E.A. Shoubridge, 2003, "Mutations in COX10 Result in a Defect in Mitochondrial Heme A Biosynthesis and Account for Multiple, Early-Onset Clinical Phenotypes Associated with Isolated COX deficiency", *Human Molecular Genetics*, Vol.12, No.20, pp. 2693–2702.

Antonicka, H., A. Mattman, C.G. C, D.M. Glerum, K.C. Hoffbuhr, S.C. Leary, N.G. Kennaway and E.A. Shoubridge, 2003, "Mutations in COX15 Produce a Defect in the Mitochondrial Heme Biosynthetic Pathway, Causing Early-Onset Fatal Hypertrophic Cardiomyopathy", *The American Journal of Human Genetics*, Vol.72, No.1, pp.101-114.

Ashfaq, A.R.Moats, H.Northrup, C.N.Singletary, S.Hashmi, M. KayKoenig, M.B.Bagg and D.Rodriguez-Buritica, 2021, "Hypoglycemia in Mitochondrial Disorders", *Mitochondrion*, Vol.58, pp.179–183.

Bacman, S. R., S.L. Williams, M. Pinto and C.T. Moraes, 2014, "The Use of Mitochondria Targeted Endonucleases to Manipulate mtDNA", *Methods in Enzymology*, Vol.547, No.C, p.373.

Bareth, B., S. Dennerlein, D. Mick, M. Nikolov, H. Urlaub, P. Rehling , 2013, "The Heme a Synthase Cox15 Associates with Cytochrome c Oxidase Assembly Intermediates during Cox1 Maturation", *Molecular and Cellular Biology*, Vol.33, No.20, p.4128.

Bar-Ziv, R., T. Bolas and A. Dillin, 2020, "Systemic effects of Mitochondrial Stress", *EMBO Reports*, Vol.21, No.6, p.e50094.

Ben-Sahra, G. Hoxhaj, S.J.H. Ricoult, J.M. Asara and B.D. Manning, 2016, "mTORC1 Induces Purine Synthesis Through Control of the Mitochondrial Tetrahydrofolate Cycle", *Science*, Vol.351 No.6274, pp.728–733.

Bezawork-Geleta. A., J. Rohlena, D. Lanfeng, P. Karel and J. Neuzil, 2017, "Mitochondrial Complex II: At the Crossroads", *In Trends in Biochemical Sciences*, Vol.42, No.4, pp.312–325.

Bhatti, J. S., G.K. Bhatti and P.H Reddy, 2017, " Mitochondrial Dysfunction and Oxidative Stress in Metabolic Disorders — A Step Towards Mitochondria Based Therapeutic Strategies", *Biochimica et Biophysica Acta - Molecular Basis of Disease*, Vol.1863, No.5, pp.1066–1077.

Bilen, M., S. Benhammouda, R.S. Slack and M. Germain, 2022, "The Integrated Stress Response as a Key Pathway Downstream of Mitochondrial Dysfunction", *Current Opinion in Physiology*, Vol.27, p.100555.

Boczonadi, M.J. Jennings, and R. Horvath, 2018, "The Role of tRNA Synthetases in Neurological and Neuromuscular Disorders", *FEBS Letters*, Vol.592, No.5, pp.703–717.

Bonnefond, L., A. Fender, J. Rudinger-Thirion, R. Giegé, C. Florentz, and M.Sissler, 2005, "Toward the Full Set of Human Mitochondrial Aminoacyl-tRNA Synthetases: Characterization of AspRS and TyrRS", *Biochemistry*, Vol.44, No.12, pp.4805–4816.

Bua, E. A., S.H. McKiernan, J. Wanagat, D. McKenzie, and J.M. Aiken, 2002, "Mitochondrial Abnormalities are More Frequent in Muscles Undergoing Sarcopenia", *Journal of Applied Physiology*, Vol.92, No.6, pp.2617–2624.

Bugiani, M., V. Tiranti, L. Farina, G. Uziel, and M. Zeviani, 2005, "Novel mutations

in COX15 in a Long Surviving Leigh Syndrome Patient with Cytochrome c Oxidase Deficiency. *Journal of Medical Genetics*, Vol.42, No.5, pp.e28–e28.

Calvo, S. E. and V.K.Mootha, 2010, "The Mitochondrial Proteome and Human Disease", *Annual Review of Genomics and Human Genetics*, Vol.11, pp.25–44.

Cannavino, J., L.Brocca, M. Sandri, R. Bottinelli and M.A. Pellegrino, 2014, "PGC-1 α Over-expression Prevents Metabolic Alterations and Soleus Muscle Atrophy in Hindlimb Unloaded Mice", *The Journal of Physiology*, Vol.592, No.20, pp.4575–4589,

Cantó, C. and J.A. Auwerx, 2009, "PGC-1alpha, SIRT1 and AMPK, an Energy Sensing Network That Controls Energy Expenditure", *Current Opinion in Lipidology*, Vol.20, No.2, pp.98.

Chang, M., S. Huhn, L. Nelson, M. Betenbaugh and Z. Du, 2022, "Significant Impact of mTORC1 and ATF4 pathways in CHO Cell Recombinant Protein Production Induced by CDK4/6 Inhibitor", *Biotechnology and Bioengineering*, Vol.119, No.5, pp.1189–1206.

Chin, H.S. and Y.F. Nai,"Physiological Functions of Mcl-1: Insights From Genetic Mouse Models", 2021, *Frontiers in Cell and Developmental Biology*, Vol.9, pp.1767.

Christian, B.E. and L.L.Spremulli, 2012, "Mechanism of Protein Biosynthesis in Mammalian Mitochondria 1. Protein Biosynthesis in Mammalian Mitochondria 1.1 Role of Mitochondria in Energy Metabolism", *Biochim Biophys Acta*, Vol.1819, No.9, pp.1035-1054.

Christian J.M.I.K., B. Thomas Budiman2 R.H. Judith R. Homberg3 , V. Dilip K. Jaap and E.M. van Schothorst, 2022, "Measuring Locomotor Activity and Behavioral Aspects of Rodents Living in the Home-Cage", *Frontiers in Behavioral Neuroscience*, Vol.16, p. 877323.

Civiletto, G., T. Varanita, R. Cerutti, T.Gorletta, S. Barbaro, S. Marchet, 2015, "Opa1 Overexpression Ameliorates the Phenotype of two Mitochondrial Disease Mouse Models", *Cell Metabolism*, Vol.21, No.6, pp.845–854.

Cohen, A., P.J.R. Barton, B. Robert, I. Garner, S. Alonso, M.E. Buckingham, 1998, "Promoter Analysis of Myosin Alkali Light Chain Genes Expressed in Mouse Striated Muscle. *Nucleic Acids Research*, Vol.16, No.21, pp.10037–10052.

Czudnochowski, N., Amy L.W., Janet F.M. and Robert M.S., 2013, "In Human Pseudouridine Synthase 1 (hPus1), a C-terminal Helical Insert Blocks tRNA From Binding in the Same Orientation as in the Pus1 Bacterial Homologue TruA, Consistent with their Different Target Selectivities", *Journal of Molecular Biology*, Vol.425, No.20, p. 3875.

Danhauser, K., T.B. Haack, B. Alhaddad, M. Melcher, A. Seibt, T.M. Strom, T. Meitinger, D. Klee, E. Mayatepek, H. Prokisch, F. Distelmaier, 2016, "EARS2 Mutations Cause Fatal Neonatal Lactic Acidosis, Recurrent Hypoglycemia and Agenesis of Corpus Callosum", *Metabolic Brain Disease*, Vol. 31, No. 3, pp. 717–721.

Dell'Agnello, C., S. Leo, A. Agostino, G. Szabadkai, C.C. Tiveron, A.A. Zulian, A. Prelle, P. Roubertoux, R. Rizzuto and M.Zeviani, 2007, "Increased Longevity and Refractoriness to Ca^2+-Dependent Neurodegeneration in *Surf1* Knockout Mice", *Human Molecular Genetics*, Vol. 16, No. 4, pp. 431–444.

Dey, S., T.D. Baird, D. Zhou, L.R. Palam, D.F. Spandau and R.C. Wek, 2010, "Both Transcriptional Regulation and Translational Control of ATF4 Are Central to the Integrated Stress Response", *The Journal of Biological Chemistry*, Vol. 285 No. 43, p.33165.

Diaz, F., C.K. Thomas, S. Garcia, D. Hernandez and C.T. Moraes, 2005, "Mice lacking COX10 in Skeletal Muscle Recapitulate the Phenotype of Progressive Mitochondrial Myopathies Associated with Cytochrome c Oxidase Deficiency", *Human Molecular*

Genetics, Vol. 14, No. 18, pp. 2737–2748.

Dikic, I., and Z. Elazar, 2018, "Mechanism and Medical Implications of Mammalian Autophagy", *Nature Reviews.* Molecular Cell Biology, Vol. 19, No. 6, pp. 349–364.

Dillon, L. M., A. P. Rebelo, and C.T. Moraes, 2012, "The Role of PGC-1 Coactivators in Aging Skeletal Muscle and Heart", *IUBMB Life*, Vol. 64, No. 3, pp. 231–241.

Diodato, D., D. Ghezzi, and V. Tiranti, 2014, "The Mitochondrial Aminoacyl tRNA Synthetases: Genes and Syndromes", *International Journal of Cell Biology*, p.787956.

Dogan, S. A., R. Cerutti, C. Benincá, G. Brea-Calvo, H.T. Jacobs, M. Zeviani, M. Szibor and C. Viscomi, 2018, " Perturbed Redox Signaling Exacerbates a Mitochondrial Myopathy", *Cell Metabolism*, Vol. 28, No. 5, pp. 764-775.

Dogan, S. A., Pujol, C., Maiti, P., Kukat, A., Wang, S., Hermans, S., Senft, K., Wibom, R., Rugarli, E. I., and Trifunovic, A., 2014, "Tissue-specific Loss of DARS2 Activates Stress Responses Independently of Respiratory Chain Deficiency in the Heart", *Cell Metabolism*, Vol. 19, Non3, pp. 458–469.

D'Souza, A. R., and M. Minczuk, M., 2018, "Mitochondrial Transcription and Translation: Overview", *Essays in Biochemistry* Vol. 62, No. 3, pp. 309–320.

Ducker, G. S., and J.D.Rabinowitz, 2017, "One-Carbon Metabolism in Health and Disease", *Cell Metabolism* Vol. 25, No. 1, pp. 27–42.

Echevarría, L., P. Clemente, R. Herńandez-Sierra, M.E. Gallardo, M.A. Ferńandez-Moreno and R. Garesse, 2014, "Glutamyl-tRNAGln Amidotransferase is Essential for Mammalian Mitochondrial Translation In Vivo", *Biochemical Journal*, Vol. 460, No.1, 91–101.

Eckl, E. M., O. Ziegemann,L. Krumwiede, E. Fessler and L.T. Jae, 2021, "Sensing,

Signaling and Surviving Mitochondrial Stress", *Cellular and Molecular Life Sciences* Vol. 78, No. 16, pp. 5925–5951.

Egan, D. F., D.B. Shackelford, M. M. Mihaylova, S. Gelino, R.A. Kohnz, W. Mair, D.S. Vasquez, A. Joshi, D.M Gwinn, R. Taylor, J.M. Asara, J. Fitzpatrick, A. Dillin, B. Viollet, M. Kundu, M. Hansen, and R. J. Shaw, 2011, "Phosphorylation of ULK1 (hATG1) by AMP-activated Protein Kinase Connects Energy Sensing to Mitophagy", *Science* (New York, N.Y.), Vol. 331, No. 6016, pp. 456–461.

Exil, V. J., R.L. Roberts, H. Sims, J.E. Mclaughlin, R. A. Malkin, C. D., Gardner, G. Ni, J.N. Rottman and A. W. Strauss, 2003, "Very-Long-Chain Acyl-Coenzyme A Dehydrogenase Deficiency in Mice, *Circulation Research*, Vol. 93, No. 5, pp. 448–455.

Fernandez-Vizarra, E., A. Berardinelli, L. Valente, V. Tiranti and M. Zeviani, 2007, "Nonsense Mutation in Pseudouridylate Synthase 1 (PUS1) in Two Brothers Affected by Myopathy, Lactic Acidosis and Sideroblastic Anaemia (MLASA)", *Journal of Medical Genetics*, Vol. 44, No. 3, p. 173.

Fernie, A. R., F. Carrari, and L.J. Sweetlove, 2004, "Respiratory Metabolism: Glycolysis, the TCA Cycle and Mitochondrial Electron Transport", *Current Opinion in Plant Biology*, Vol. 7, No. 3, pp. 254–261.

Fine, A. S., C.L. Nemeth, M. L., Kaufman and A. Fatemi, 2019, "Mitochondrial Aminoacyl-tRNA Synthetase Disorders: An Emerging Group of Developmental Disorders of Myelination", *Journal of Neurodevelopmental Disorders* Vol. 11, No. 1, p. 29.

Forsström, S., C.B. Jackson, C. J. Carroll, M. Kuronen, E. Pirinen, S. Pradhan, A. Marmyleva, M. Auranen, I.M. Kleine, N. A. Khan, A. Roivainen, P. Marjamäki, H. Liljenbäck, L. Wang, B. J.Battersby, U. Richter, V. Velagapudi, J. Nikkanen, L. Euro and A. Suomalainen, 2019, "Fibroblast Growth Factor 21 Drives Dynamics

of Local and Systemic Stress Responses in Mitochondrial Myopathy with mtDNA Deletions", *Cell Metabolism*, Vol. 30 No.6, pp. 1040-1054.

Frias, D. P., R. L. N. Gomes, K. Yoshizaki, R. Carvalho-Oliveira, M. Matsuda, de S.M. Junqueira, W. R. Teodoro, P. de C. Vasconcellos, D. C. de A. Pereira, P. R. da Conceição, P. H. N. Saldiva, T. Mauad and M. Macchione, 2020, "Nrf2 Positively Regulates Autophagy Antioxidant Response in Human Bronchial Epithelial Cells Exposed to Diesel Exhaust Particles", *Scientific Reports* Vol. 10, No. 1, pp. 1–13.

Gardeitchik, T., M. Mohamed, B. Ruzzenente, D. Karall, S. Guerrero-Castillo, D. Dalloyaux, M. van den Brand, S. van Kraaij, E. van Asbeck, Z. Assouline, M. Rio, P. de Lonlay, S. Scholl-Buergi, D.F.G.J. Wolthuis, A. Hoischen, R.J. Rodenburg, W. Sperl, Z. Urban, U. Brandt, ... E. Morava, 2018, "Bi-allelic Mutations in the Mitochondrial Ribosomal Protein MRPS2 Cause Sensorineural Hearing Loss, Hypoglycemia, and Multiple OXPHOS Complex Deficiencies", *The American Journal of Human Genetics*, Vol. 102, No. 4, pp. 685–695.

Garin, S., O. Levi, B. Cohen, A. Golani-Armon and Y.S. Arava, 2020, "Localization and RNA Binding of Mitochondrial Aminoacyl tRNA Synthetases", *Genes* Vol. 11, No. 10, pp. 1–20.

Garone, C., and C. Viscomi, 2018, "Towards a Therapy for Mitochondrial Disease: An Update", *Biochemical Society Transactions* Vol. 46, No. 5, pp. 1247–1261.

Gehrig, S. M., V. Mihaylova, S. Frese, S.M. Mueller, M. Ligon-Auer, C.M. Spengler, J.A. Petersen, C. Lundby and H.H. Jung, 2016, "Altered Skeletal Muscle (Mitochondrial) Properties in Patients with Mitochondrial DNA Single Deletion Myopathy", *Orphanet Journal of Rare Diseases*, Vol. 11, No. 1, p.105.

Guo, M., X.L. Yang and P. Schimmel, 2010, "New Functions of Aminoacyl-tRNA Synthetases Beyond Translation", *Nature Reviews. Molecular Cell Biology*, Vol. 11, No. 9, pp. 668–674.

Hahn, A., and s. Zuryn, 2019, "The Cellular Mitochondrial Genome Landscape in Disease", *Trends in Cell Biology*, Vol. 29, No.3, pp. 227–240.

Halperin, D., M. Drabkin, O. Wormser, Y. Yogev, V. Dolgin, Z. Shorer, L. Gradstein, I. Shelef, H. Flusser and O.S. Birk, 2020, "Phenotypic Variability and Mutation Hotspot in COX15-Related Leigh Syndrome", *American Journal of Medical Genetics*, Vol. 182, No.6, pp. 1506–1512.

Hassani, A., R. Horvath and P.F. Chinnery, 2010, "Mitochondrial Myopathies: Developments in Treatment", *Current Opinion in Neurology* Vol. 23, No. 5, pp. 459–465,

Hellyer, J. A., S.K. Padda, M. Diehn, and H.A. Wakelee, 2021, "Clinical Implications of KEAP1-NFE2L2 Mutations in NSCLC", *Journal of Thoracic Oncology: Official Publication of the International Association for the Study of Lung Cancer*, Vol. 16, No.3, pp. 395–403.

Hwang, H.J., H. Ha, B.S. Lee, B.H. Kim, H.K. Song and Y.K. Kim, 2022, "LC3B is an RNA-binding Protein to Trigger Rapid mRNA Degradation During Autophagy", *Nature Communications*, Vol. 13 No. 1, p. 1436.

Jäer, S., C. Handschin, J. St-Pierre and B.M. Spiegelman, 2007, "AMP-activated Protein Kinase (AMPK) Action in Skeletal Muscle via Direct Phosphorylation of PGC-1 α", *Proceedings of the National Academy of Sciences of the United States of America*, Vol. 104, No. 29, pp. 12017–12022.

Jain, A., T. Lamark, E. Sjøttem, K.B. Larsen, J.A. Awuh, A. Øvervatn, M. McMahon, J.D. Hayes and T. Johansen, 2010, "p62/SQSTM1 Is a Target Gene for Transcription Factor NRF2 and Creates a Positive Feedback Loop by Inducing Antioxidant Response Element-driven Gene Transcription", *Journal of Biological Chemistry*, Vol. 285, No. 29, pp. 22576–22591.

Kang, I., C.T. Chu and B.A. Kaufman, 2018, "The Mitochondrial Transcription Factor

TFAM in Neurodegeneration: Emerging Evidence and Mechanisms", *FEBS Letters*, Vol. 592 No. 5, pp. 793–811.

Kasai, S., S. Shimizu, Y. Tatara, J. Mimura and K. Itoh, 2020, "Regulation of Nrf2 by Mitochondrial Reactive Oxygen Species in Physiology and Pathology", *Biomolecules*, Vol. 10, No. 2.

Khan, N. A., J. Nikkanen, S. Yatsuga, C. Jackson, L. Wang, S. Pradhan, R. Kivelä, A. Pessia, V. Velagapudi and A. Suomalainen, 2017, "mTORC1 Regulates Mitochondrial Integrated Stress Response and Mitochondrial Myopathy Progression", *Cell Metabolism*, Vol. 26, No. 2, 419-428.

Klaus, S. and M. Ost, 2020, "Mitochondrial Uncoupling and Longevity – A Role for Mitokines?" *Experimental Gerontology*, Vol, 130 p. 110796.

Konovalova, S. and H. Tyynismaa, 2013, "Mitochondrial Aminoacyl-tRNA Synthetases in Human Disease", *Molecular Genetics and Metabolism*, Vol. 108, No. 4, pp. 206–211.

Kose, M., E. Canda, M. Kagnici, A. Aykut, O. Adebali, A. Durmaz, A. Bircan, G. Diniz, C. Eraslan, E. Kose, A. Ünalp, A.Ü. Yılmaz, B. Ozyilmaz, T.R. Özdemir, T. Atik, S.K. Uçar, R. McFarland, R.W. Taylor, G. K. Brown, ... F. Özkınay, 2020, "*SURF1* Related Leigh Syndrome: Clinical and Molecular Findings of 16 Patients from Turkey", *Molecular Genetics and Metabolism Reports*, Vol.25, p. 100657.

Kruse, S. E., W.c. Watt, D.J. Marcinek, R.P. Kapur, K.A. Schenkman, and R.D. Palmiter, 2008, "Mice with Mitochondrial Complex I Deficiency Develop a Fatal Encephalomyopathy", *Cell Metabolism*, Vol. 7, No. 4, pp. 312–320.

Kühl, I., M. Miranda, I. Atanassov, I. Kuznetsova, Y. Hinze, A. Mourier, A. Filipovska and N.G. Larsson, 2017, "Transcriptomic and Proteomic Landscape of mitochondrial dysfunction Reveals Secondary Coenzyme Q Deficiency in Mammals", *ELife*, Vol.6,

pp. 1–3.

Kummer, E. and N. Ban, 2021, "Mechanisms and Regulation of Protein Synthesis in Mitochondria", *Nature Reviews Molecular Cell Biology*, Vol. 22, No. 5, pp. 307–325.

Kuszak, A. J., M.G. Espey, M. J. Falk, M. A. Holmbeck, G. Manfredi, G.S. Shadel, H. J. Vernon and Z. Zolkipli-Cunningham, 2018, "Nutritional Interventions for Mitochondrial OXPHOS Deficiencies: Mechanisms and Model Systems", *Annual Review of Pathology: Mechanisms of Disease*, Vol. 13, pp. 163–191.

Lane, N. and W. Martin, 2010, "The Energetics of Genome Complexity", *Nature* Vol. 467, No. 7318, pp. 929–934.

Larsson, N. G. and A. Oldfors, 2001, "Mitochondrial Myopathies", *Acta Physiologica Scandinavica*, Vol. 171, No. 3, pp. 385–393.

Larsson, N.-G. and P. Rustin, 2001, "Animal Models for Respiratory Chain Disease", *Trends in Molecular Medicine*, Vol. 7, No. 12.

Licari, E., L. Sánchez-del-Campo and P. Falletta, 2021, "The Two Faces of the Integrated Stress Response in Cancer Progression and Therapeutic Strategies", *The International Journal of Biochemistry and Cell Biology*, Vol.139. p. 106059.

Li, J.-L., K.J. Tsai, C.C. Chan, T.Y. Lin, P.L. Chen, T.N. Guo, S.Y. Huang, C.H. Chen, C.H. Lin, 2021, "Mitochondrial Function and Parkinson's Disease: From the Perspective of the Electron Transport Chain", *Frontiers in Molecular Neuroscience* Vol. 14. pp. 797833-797833.

Lin, Y. F., A.M. Schulz, M.W. Pellegrino, Y. Lu, S. Shaham and C.M. Haynes, 2016, "Maintenance and Propagation of a Deleterious Mitochondrial Genome by the Mitochondrial UPR", *Nature*, Vol. 533, No. 7603, p. 416.

Liu, S., S. Li and H. Jiang, 2021, "Multifaceted Roles of Mitochondrial Stress Responses under ETC Dysfunction – Repair, Destruction and Pathogenesis", *FEBS Journal*.

Liu, W. J., L. Ye, W.F. Huang, L.J. Guo, Z.G. Xu, H.L. Wu, C. Yang and H.F. Liu, 2016, "p62 Links the Autophagy Pathway and the Ubiqutin-proteasome System upon Ubiquitinated Protein Degradation", *Cellular and Molecular Biology Letters*, Vol. 21 No. 1, pp. 1–14.

Lyons, G. E., S. Muhlebach, A. Moser, R. Masood, B.M. Paterson, M.E. Buckingham and J.C. Perriard, 1991, "Developmental Regulation of Creatine Kinase Gene Expression by Myogenic Factors in Embryonic Mouse and Chick Skeletal Muscle", *Development* Vol. 113, No. 3, pp. 1017-1029.

Mangum, J. E., J.P. Hardee, D.K. Fix, M.J. Puppa, J. Elkes, D. Altomare, Y. Bykhovskaya, D.R. Campagna, P.J. Schmidt, A.K. Sendamarai, H.G.W. Lidov, S.C. Barlow, N. Fischel-Ghodsian, M.D. Fleming, J.A. Carson and J.R. Patton, 2016, "Pseudouridine Synthase 1 Deficient Mice, a Model for Mitochondrial Myopathy with Sideroblastic Anemia, Exhibit Muscle Morphology and Physiology Alterations", *Scientific Reports*, Vol. 6, No. 1, p. 26202.

Melber, A. and C.M. Haynes, 2018, "UPR mt Regulation and Output: a Stress Response Mediated by Mitochondrial-nuclear Communication", *Nature Publishing Group*, Vol. 28, pp. 281–295.

Merry, T. L., M. Ristow, T.L. Merry and M. Ristow, 2016, "Nuclear factor erythroid-derived 2-like 2 (NFE2L2, Nrf2) Mediates Exercise-induced Mitochondrial Biogenesis and the Anti-oxidant Response in Mice, *The Journal of Physiology* Vol. 594, pp. 5195–5207.

Miniou, P., D. Tiziano, T. Frugier, N. Roblot, M. le Meur and J. Melki, 1999, "Gene Targeting Restricted to Mouse striated muscle lineage", *Nucleic Acids Research*, Vol.27 No. 19, pp. e27–e30.

Mito, T., A. E. Vincent, J. Faitg, R.W. Taylor, N.A. Khan, T.G. McWilliams and A. Suomalainen, 2022, "Mosaic Dysfunction of Mitophagy in Mitochondrial Muscle Disease", *Cell Metabolism*, Vol. 34 No. 2, pp. 197-208.

Moraes, C. T., 2009, "Making the Most of What You've Got: Optimizing Residual OXPHOS Function in Mitochondrial Diseases", *EMBO Molecular Medicine*, Vol. 1, pp. 357–359.

Murphy, M. P., 2009, "How Mitochondria Produce Reactive Oxygen Species", *Biochemical Journal*, Vol. 417, No. 1, pp. 1–13.

Muthiah, A., G.D. Housley, M. Klugmann and D. Fröhlich, 2021, "The Leukodystrophies HBSL and LBSL—Correlates and Distinctions", *Frontiers in Cellular Neuroscience*, Vol. 14, p. 626610.

N'gbo N'gbo Ikazabo, R., C. Mostosi, P. Jissendi, M.A. Labaisse and I. Vandernoot, 2020, "A New DARS2 Mutation Discovered in an Adult Patient", *Case Reports in Neurology*, Vol. 12, No. 1, p.107.

Ngo, H. B., G.A. Lovely, R. Phillips and D.C. Chan, 2014, "Distinct Structural Features of TFAM Drive Mitochondrial DNA Packaging Versus Transcriptional Activation", *Nature Communications* Vol. 5, No. 1, pp. 1–12.

Nguyen, T., P.J. Sherratt, H.C. Huang, C.S. Yang and C.B. Pickett, 2003, "Increased Protein Stability as a Mechanism That Enhances Nrf2-mediated Transcriptional Activation of the Antioxidant Response Element: Degradation of Nrf2 BY THE 26 S Proteosome", *Journal of Biological Chemistry*, Vol. 278, No. 7, pp. 4536–4541.

Niemann, M., A. Harsman, J. Mani, C.D. Peikert, S. Oeljeklaus, B. Warscheid, R. Wagner and A. Schneider, 2017, "tRNAs and Proteins Use the Same Import Channel for Translocation Across the Mitochondrial Outer Membrane of Trypanosomes", *Proceedings of the National Academy of Sciences of the United States of America*,

Vol. 114, No. 37, pp. E7679–E7687.

Niklaus, M., O. Adams, S. Berezowska, I. Zlobec, F. Graber, J. Slotta-Huspenina, U. Nitsche, R. Rosenberg, M.P. Tschan, and R. Langer, 2017, "Expression Analysis of LC3B and p62 Indicates Intact Activated Autophagy is Associated with an Unfavorable Prognosis in Colon Cancer", *Oncotarget*, Vol. 8, No. 33, p. 54604.

Nilsson, R., M. Jain, N. Madhusudhan, N.G. Sheppard, L. Strittmatter, C. Kampf, J. Huang, A. Asplund and V.K. Mootha, 2014, "Metabolic enzyme expression highlights a key role for MTHFD2 and the mitochondrial folate pathway in cancer", *Nature Communications* Vol. 5, p. 3128.

Niyazov, D. M., S.G. Kahler and R.E. Frye, 2016, "Primary Mitochondrial Disease and Secondary Mitochondrial Dysfunction: Importance of Distinction for Diagnosis and Treatment", *Molecular Syndromology*, Vol. 7, No. 3, pp. 122–137.

Nolfi-Donegan, D., A. Braganza and S. Shiva, 2020, "Mitochondrial Electron Transport Chain: Oxidative Phosphorylation, Oxidant Production, and Methods of Measurement", *Redox Biology*, Vol. 37, p. 101674.

Nunnari, J. and A. Suomalainen, 2012, "Mitochondria: In Sickness and in Health", *Cell*, Vol. 148, No. 6, pp. 1145–1159.

Ost, M., . Igual Gil, V. Coleman, S. Keipert, S. Efstathiou, V. Vidic, M. Weyers and S. Klaus, 2020, "Muscle-derived GDF15 Drives Diurnal Anorexia and Systemic Metabolic Remodeling During Mitochondrial Stress", *EMBO Reports*, Vol. 21 No. 3, p. e48804.

Pajares, M., N. Jiménez-Moreno, A.J. García-Yagüe, M. Escoll, M.L. de Ceballos, F. van Leuven, A. Rábano, M. Yamamoto, A.I. Rojo and A. Cuadrado, 2016, "Transcription Factor NFE2L2/NRF2 is a Regulator of Macroautophagy Genes", *Autophagy*, Vol. 12, No. 10, pp. 1902–1916.

Pakos-Zebrucka, K., I. Koryga, K. Mnich, M. Ljujic, A. Samali and A. M. Gorman, 2016, "The Integrated Stress Response", *EMBO Reports*, Vol. 17, No. 10, pp. 1374–1395.

Palikaras, K., E. Lionaki and N. Tavernarakis, 2015, "Balancing Mitochondrial Biogenesis and Mitophagy to Maintain Energy Metabolism Homeostasis", *Cell Death and Differentiation*, Vol. 22, No. 9, pp. 1399–1401.

Palikaras, K. and N. Tavernarakis, N., 2014, "Mitochondrial Homeostasis: The Interplay Between Mitophagy and Mitochondrial Biogenesis", *Experimental Gerontology*, Vol. 56, pp. 182–188.

Park, C. B., J. Asin-Cayuela, Y. Cámara, Y. Shi, M. Pellegrini, M. Gaspari, R. Wibom, K. Hultenby, H. Erdjument-Bromage, P. Tempst, M. Falkenberg, C.M. Gustafsson and N.G. Larsson, 2007, "MTERF3 Is a Negative Regulator of Mammalian mtDNA Transcription", *Cell*, Vol. 130, No. 2, pp. 273–285.

Parzych, K. R. and D.J. Klionsky, 2014, "An Overview of Autophagy: Morphology, Mechanism, and Regulation. *Antioxidants and Redox Signaling*, Vol. 20, No. 3, pp. 460–473.

Pasyukova, E. G., N. Chatterjee, A.P. Gureev, E.A. Shaforostova and V.N. Popov, 2019, "Regulation of Mitochondrial Biogenesis as a Way for Active Longevity: Interaction Between the Nrf2 and PGC-1 α Signaling Pathways", *Frontiers in genetics*, Vol. 10, p. 435.

Pearce, S., Nezich, C.L. and A. Spinazzola, 2013, "Mitochondrial Diseases: Translation Matters", *Molecular and Cellular Neurosciences*, Vol. 55, pp. 1–12.

Peter, B. and M. Falkenberg, 2020, "TWINKLE and Other Human Mitochondrial DNA Helicases: Structure, Function and Disease", *Genes*, Vol. 11, p. 408.

Pfeffer, G. and P.F. Chinnery, 2013, "Diagnosis and Treatment of Mitochondrial Myopathies", *Annals of Medicine*, Vol. 45, No. 1, pp. 4–16.

Piantadosi, C. A., M.S. Carraway, A. Babiker and H.B. Suliman, 2008, "Heme oxygenase-1 Regulates Cardiac Mitochondrial Biogenesis via Nrf2-mediated Transcriptional Control of Nuclear Respiratory Factor-1", *Circulation Research*, Vol. 103, No. 11, pp. 1232–1240.

Protasoni, M. and M. Zeviani, 2021, "Mitochondrial Structure and Bioenergetics in Normal and Disease Conditions", *International Journal of Molecular Sciences*, Vol. 22, No. 2, pp. 1–55.

Pulliam, D. A., S.S. Deepa, Y. Liu, S. Hill, A.L. Lin, A. Bhattacharya, Y. Shi, L. Sloane, C. Viscomi, M. Zeviani and H. van Remmen, 2014, "Complex IV-deficient *Surf1*$^{-/-}$ Mice Initiate Mitochondrial Stress Responses", *Biochemical Journal*, Vol. 462, No. 2, pp. 359–371.

Punsoni, M., S. Mangray, K.A. Lombardo, N. Heath, E.G. Stopa and E. Yakirevich, 2017, "Succinate Dehydrogenase B (SDHB) Immunohistochemistry for the Evaluation of Muscle Biopsies", *Applied immunohistochemistry and molecular morphology*, Vol. 25, No. 9, pp. 645–650.

Rebelo, A. P., L.M. Dillon and C.T. Moraes, 2011, "Mitochondrial DNA Transcription Regulation and Nucleoid Organization", *Journal of Inherited Metabolic Disease*, Vol. 34, No. 4, pp. 941–951.

Ren, J., L. Pulakat, A. Whaley-Connell and J.R. Sowers, 2010, "Mitochondrial Biogenesis in the Metabolic Syndrome and Cardiovascular Disease", *Journal of Molecular Medicine*, Vol. 88, No. 10, pp. 993–1001.

Rossignol, R., B. Faustin, C. Rocher, M. Malgat, J.P. Mazat and T. Letellier, 2003, "Mitochondrial Threshold Effects", *Biochemistry* Vol. 370, pp. 751–762.

Rubio, M. A. T., J.J. Rinehart, B. Krett, S. Duvezin-Caubet, A.S. Reichert, D. Söll, and J.D. Alfonzo, 2008, "Mammalian Mitochondria Have the Innate Ability to Import tRNAs by a Mechanism Distinct from Protein Import", *Proceedings of the National Academy of Sciences of the United States of America*, Vol. 105, No. 27, pp. 9186–9191.

Ryoo, H. D. and D. Vasudevan, 2017, "Two Distinct Nodes of Translational Inhibition in the Integrated Stress Response", *BMB Reports*, Vol. 50, No. 11, p. 539.

Sagan, L., 1967, "On the Origin of Mitosing Cells", *Journal of Theoretical Biology*, Vol. 14, No. 3, pp. 255–274.

Salinas-Giegé, T., R. Giegé and P. Giegé, 2015, "tRNA Biology in Mitochondria", *Int. J. Mol. Sci*, Vol. 16, p. 16.

Sasarman, F., G. Karpati and E.A. Shoubridge, 2002, "Nuclear Genetic Control of Mitochondrial Translation in Skeletal Muscle Revealed in Patients with Mitochondrial Myopathy", *Human Molecular Genetics*, Vol. 11, No. 14, pp. 1669–1681.

Scheper, G. C., T. van der Klok, R.J. van Andel, C.G.M. van Berkel, M. Sissler, J. Smet, T.I. Muravina, S.V. Serkov, G. Uziel, M. Bugiani, R. Schiffmann, I. Krägeloh-Mann, J.A.M. Smeitink, C. Florentz, R. van Coster, J.C. Pronk and M.S. van der Knaap, 2007, "Mitochondrial aspartyl-tRNA Synthetase Deficiency Causes Leukoencephalopathy with Brain Stem and Spinal Cord Involvement and Lactate Elevation", *Nature Genetics*, Vol. 39, No. 4, pp. 534–539.

Sharma, L., J. Lu and Y. Bai, 2009, "Mitochondrial Respiratory Complex I: Structure, Function and Implication in Human Diseases", *Current Medicinal Chemistry*, Vol. 16, No. 10, pp. 1266–1277.

Shimojima, K., T. Higashiguchi, K. Kishimoto, S. Miyatake, N. Miyake, J.I. Takanashi, N. Matsumoto and T. Yamamoto, 2017, "A novel DARS2 Mutation in a Japanese

Patient with Leukoencephalopathy with Brainstem and Spinal Cord Involvement but no Lactate Elevation", *Human Genome Variation*, Vol. 4, No. 1, p. 17051.

Signes, A. and E. Fernandez-Vizarra, 2018, "Assembly of Mammalian Oxidative Phosphorylation Complexes I–V and Supercomplexes", *Essays in Biochemistry*, Vol. 62, No. 3, pp. 255–270.

Sissler, M., L.E. González-Serrano, and E. Westhof, 2017, "Recent Advances in Mitochondrial Aminoacyl-tRNA Synthetases and Disease", *Trends in Molecular Medicine*, Vol. 23, No. 8, pp. 693–708.

Srivastava, S. and C.T. Moraes, 2005, "Double-strand Breaks of Mouse Muscle mtDNA Promote Large Deletions Similar to Multiple mtDNA Deletions in Humans", *Human Molecular Genetics*, Vol. 14, No. 7, pp. 893–902.

Stewart, J. B. and P.F. Chinnery, 2015, "The Dynamics of Mitochondrial DNA Heteroplasmy: Implications for Human Health and Disease", *Nature Reviews Genetics*, Vol. 16, No. 9, pp. 530–542.

Su, H. and X. Wang, 2012, "p62 Stages an Interplay Between the Ubiquitin-Proteasome System and Autophagy in the Heart of Defense against Proteotoxic Stress", *Trends in cardiovascular medicine*, Vol. 21, No. 8, pp. 224–228.

Sulaiman, S. A., Z. Mohd Rani, F.Z. Mohd Radin and N.A. Abdul Murad, 2020, "Advancement in the Diagnosis of Mitochondrial Diseases", *Journal of Translational Genetics and Genomics*, Vol. 4, No. 3, pp. 159–187.

Suomalainen, A., and B.J. Battersby, 2018, "Mitochondrial diseases: The Contribution of Organelle Stress Responses to Pathology", *Nature Reviews Molecular Cell Biology*, Vol. 19, No. 2, pp. 77–92.

Suzuki, T., A. Nagao and T. Suzuki, 2011, "Human Mitochondrial tRNAs: Biogenesis,

Function, Structural Aspects, and Diseases", *Annual Review of Genetics*, Vol. 45, pp. 299–329. Taivassalo, T. and R.G. Haller, 2005, "Exercise and Training in Mitochondrial Myopathies", *Medicine and Science in Sports and Exercise*, Vol. 37, No. 12, pp. 2094–2101.

Trifunovic, A., A. Hansson, A. Wredenberg, A.T. Rovio, E. Dufour, I. Khvorostov, J.N. Spelbrink, R. Wibom, and H.T. Jacobs, 2005, "Somatic mtDNA Mutations Cause Aging Phenotypes without Affecting Reactive Oxygen Species Production", *PNAS* Vol. 102, No. 50, pp. 17993–17998.

Tyynismaa, H., 2013, "Mitochondrial aminoacyl-tRNA Synthetases", *Mitochondrial Disorders Caused by Nuclear Genes*, Vol. 9781461437222, pp. 263–276.

Tyynismaa, H., C.J. Carroll, N. Raimundo, S. Ahola-erkkilä, T. Wenz, H. Ruhanen, K. Guse, A. Hemminki, K.E. Peltola-Mjøsund, V. Tulkki, M. Orešič, C.T. Moraes, K. Pietiläinen, I. Hovatta, and A. Suomalainen, 2010, "Mitochondrial Myopathy Induces a Starvation-like Response", *Human Molecular Genetics*, Vol. 19, No. 20, pp. 3948–3958.

Tyynismaa, H., K.P. Mjosund, S. Wanrooij, I. Lappalainen, E. Ylikallio, A. Jalanko, J.N. Spelbrink, A. Paetau and A. Suomalainen, 2005, "Mutant Mitochondrial Helicase Twinkle Causes Multiple mtDNA Deletions and a Late-onset Mitochondrial Disease in Mice", *Proceedings of the National Academy of Sciences of the United States of America*, Vol. 102, No.49, pp. 17687–17692.

Valera-Alberni, M. and C. Canto, 2018, "Mitochondrial Stress Management: A Dynamic Journey", *Cell Stress*, Vol. 2, No. 10, pp. 253–274.

van Berge, L., S. Dooves, C.G.M. van Berkel, E. Polder, M.S. van der Knaap and G.C. Scheper, 2012, "Leukoencephalopathy with Brain Stem and Spinal Cord Involvement and Lactate Elevation is Associated with Cell-type-dependent Splicing of mtAspRS mRNA", *Biochemical Journal*, Vol. 441, No. 3, pp. 955–962.

van de Wal, M. A. E., M.J.W. Adjobo-Hermans, J. Keijer, T.J.J. Schirris, J.R. Homberg, M.R. Wieckowski, S. Grefte, E.M. van Schothorst, C. van Karnebeek, A. Quintana and W.J.H. Koopman, 2022, "Ndufs4 Knockout Mouse Models of Leigh Syndrome: Pathophysiology and Intervention", *Brain*, Vol. 145, No. 1, pp. 45–63.

Vincent, A. E., Y.S. Ng, K. White, T. Davey, C. Mannella, G. Falkous, C. Feeney, A.M. Schaefer, R. McFarland, G.S. Gorman, R.W. Taylor, D.M. Turnbull and M. Picard, 2016, "The Spectrum of Mitochondrial Ultrastructural Defects in Mitochondrial Myopathy", *Scientific Reports*, Vol. 6, No. 1, pp. 1–12.

Vincent, A.E. and M. Picard, 2018, "Multilevel Heterogeneity of Mitochondrial Respiratory Chain Deficiency", *Journal of Pathology*, Vol. 246, No.3, pp. 261–265.

Viscomi, C., E. Bottani, G. Civiletto, R. Cerutti, M. Moggio, G. Fagiolari, E.A. Schon, C. Lamperti and M. Zeviani, 2011, "In vivo Correction of COX Deficiency by Activation of the AMPK/PGC-1 α Axis", *Cell Metabolism*, Vol. 14, No. 1, pp. 80–90.

Viscomi, C. and M. Zeviani, 2020, "Strategies for Fighting Mitochondrial Diseases", *Journal of Internal Medicine*, Vol. 287, No. 6, pp. 665–684.

Vogel, C., Monteiro Silva, G. and E.M. Marcotte, 2011, "Protein Expression Regulation Under Oxidative Stress", *Molecular & Cellular Proteomics* Vol. 10, No.12, pp. M111.009217-M111.009217.

Vogel, H., 2001, "Mitochondrial Myopathies and the Role of the Pathologist in the Molecular Era", *Journal of Neuropathology and Experimental Neurology*, Vol. 60, No. 3, pp. 217–227.

Voos, W. and K. Röttgers, 2002, "Molecular Chaperones as Essential Mediators of Mitochondrial Biogenesis", *Biochimica et Biophysica Acta - Molecular Cell Research*, Vol. 1592, No. 1, pp. 51–62.

Wallen, R.C. and A. Antonellis, 2013, "To Charge or not to Charge: Mechanistic Insights into Neuropathy-associated tRNA Synthetase Mutations", *Current Opinion in Genetics and Development*, Vol. 23, No. 3, pp. 302–309.

Wang, F., D. Zhang, D. Zhang, P. Li and Y. Gao, 2021, "Mitochondrial Protein Translation: Emerging Roles and Clinical Significance in Disease", *Frontiers in Cell and Developmental Biology*, Vol. 9, pp. 675465-675465.

Wang, J., H. Wilhelmsson, C. Graff, H. Li, A. Oldfors, P. Rustin, J.C. Brüning, C.R. Kahn, D.A. Clayton, G.S. Barsh, P. Thorén and N.G. Larsson, 1999, "Dilated Cardiomyopathy and Atrioventricular Conduction Blocks Induced by Heart-specific Inactivation of Mitochondrial DNA Gene Expression", *Nature genetics*, Vol. 21, No. 1, pp. 133–137.

Wang, X., M. Bathina, J. Lynch, B. Koss, C. Calabrese, S. Frase, J.D. Schuetz, J.E. Rehg and J.T. Opferman, 2013, "Deletion of MCL-1 Causes Lethal Cardiac Failure and Mitochondrial Dysfunction", *Genes and Development*, Vol. 27, No. 12, pp. 1351–1364.

Webb, B. D., Diaz, G. A. and P. Prasun, 2020, "Mitochondrial Translation Defects and Human Disease", *Journal of Translational Genetics and Genomics*, Vol. 4, p. 71.

Wredenberg, A., R. Wibom, H. Wilhelmsson, C. Graff, H.H. Wiener, S.J. Burden, A. Oldfors, H. Westerblad and N.G. Larsson, 2002, "Increased Mitochondrial Mass in Mitochondrial Myopathy Mice", *Proceedings of the National Academy of Sciences of the United States of America*, Vol. 99, No.23, pp. 15066–15071.

Wu, Z., P. Puigserver, U. Andersson, C. Zhang, G. Adelmant, V. Mootha, A. Troy, S. Cinti, B. Lowell, R.C. Scarpulla and B.M. Spiegelman, 1999, "Mechanisms Controlling Mitochondrial Biogenesis and Respiration through the Thermogenic Coactivator PGC-1", *Cell*, Vol. 98, No. 1, pp. 115–124.

Xiong, D., H. He, J. James, C. Tokunaga, C. Powers, Y. Huang, H. Osinska, J.A. Towbin, E. Purevjav, J.A. Balschi, S. Javadov, F.X. McGowan, A.W. Strauss, Z. Khuchua and M.F. Jr, 2014, "Cardiac-specific VLCAD Deficiency Induces Dilated Cardiomyopathy and Cold Intolerance", *Am J Physiol Heart Circ Physiol*, Vol. 306, pp. 326–338.

Yan, Z., M. Okutsu, Y.N. Akhtar and V.A. Lira, 2011, "Signals Mediating Skeletal Muscle Remodeling by Activity: Regulation of Exercise-induced Fiber Type Transformation, Mitochondrial Biogenesis, and Angiogenesis in Skeletal Muscle. Journal of Applied Physiology, Vol. 110, No. 1, p.264.

Yao, P. and P.L. Fox, 2013, "Aminoacyl-tRNA Synthetases in Medicine and Disease", *EMBO Molecular Medicine*, Vol. 5, No. 3, pp. 332–343.

Zaragoza, M. v., J. Fass, M. Diegoli, D. Lin and E. Arbustini, 2010, "Mitochondrial DNA Variant Discovery and Evaluation in Human Cardiomyopathies through Next-Genera-tion Sequencing", *PLoS One*, Vol. 5, No. 8, p. 12295.

Zeviani, M. and S. di Donato, 2004, "Mitochondrial Disorders", *Brain*, Vol. 127, No. 10, pp. 2153–2172.

Zhang, Y., Y. Qu, K. Gao, Q. Yang, B. Shi, P. Hou, and M. Ji, 2015, "High Copy Number of Mitochondrial DNA (mtDNA) Predicts Good Prognosis in Glioma Patients", *Am J Cancer Res*, Vol. 5, No. 3, pp. 1207–1216.